Burnham

A.R.A.P. REPORT NO. 245

ANALYSIS OF THE VORTEX WAKES OF THE BOEING 727, LOCKHEED L-1011, MCDONNELL DOUGLAS DC-10, AND BOEING 747 AIRCRAFT

Richard S. Snedeker
Alan J. Bilanin

July 1975

Final Report

Prepared for

U.S. DEPARTMENT OF TRANSPORTATION
Transportation Systems Center
Cambridge, Massaschusetts 02142

NOTICE

Technical Report Documentation Page

1. Report No.	2. Government Accession No.	3. Recipient's Catalog No.

4. Title and Subtitle
Analysis of the Vortex Wakes of the Boeing 727, Lockheed L-1011, McDonnell Douglas DC-10, and Boeing 747 Aircraft

5. Report Date
July 1975

6. Performing Organization Code
1A844

7. Author(s)
Richard S. Snedeker & Alan J. Bilanin

8. Performing Organization Report No.
A.R.A.P. Rept. 245

9. Performing Organization Name and Address
Aeronautical Research Associates of Princeton, Inc.
50 Washington Road, Princeton, N.J. 08540

10. Work Unit No. (TRAIS)

11. Contract or Grant No.
DOT-TSC 845

12. Sponsoring Agency Name and Address
U.S. Department of Transportation
Transportation Systems Center
Cambridge, Massachusetts

13. Type of Report and Period Covered
Final Report
June 1974-July 1975

14. Sponsoring Agency Code
AWCK

15. Supplementary Notes

16. Abstract

A study has been made of the vortex wakes behind Boeing 727, Lockheed L-1011, McDonnell Douglas DC-10, and Boeing 747 aircraft in several flight configurations. An analytical method is developed for the computation of the wake vortex patterns and their velocity profiles for these aircraft. The method, which is based on Donaldson's extension of the Betz method for an inviscid wake, is further modified herein to include the effects of distributed wing drag and the computation of axial velocity profiles. Comparisons are made between wake vortex swirl velocity profiles computed for these aircraft and corresponding measurements made by the FAA in full-scale flyby tests at NAFEC.

The results indicate that the inviscid calculation works well for simple wakes containing one predominant pair of vortices, such as those shed with the aircraft in its cruise or holding configuration. With flaps deployed for take-off or landing, these aircraft, because of the segmented design of their flaps, produce complex wakes, which may contain as many as five pairs of vortices. Agreement between computed and

(Cont.)

17. Key Words	18. Distribution Statement
Vortices Vortex wakes Aircraft wakes Wake vortices Wake turbulence	Document is available to the public through the National Technical Information Service, Springfield, Virginia 22161.

19. Security Classif. (of this report)	20. Security Classif. (of this page)	21. No. of Pages	22. Price
UNCLASSIFIED	UNCLASSIFIED		

Form DOT F 1700.7 (8-72) Reproduction of completed page authorized

16. ABSTRACT (cont.)

measured profiles for these cases is not satisfactory, and it is surmised that under these conditions the actual vortices tend to merge through the action of turbulent transport. Thus, the measured profiles, in many cases, appear to represent vorticity concentrations that are the result of two or more vortices merging together.

It is concluded that the effects of drag on the inviscid structure of the vortices are small. Although there is a reduction in peak swirl velocities, this effect is confined to a small radial region. It is recommended that further efforts be made to understand the role of turbulent transport in the merging of vortices due to complex wing loadings, since it appears that this phenomenon is of major importance in the reduction of wake hazard.

PREFACE

The authors acknowledge with thanks the assistance and cooperation of the following individuals for providing necessary data and information:

L. J. Garodz, FAA-NAFEC
N. Miller, FAA-NAFEC
J. Thelander, Douglas Aircraft Co.
O. R. Dunn, Douglas Aircraft Co.
W. A. Stauffer, Lockheed-California Co.
A. S. Mahal, Boeing Co.
P. W. Tracy, Boeing Co.

The authors also extend their appreciation to Mrs. Lois Ridgway of A.R.A.P. for typing the manuscript and to Mrs. Patricia Tobin of A.R.A.P. for preparation of the figures.

TABLE OF CONTENTS

1. INTRODUCTION

Significant progress has been made over the past four years in the understanding of the formation and decay of aircraft vortex wakes. An essential element in this progress has been the adaptation of the inviscid wake model first postulated by Betz in 1932 (Ref. 1). The Betz model relates the spanwise distribution of circulation about a wing to the radial distribution in a trailed, rolled-up vortex and depends on the assumption that the moments of vorticity during roll up are invariant. The initial application of this model to the present-day wake hazard problem associated with large aircraft was given by Donaldson in 1972 (Ref. 2). Since that time numerous studies have been carried out, at A.R.A.P. and elsewhere, which involve the modification or extension of the Betz approach to a variety of wake formation situations.

As a result of a study carried out with FAA and AFOSR support, Donaldson, et al. (Ref. 3), reported in 1973 that wake vortex velocity profiles computed using the Betz approach showed remarkably good agreement with those measured by the FAA during full-scale tower flyby tests of DC-7, DC-9, and C-141 aircraft at its NAFEC facility. In that report, it was further demonstrated that the principles of the Betz approach could be successfully applied to wakes other than those from wings that were approximately elliptically loaded. It was shown that the initial rolled-up form of the wake from a flapped wing of more complex spanwise loading could also be calculated successfully. Comparisons of the FAA data for flaps-down flybys of those aircraft with calculated vortex profiles showed good agreement if it was assumed that the measured vortex in such cases was always the interior or "flap" vortex, rather than the tip vortex. Such an assumption was reasonable in view of the fact that for most cases the spanwise loading was such that the tip vortices were significantly weaker than the flap vortices. Nevertheless, the question was left unresolved as to the fate of the tip vortices

and whether or not they contributed to the rolled-up wake profiles. In the case of the C-141, in particular, with flaps set for take-off and landing, the tip vortices, while weaker than the flap vortices, were still of significant strength. It could not be determined whether these vortices ultimately became diffused with the flap vortices or whether, through the effects of mutual induction, they had moved to a position where they could not be detected at the instrumentation tower. In fact, they may also have been subject to some form of breakdown brought on by self-induced or atmospheric turbulence interaction. It is important to note that all three of the aircraft used for the reported flyby tests had flaps that were aerodynamically continuous in spanwise extent (Fig. 1-1a). That is, there was no segmentation of the flaps that might give rise to additional vortex roll-up centers. Thus, only one significant interior vortex might have been expected in the wakes from these aircraft. As will be shown, the four aircraft involved in the study to be reported here, the Boeing 727, Boeing 747, McDonnell Douglas DC-10, and Lockheed L-1011, all have flaps that are arranged in two spanwise segments with a substantial gap between them (Fig. 1-1b). This arrangement can give rise to as many as four interior vortices of comparable strength.

In this report, the modified Betz method will be applied to the wake formation of the 727, 747, DC-10, and L-1011 aircraft. The inviscid, rolled-up velocity profiles will be calculated for several flight configurations. In addition, a method will be described for the inclusion of profile and induced drag in the roll-up calculation. Finally, the calculated wake velocity profiles, with and without drag, will be compared with the NAFEC flyby results for these aircraft. Anticipating the results somewhat, it will be seen that the individual interior vortices calculated for these aircraft with flaps extended do not show as good agreement with the vortex profiles measured at the tower as in the cases reported previously (DC-7, DC-9, C-141). Possible reasons for this finding will be discussed.

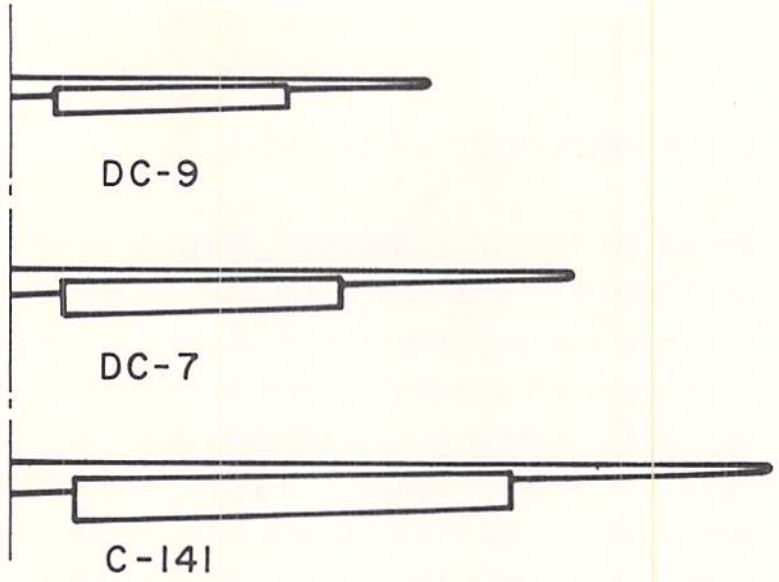

(a) Aircraft with continuous flaps

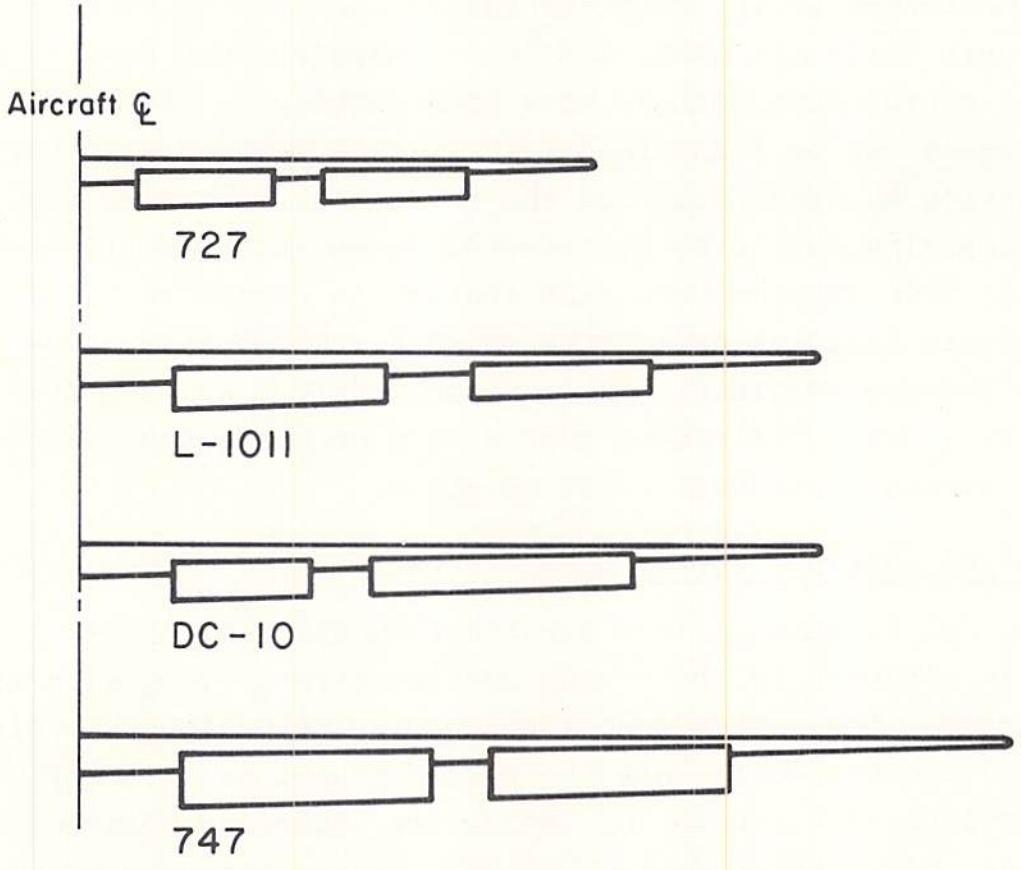

(b) Aircraft with segmented flaps

Fig. 1-1. Rear view wing profiles of NAFEC test aircraft showing (a) continuous and (b) segmented flaps. Spanwise dimensions to scale; otherwise schematic.

2. ESTIMATION OF THE VELOCITIES IN AN INVISCID VORTEX WAKE

As has been mentioned in the introduction, the Betz roll-up technique has received widespread attention in the literature. The popularity of this technique has no doubt been largely a result of the favorable comparisons between predicted and measured vortex swirl velocities (Refs. 2-6). Since a significant portion of the effort of this investigation is to compare the measured swirl velocities obtained from full-scale flyby tests with those velocity distributions computed with the Betz technique, it is appropriate to review the Betz method here.

The computation of the complete vortex wake behind an aircraft is a very difficult task, and it is therefore not surprising that several approximate methods have been developed. (A review of these techniques can be found in Ref. 7.) Betz avoided this difficult computation by specifying how the streamwise vorticity trailed from a lifting wing should be distributed in an axisymmetric vortex down stream. This axisymmetric distribution is chosen so as to preserve certain integral invariants of an incompressible, two-dimensional bounded vorticity distribution. Before delving into the Betz model, some preliminary ground work on the general nature of aircraft vortex wakes must first be given.

2.1 Single and multiple vortex wakes

In Fig. 2-1 is shown a load distribution which might be typical of an aircraft in the cruise configuration, i.e., with its flaps retracted. The vortex system which results behind this aircraft is well understood in that the wake contains two counter rotating vortices of strength Γ_o which are separated horizontally by a distance b'. The function $-d\Gamma/dy$ is the strength of the vortex sheet trailed from the wing. A maximum of sheet strength implies a maximum in the trailed vorticity, and it is reasonable to presume that in this case roll up begins at the wing tip. This of course is what is observed.

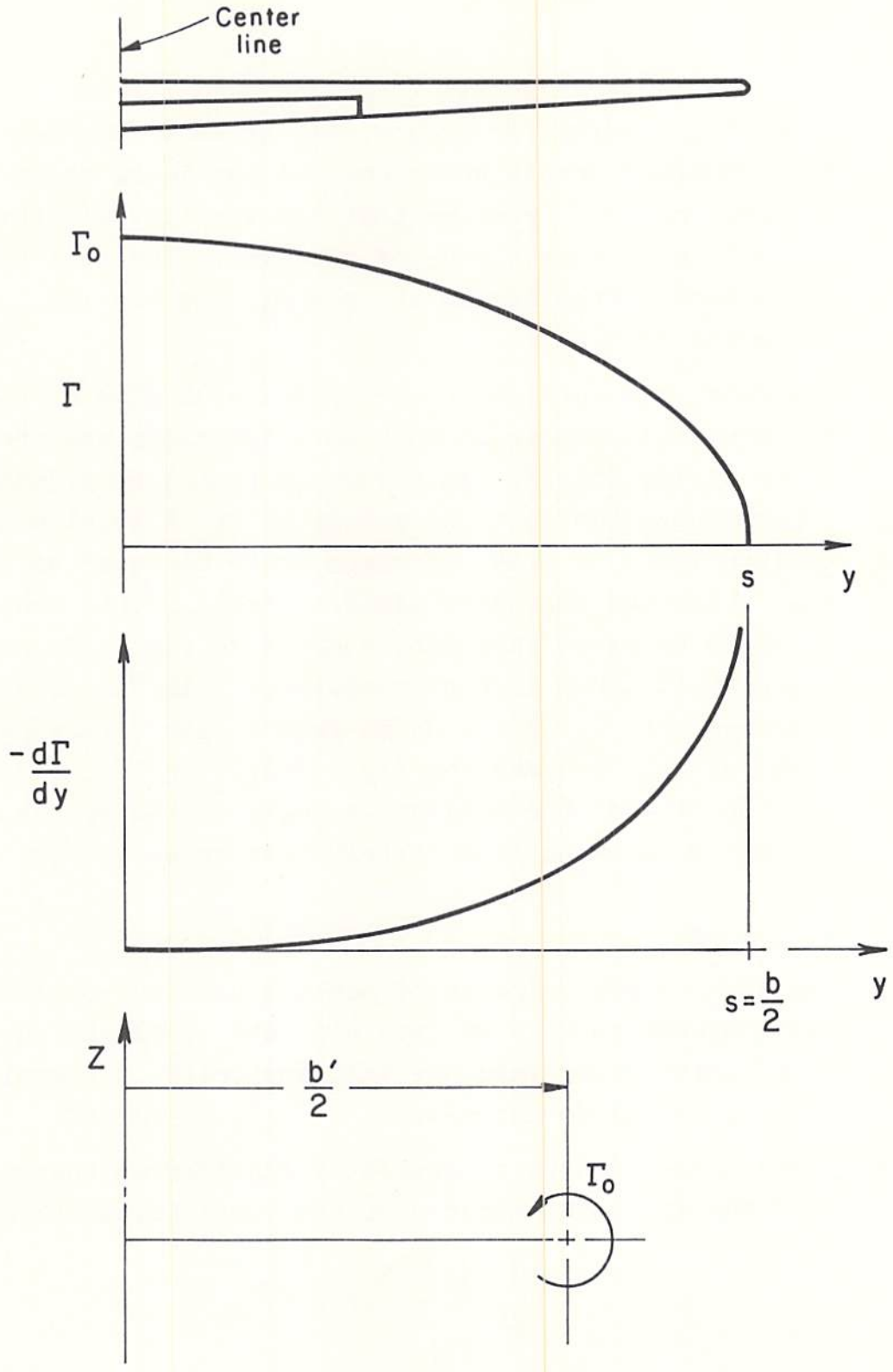

Fig. 2-1. The wing loading, sheet strength, and vortex system for a simply loaded wing.

Now suppose an aircraft has flaps deployed for landing. A typical load distribution for such a case is shown in Fig. 2-2. Note that the trailed vortex sheet now has two local maximums, and it is not unreasonable to presume that two vortices of like sign proceed to roll up from each side of the wing. The roll up of the flap or "interior" vortex begins at $y = y_m$ and the roll up of the tip vortex begins at $y = s$.

If, in fact, two vortices roll up from each side of the wing, one might immediately wonder at what location along the sheet does the vorticity divide itself. As a rule of thumb, Donaldson, et al. (Ref. 3), have suggested that the points at which local minimums of the absolute value of sheet strength occur be taken as the locations at which the vorticity divides itself. This conjecture has been checked by exact calculation by Yates (Ref. 10), and was shown to be correct under most circumstances. In Fig. 2-2 the vorticity inboard of y_B rolls up to form a flap vortex, while that outboard of y_B becomes the tip vortex. In Fig. 2-3 is shown an illustration of what the roll-up geometry of the vortex sheet might be like for the wing load distribution shown in Fig. 2-2.

2.2 Betz roll up

Having given a prescription of how the trailed vorticity divides and proceeds to roll up into discrete vortices, we will now give a method which determines how this vorticity is distributed in an axisymmetric vortex downstream.

The Betz method can be motivated by considering the time rates of change of the following moments of the vorticity distribution.

$$\Gamma = \int \zeta dA \tag{1}$$

$$\Gamma_y = \int y\zeta dA \tag{2}$$

$$\Gamma_z = \int z\zeta dA \tag{3}$$

$$\Gamma_r = \int (y^2 + z^2)\zeta dA \tag{4}$$

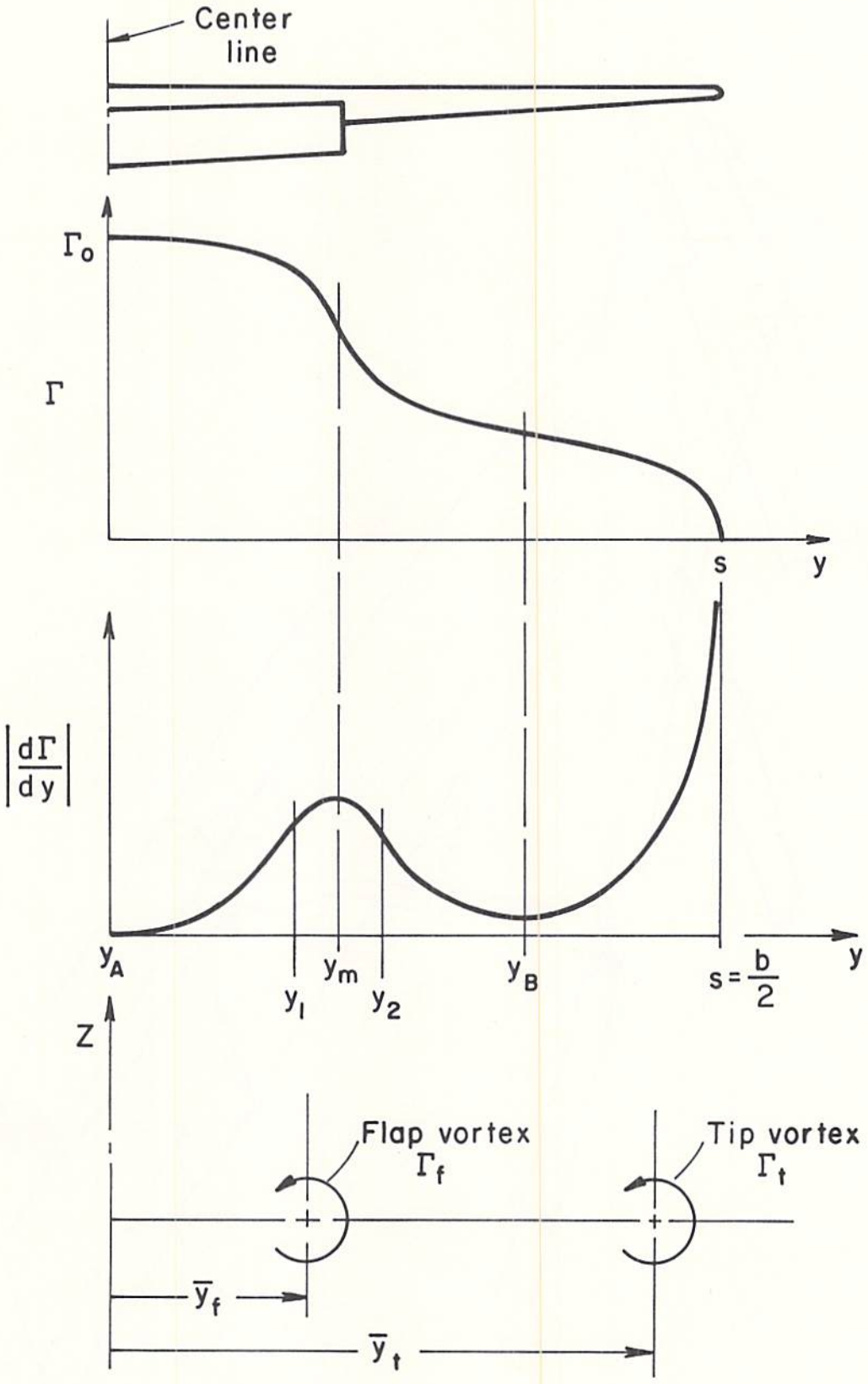

Fig. 2-2. The wing loading, sheet strength, and vortex system for a flapped wing.

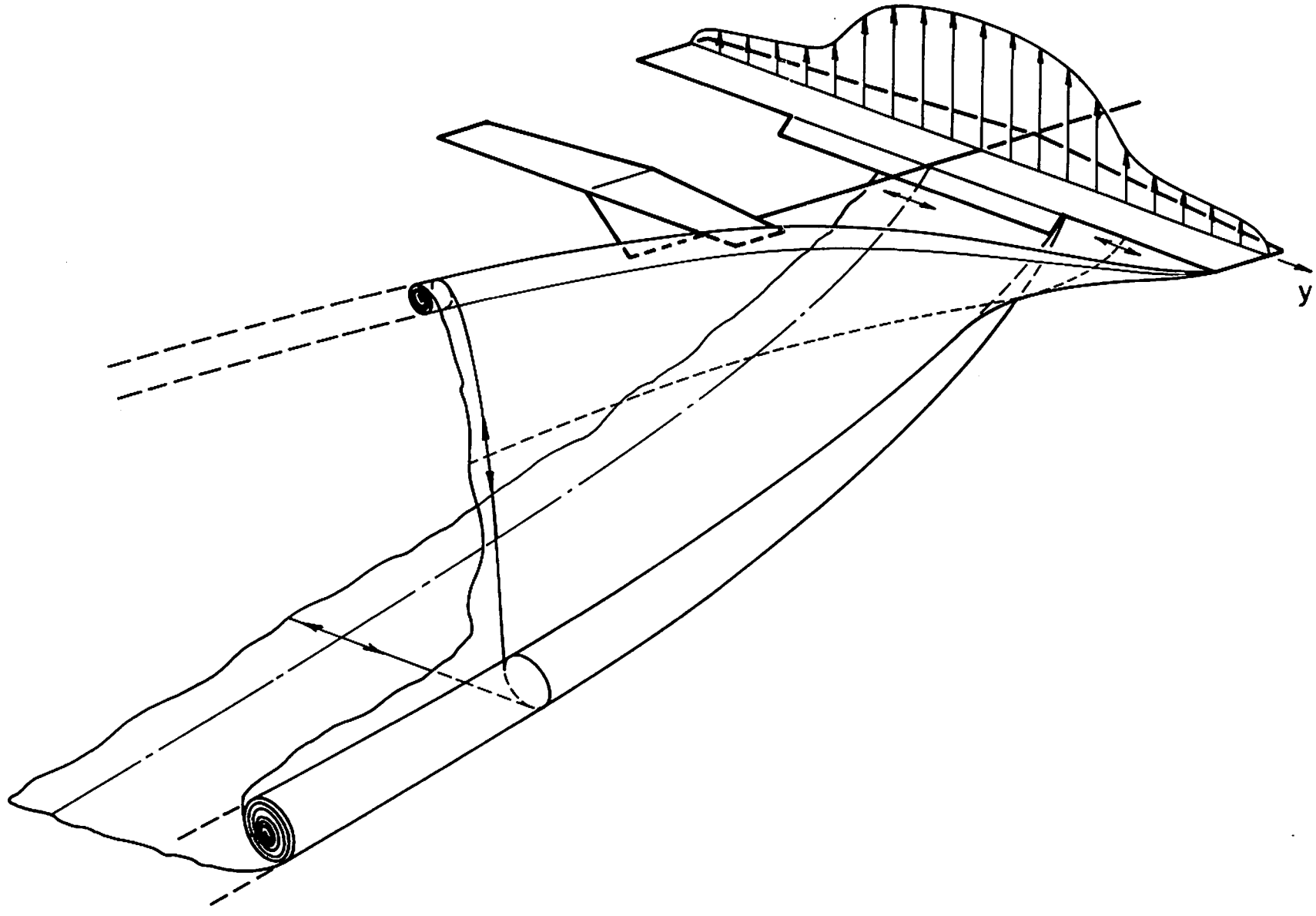

Fig. 2-3. The roll up of the flap and tip vortices from the load distribution shown in Fig. 2-1 (from Ref. 7).

where ζ is the trailed vorticity. The trailed vorticity as viewed in a plane normal to the flight direction is shown in Fig. 2-4. The area over which the integrations in Eqs. (1-4) are to be taken is given by $y \geq 0$.

The wake strength is the circulation Γ and the y and z moments are used to define centroids

$$\bar{y} = \frac{1}{\Gamma} \int y\zeta dA \tag{5}$$

$$\bar{z} = \frac{1}{\Gamma} \int z\zeta dA \tag{6}$$

The polar moment Γ_r when y and z are measured from $\bar{y}$ and $\bar{z}$, respectively, can be used to define a length squared, which is a measure of the spread or dispersion of the vorticity distribution.

For a constant density fluid, using continuity and the two-dimensional vorticity equation, it is not difficult to show that the time rates of change of Eqs. (1-4) are given by

$$\frac{d\Gamma}{dt} = -\nu \int_{-\infty}^{\infty} \left.\frac{\partial \zeta}{\partial y}\right|_{y=o} dz \tag{7}$$

$$\frac{d\Gamma_y}{dt} = 0 \tag{8}$$

$$\frac{d\Gamma_z}{dt} = -\int_{-\infty}^{\infty} \left(\left.\frac{W^2}{2}\right|_{y=o} + \nu z \left.\frac{\partial \zeta}{\partial y}\right|_{y=o} \right) dz \tag{9}$$

$$\frac{d\Gamma_r}{dt} = -\int_{-\infty}^{\infty} (z - \bar{z}) \left.\frac{W^2}{2}\right|_{y=o} dz + 2\nu\Gamma \tag{10}$$

where ν is the kinematic viscosity and where it is assumed that $V(0,z,t) = 0$. In the absence of viscosity, the circulation cannot change in the half-plane. This implies that $\bar{y}$, the horizontal centroid of the vorticity distribution, remains constant. The fact

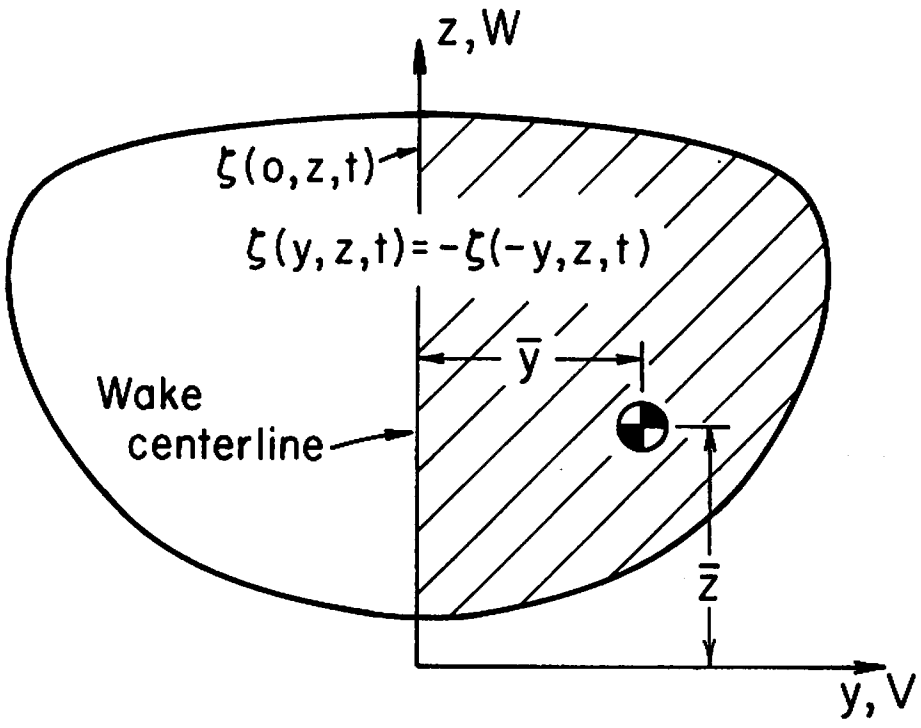

Fig. 2-4. The streamwise vorticity as viewed in a plane normal to the flight direction (from Ref. 7).

that Γ_z is a function of time is perhaps not surprising since

$$\frac{d\bar{z}}{dt} = \frac{1}{\Gamma}\frac{d\Gamma_z}{dt} \tag{11}$$

can be shown to be the observed descent rate of the vortex wake.

The time rate of change of Γ_r is directly related to the symmetry of $W^2(0,z,t)$ about $\bar{z}$. Betz argued that during roll up of the flat sheet of vorticity trailed from the wing Γ_r should not, in fact, vary much so that Γ_r could be taken to be approximately constant. In fact, Betz argued that the polar moment should be preserved during roll up locally as well. Therefore, for a simply loaded wing, the relationship between the vorticity immediately behind the wing to that downstream where roll up is complete is given by

$$-\int_y^s \frac{d\Gamma}{d\eta}(\eta)[\eta - \bar{y}(y)]^2 d\eta = \int_0^r \xi^2 \frac{d\Gamma'}{d\xi}(\xi)d\xi \tag{12}$$

where η and ξ are dummy variables for y and r, respectively, and

$$\bar{y}(y) = -\frac{1}{\Gamma(y)}\int_y^s \frac{d\Gamma(\eta)}{d\eta}\eta d\eta \tag{13}$$

is the centroid of the vorticity shed between wing station y and the wing tip. An implicit assumption is that the vortices roll up independently of each other. For high aspect ratio, simply loaded wings, this assumption appears to be valid.

It can be shown that Eq. (12) is equivalent to specifying that as roll up of a vortex proceeds from the wing tip, the torque exerted on the fluid by the wing about $\bar{y}(y)$ must equal the axial flux of angular momentum of the vortex from a circular area of radius r. If the axial velocity in the vortex is not uniform, the circulation at wing station y is the same as the circulation in the vortex at radius r. In this case, the relation between r and y is obtained from

$$u(r) \frac{dr^2}{dy} = U_\infty \frac{d}{dy} (\bar{y}(y) - y)^2$$

This follows, since a statement of Kelvin's theorem requires that

$$\Gamma(y) = \Gamma'(r) \tag{15}$$

When the axial velocity is uniform the relation between r and y was shown in Refs. 3, 4, 8, and 9 to be

$$r = \bar{y}(y) - y \tag{16}$$

Equations (15) and (16) prescribe the distribution of vorticity in the rolled-up vortex. The roll-up relations for a simply loaded wing are shown in Fig. 2-5.

The first comparison of the Betz method with the swirl velocities obtained from measurements was made by Donaldson (Ref. 2) for the wake of a C5 aircraft (Ref. 11). As can be seen in Fig. 2-6, the swirl velocity distribution obtained from the Betz method is in considerably better agreement with data than the distribution obtained from the Prandtl model (Ref. 12), or solid body core model as it is sometimes called. Additional swirl velocity distribution data have been shown to agree equally well with the swirl velocity distributions obtained by the Betz method provided that a reasonably accurate estimate of the wing load distribution has been made. The complete wake description behind a simply loaded wing therefore appears to be well in hand. The effect of distributed wing drag, as we will show below, can be included in a rational manner.

2.3 The inclusion of distributed drag

The vortex wake hazard problem motivated the need for a description of the wake behind a flapped wing when two or more vortices might roll up from each half of the wing. Donaldson, et al. (Ref. 3), showed how the Betz method could be extended to treat this case. Later, Bilanin, et al. (Ref. 6) also included the effect of distributed wing drag on vortex structure. It is convenient to develop the most general roll-up model here.

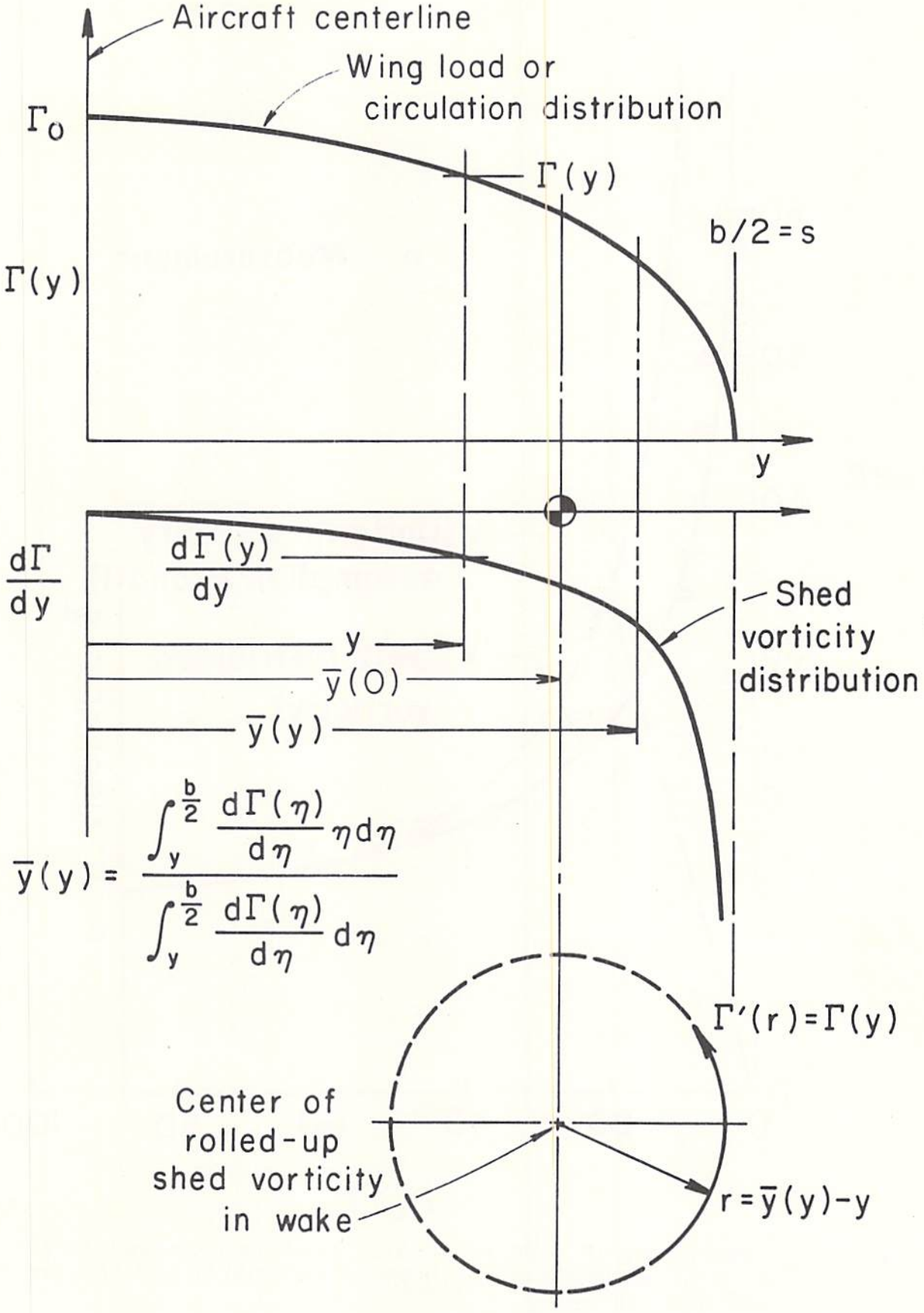

Fig. 2-5. The Betz roll-up relations for a simply loaded wing (Ref. 7).

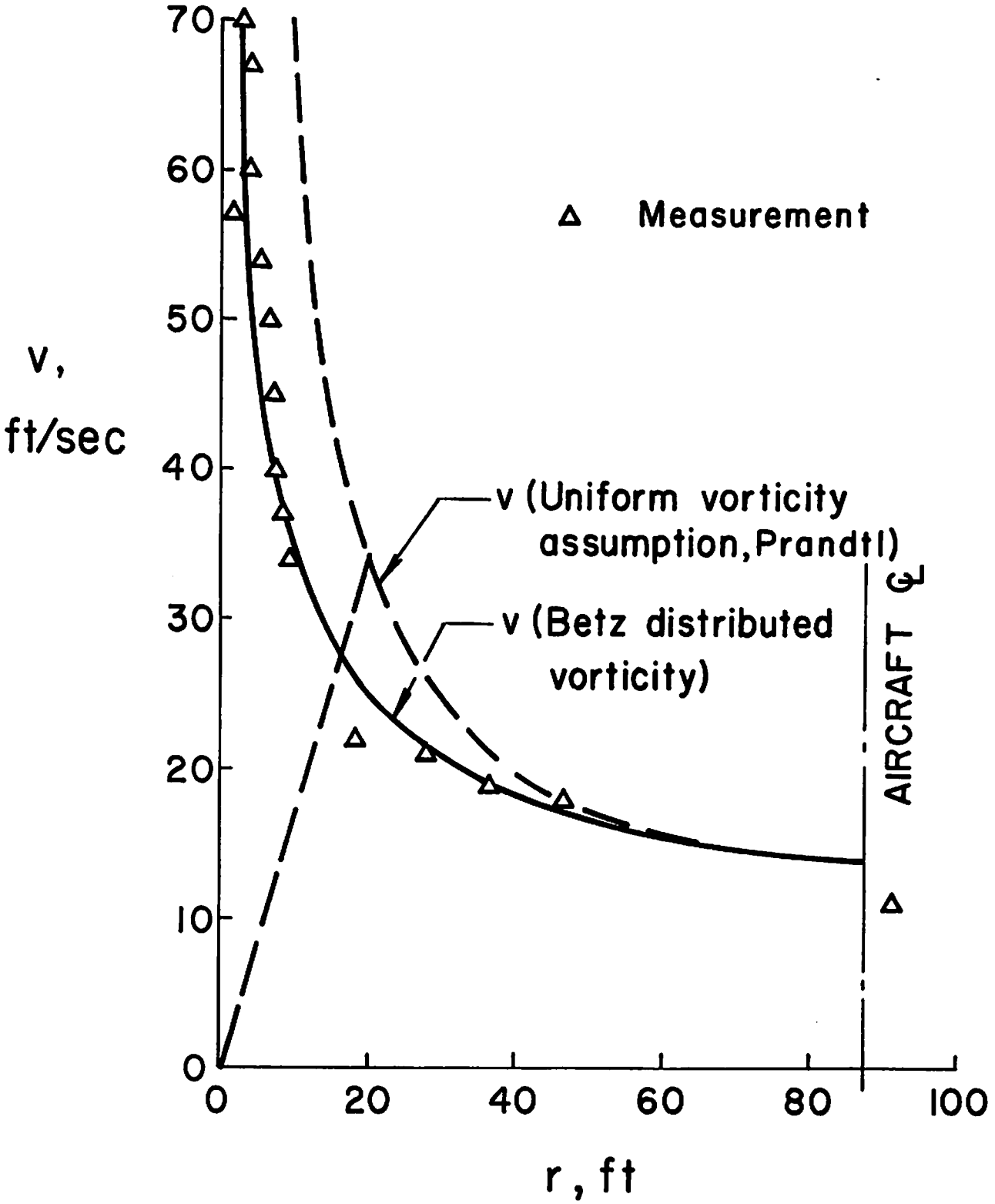

Fig. 2-6. Comparison of vortex velocity profile measured in the wake of a C5 aircraft with those calculated using the Prandtl and Betz theories.

If Eq. (12) is multiplied by $-\rho U_\infty/2$ and integrated by parts, it can be shown that

$$\int_y^s \ell(\eta)[\eta - \bar{y}(y)]d\eta = 2\pi\rho U_\infty \int_o^r v(\xi)\xi^2 d\xi \tag{17}$$

where Eqs. (15) and (16) have been used and $\ell(y) = -\rho U_\infty \Gamma(y)$ is the wing sectional lift exerted on the fluid. The Betz model is therefore equivalent to specifying that as the vortex rolls up, the torque exerted by the wing on the fluid between wing station y and the tip s about $\bar{y}(y)$ equals the axial flux of angular momentum from the vortex through a circular cross section of radius r. It is then postulated that the "interior" vortex should roll up according to

$$\int_{y_1}^{y_2} \ell(\eta)(\eta - \bar{y}_{12})d\eta = \int_o^r \rho\xi v(\xi)u(\xi)2\pi\xi d\xi \tag{18}$$

where

$$\bar{y}_{12} = \frac{1}{\Gamma(y_2) - \Gamma(y_1)} \int_{y_1}^{y_2} \eta \frac{d\Gamma}{d\eta} d\eta \tag{19}$$

The quantity $\bar{y}_{12}$ is the centroid of the vorticity shed between wing stations y_1 and y_2 which, for the moment, are the arbitrary points inboard and outboard of y_m in Fig. 2-2. Note that the axial velocity in the term which represents the axial flux of angular momentum in Eq. (18) has been taken under the integral and is not necessarily uniform nor equal to the flight speed U_∞.

A consequence of Kelvin's theorem for an "interior" roll up is that

$$\Gamma(r) = \Gamma(y_1) - \Gamma(y_2) \tag{20}$$

However, unlike roll up of a tip vortex where $y_2 = s$, a relationship between y_1 and y_2 is needed. Donaldson, et al. (Ref. 6), assumed that

$$(y_2 - \bar{y}_{12})^2 = (y_1 - \bar{y}_{12})^2 \tag{21}$$

which specifies how the vorticity enters the "interior" vortex from each side of the point $\bar{y}_{12}$. Differentiating Eq. (18) and using Eqs. (19-21) yields

$$U_\infty d(y_1 - \bar{y}_{12})^2 = u(r)dr^2 \tag{22}$$

and gives the relation for an interior vortex between wing station y_1 , radial position in the vortex r , and axial velocity in the vortex. The expression to be used to compute the roll up of a tip vortex is obtained by setting $y_2 = s$ in $\bar{y}_{12}$, whereby Eq. (22) becomes Eq. (14).

Before proceeding to discuss how the wing drag enters into the determination of $u(r)$, an interesting result using Eq. (22) will be noted. It can be shown that the swirling velocity at the center of the rolled-up flap or tip vortex is given by

$$v(0) = -\frac{1}{\pi}\left[\frac{u(0)}{U_\infty}\right]^{1/2} \left.\frac{dr}{dy}\right|_{\substack{y=y_m \\ \text{or} \\ y=s}} \tag{23}$$

where it is necessary to assume that $u(0)$ is bounded to determine this result. This result is significant in that it shows that the inviscid magnitude of the swirling velocity at the center of the vortex is directly determined by the maximum values of sheet strength. Note also that deficits in axial velocity $u/U_\infty < 1$ reduce the swirling velocity at the vortex center while axial velocity excesses intensify the vortex.

To couple the axial velocity to the wing drag distribution, axial momentum is balanced across a "cylindrical" control volume of radius r containing the portion of the wing between stations y_1 and y_2 . The details and approximations involved are discussed in Ref. 7. The result is that

$$c_d(y_1)c(y_1) - c_d(y_2)c(y_2)\frac{dy_2}{dy_1} = \pi u\left[\frac{p}{u} + \rho(u - U_\infty)\right]\frac{d(y_1-\bar{y}_{12})^2}{dy_1} \tag{24}$$

where c_d is the wing sectional drag coefficient and c is the local chord. When the u^2 term is linearized, Eq. (24) is that given by Brown (Ref. 13). The appropriate axial momentum equation for a tip roll up is obtained by setting $dy_2/dy_1 = 0$. The pressure p in the vortex is primarily a result of the swirling velocity and may be calculated from

$$\frac{dp}{dr} = -\rho\frac{v^2}{r} \tag{25}$$

Equations (22), (24), and (25) with the boundary conditions

$$p\Big|_{y_1=y_A} = -\frac{\rho}{2}v^2\Big|_{y_1=y_A} \quad \text{and} \quad r\Big|_{y_1=y_m} = 0 \quad \text{interior}$$

$$p\Big|_{y=y_B} = -\frac{\rho}{2}v^2\Big|_{y=y_B} \quad \text{and} \quad r\Big|_{y=s} = 0 \quad \text{tip} \tag{26}$$

form a coupled system of nonlinear equations with two-point boundary values. These equations have been programmed and their solution is now straightforward.

2.4 The effect of distributed drag on vortex intensity

Linear wing loading permits an analytic solution for a tip roll up with drag. This, then, provides an example of how much intensification or deintensification of a vortex results from distributed drag. The inverse problem, where the axial velocity is also prescribed and the distributed drag is computed, is given in Ref. 6. The results are shown in Fig. 2-7. Case 3 has the axial velocity uniform and equal to the free stream value, and, as can be seen, the drag required is of the order of that typical of current aircraft. As can be seen from Case 2, a modest

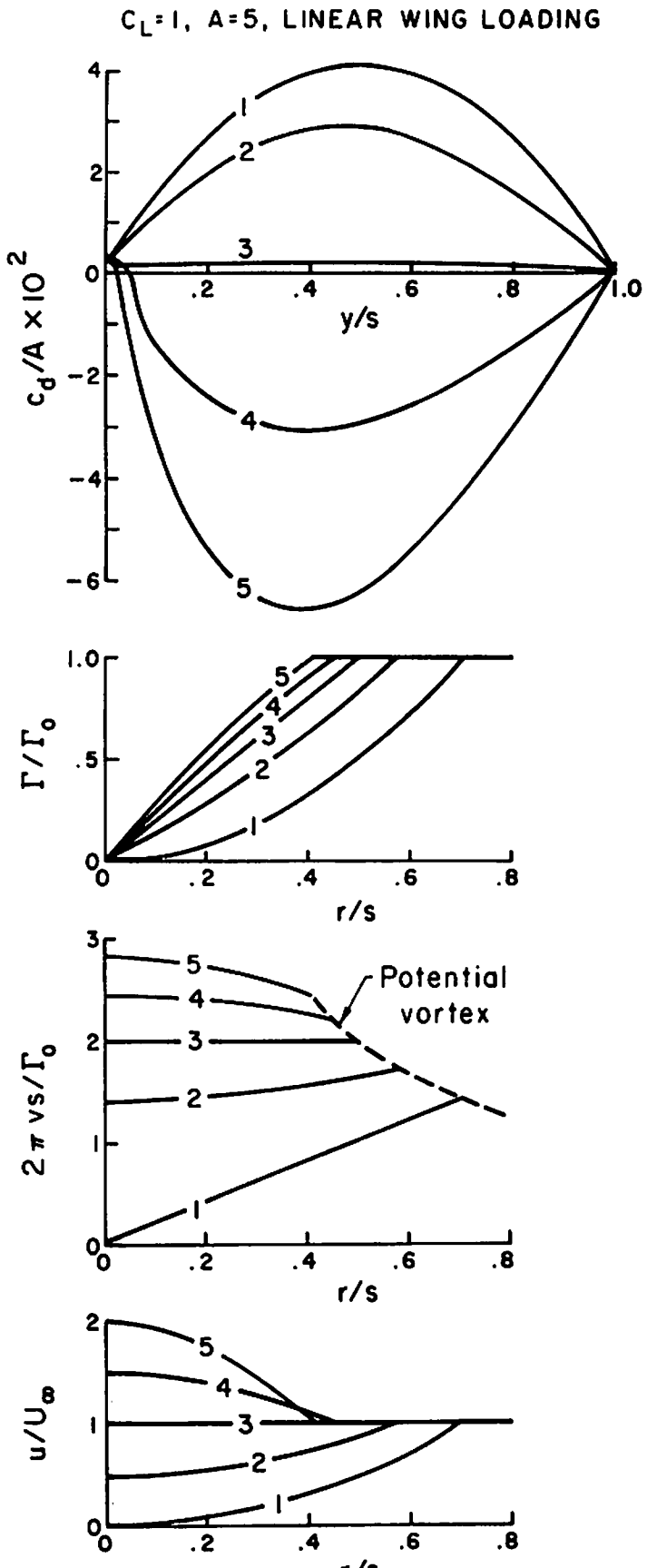

Fig. 2-7. The vortex wake structure for a linearly loaded wing (Ref. 7).

reduction in the vortex swirling velocity requires a rather sizable increase in drag (nearly an order of magnitude).

Experience has shown that the levels of drag typical of today's aircraft do not significantly alter the roll-up structure of the vortex except in the central region of the vortex. This is not particularly significant, however, since the amount of axial flux of angular moment from this region is a rather small fraction of the total flux in the vortex. This is not to say that drag is not important in determining vortex structure. Drag, in general, results in the production of turbulence and hence ages the vortex. However, turbulent transport and the resulting aging process are not treated here.

In closing this section, we would like to reemphasize one point. The Betz roll-up procedure assumes that vortices roll up essentially independently of each other. That is to say that no interactions between vortices are assumed to take place. Analysis of the NAFEC fly-by results suggests that under conditions where several vortices are shed from each side of the wing, this assumption might have to be reexamined. We will return to this point below.

3. CALCULATION OF SPANWISE LOAD DISTRIBUTIONS

The spanwise load distributions needed for the calculation of the rolled-up vortex velocity profiles were determined on the basis of information supplied by the aircraft manufacturers. Where available, this information included spanwise lift distributions as a function of both lift coefficient C_L and flap deflection δ_f. Otherwise, the manufacturers supplied wing section and planform information sufficient to enable a calculation of the spanwise lift distribution to be made at A.R.A.P. by means of a vortex-lattice program.* Induced drag distributions were calculated on the basis of the lift distributions in the usual manner. Profile drag distributions were derived from the airfoil section and planform data supplied.

The results of the spanwise load calculation for the 727, L-1011, DC-10, and 747 aircraft are presented in Figs. 3-1 through 3-14 for a range of values of aircraft C_L. The range of C_L chosen for these curves encompasses all of the values of C_L for each aircraft in each flight configuration for those NAFEC flyby tests that were analyzed. In Section 4, where comparisons are made of velocity profiles computed for specific cases, the load distributions were calculated for the exact C_L of each case. Some details of the calculation of these distributions will be reviewed in the following subsections.

3.1 Lift distributions

In the case of the L-1011 and DC-10, the manufacturers supplied computed curves of the spanwise loading parameter $c_\ell c/\bar{c}$, where c_ℓ is the local section lift coefficient, c the local chord, and $\bar{c}$ the mean aerodynamic chord. These curves were presented in the usual way, including one set of curves of "basic"

*The authors wish to thank Richard J. Margason of NASA Langley for making this program available to A.R.A.P.

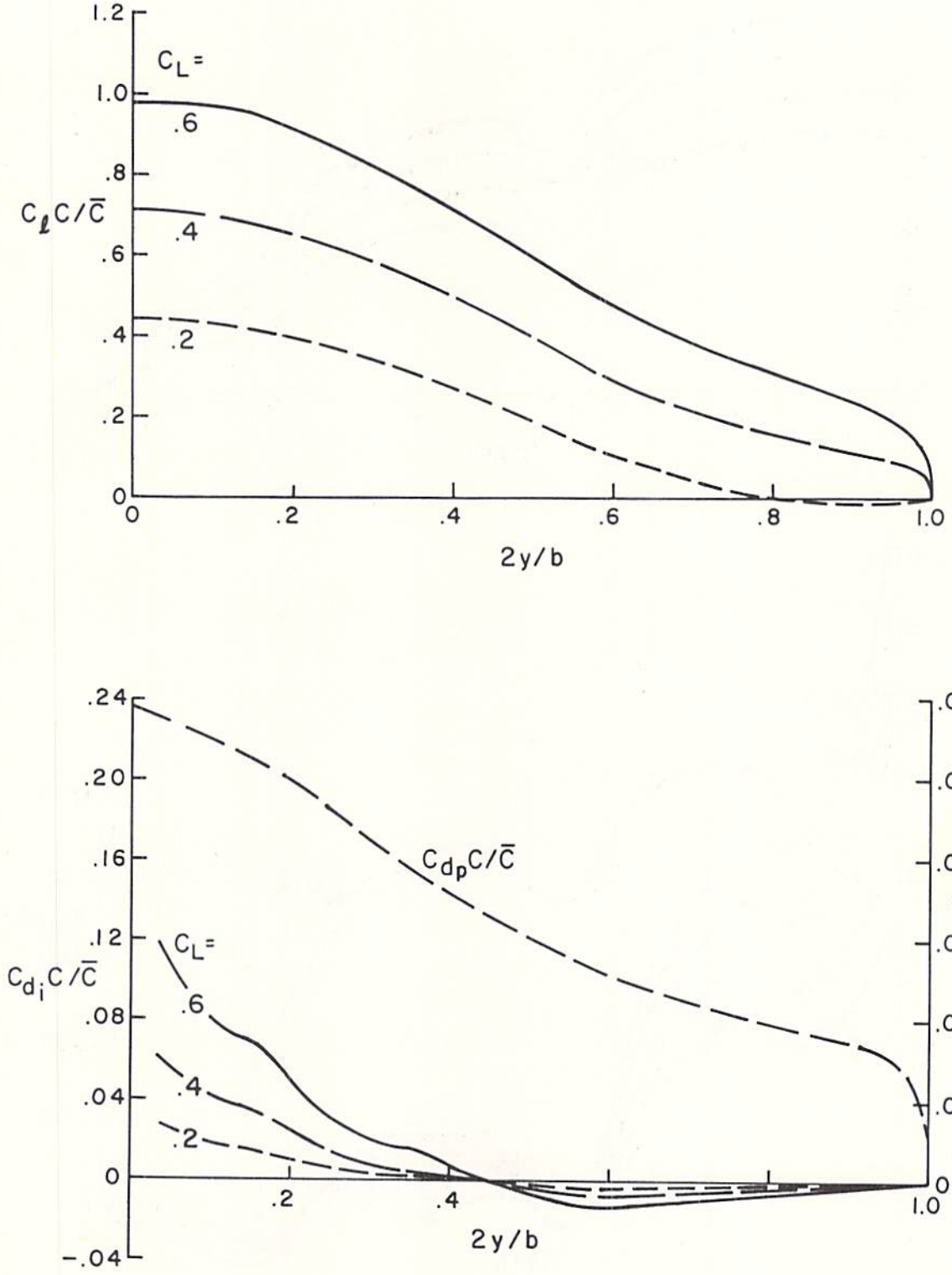

Fig. 3-1. Spanwise lift and drag distributions. 727 aircraft, holding configuration, $\delta_f = 0^o$.

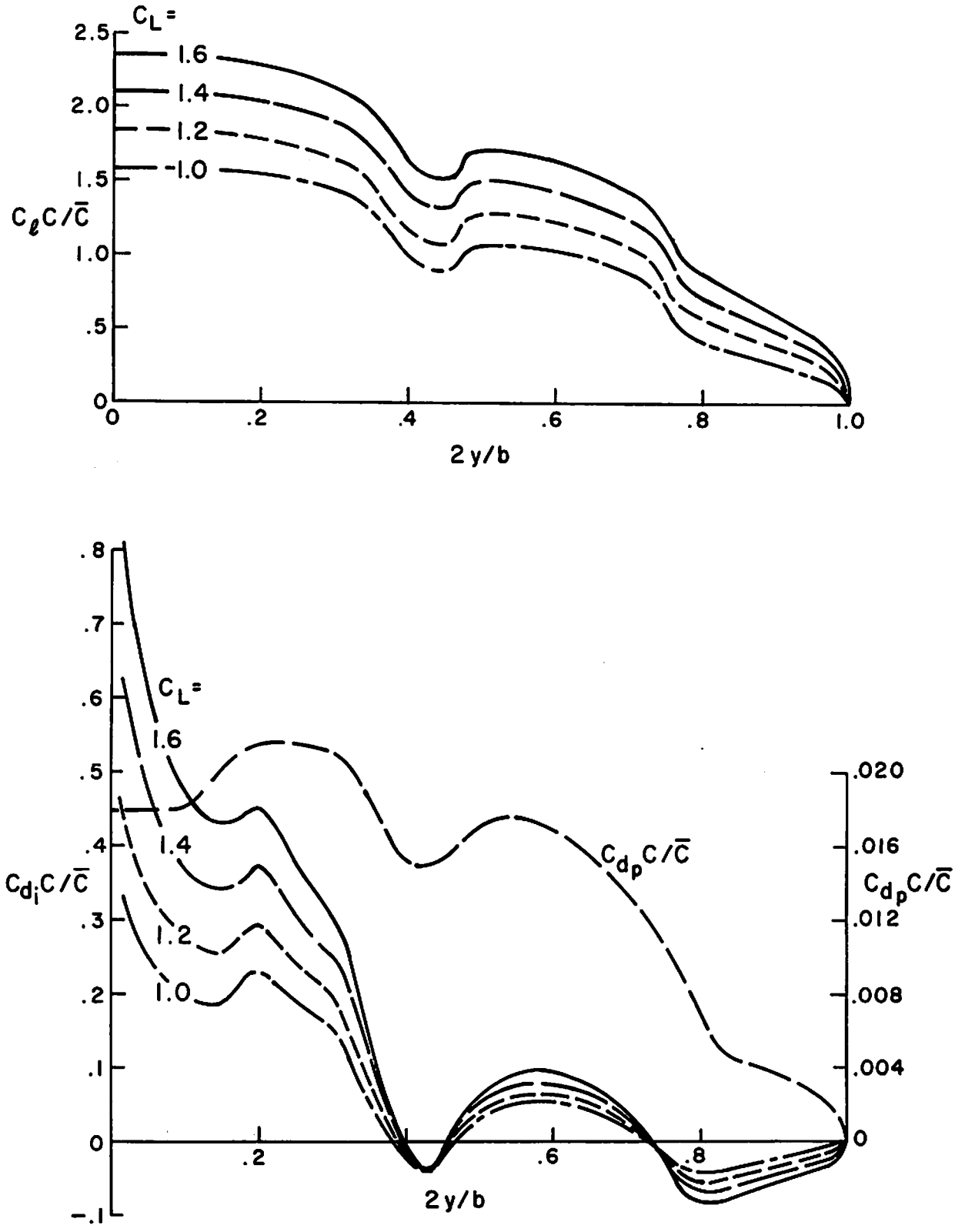

Fig. 3-2. Spanwise lift and drag distributions. 727 aircraft, take-off configuration, $\delta_f = 25^o$.

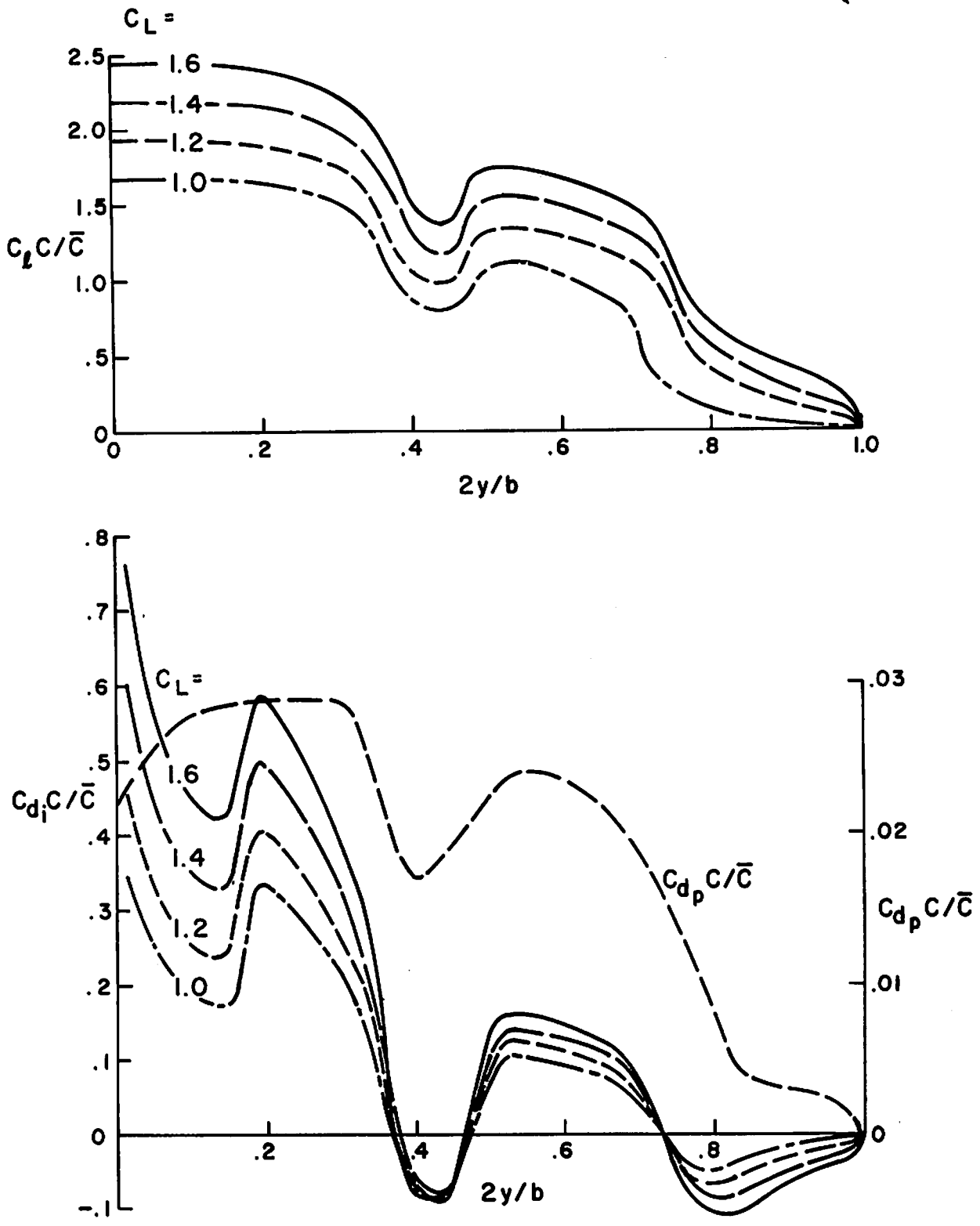

Fig. 3-3. Spanwise lift and drag distributions. 727 aircraft, landing configuration, $\delta_f = 40^\circ$.

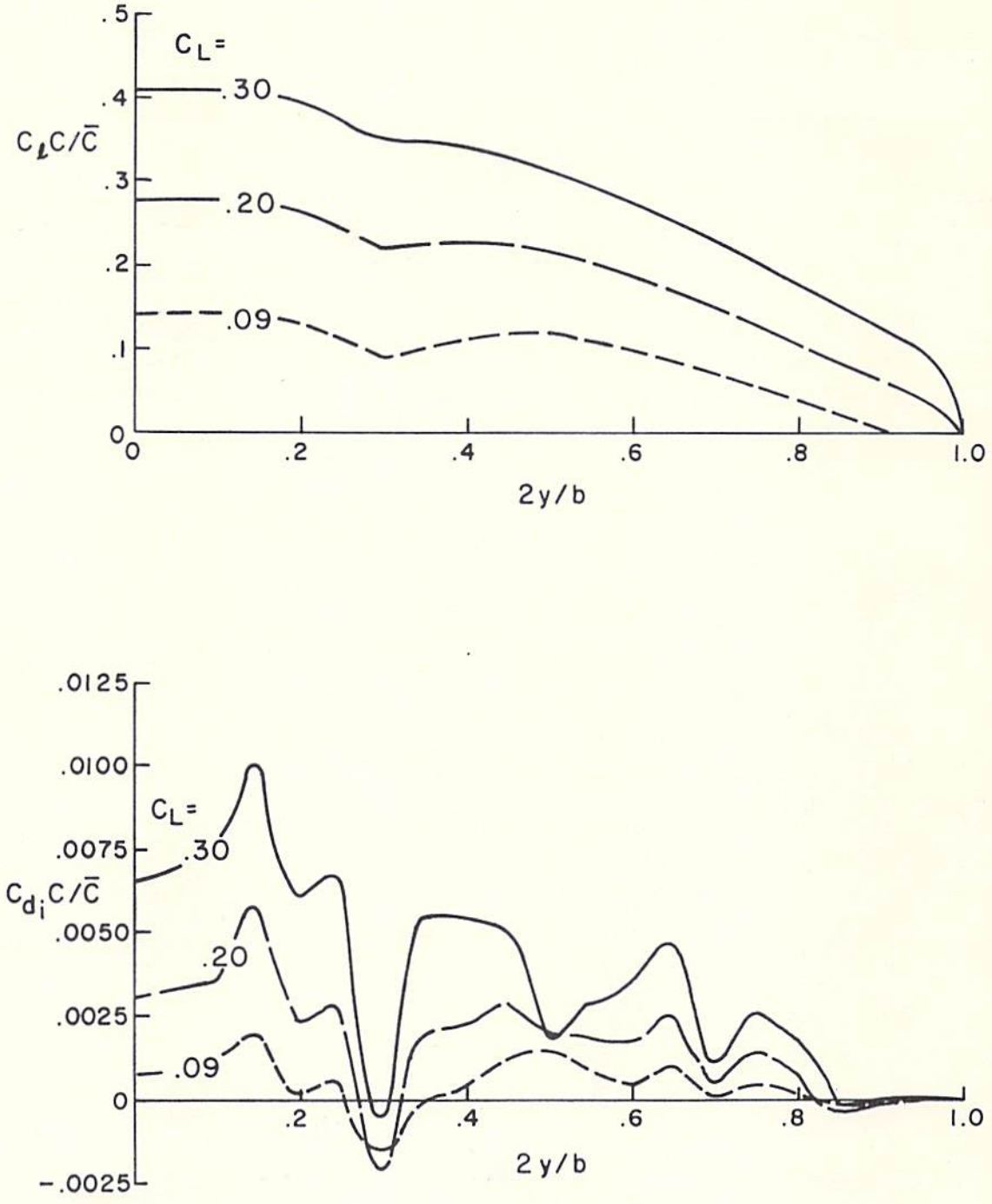

Fig. 3-4. Spanwise lift and drag distributions. L-1011 aircraft, cruise configuration, $\delta_f = 0^\circ$.

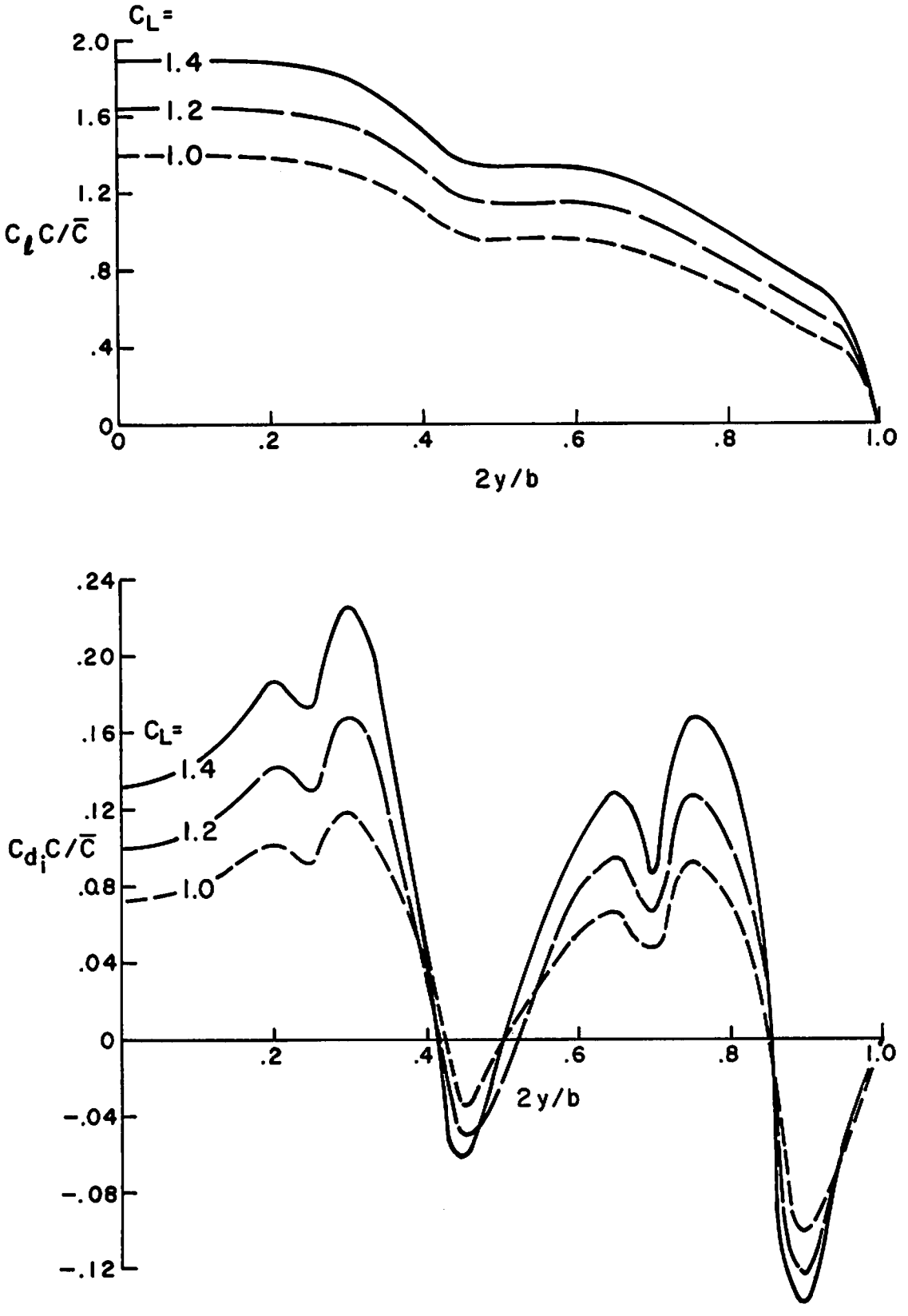

Fig. 3-5. Spanwise lift and drag distributions. L-1011 aircraft, take-off configuration, $\delta_f = 10^o$.

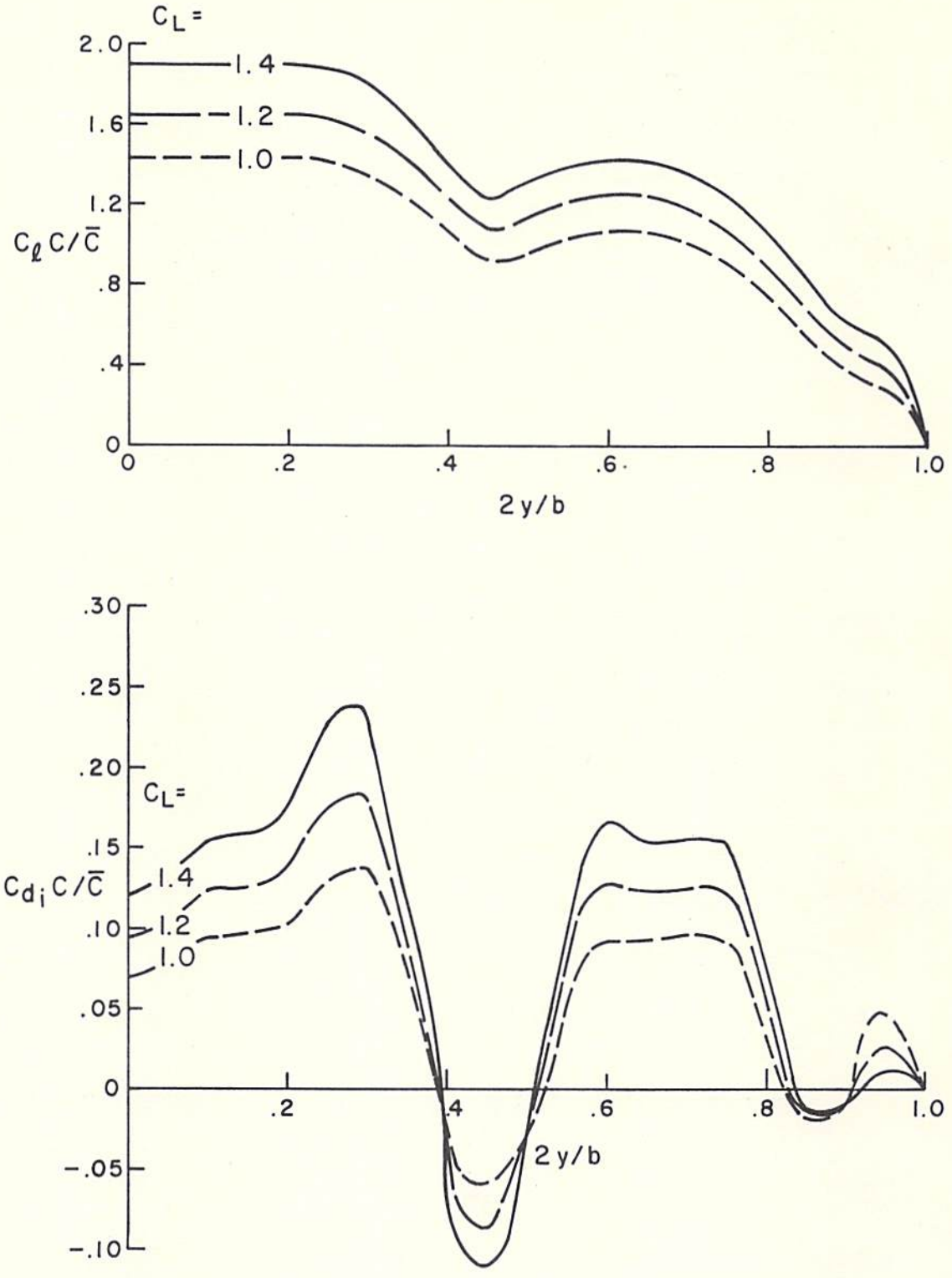

Fig. 3-6. Spanwise lift and drag distributions. L-1011 aircraft, take-off/approach configuration, $\delta_f = 25^o$.

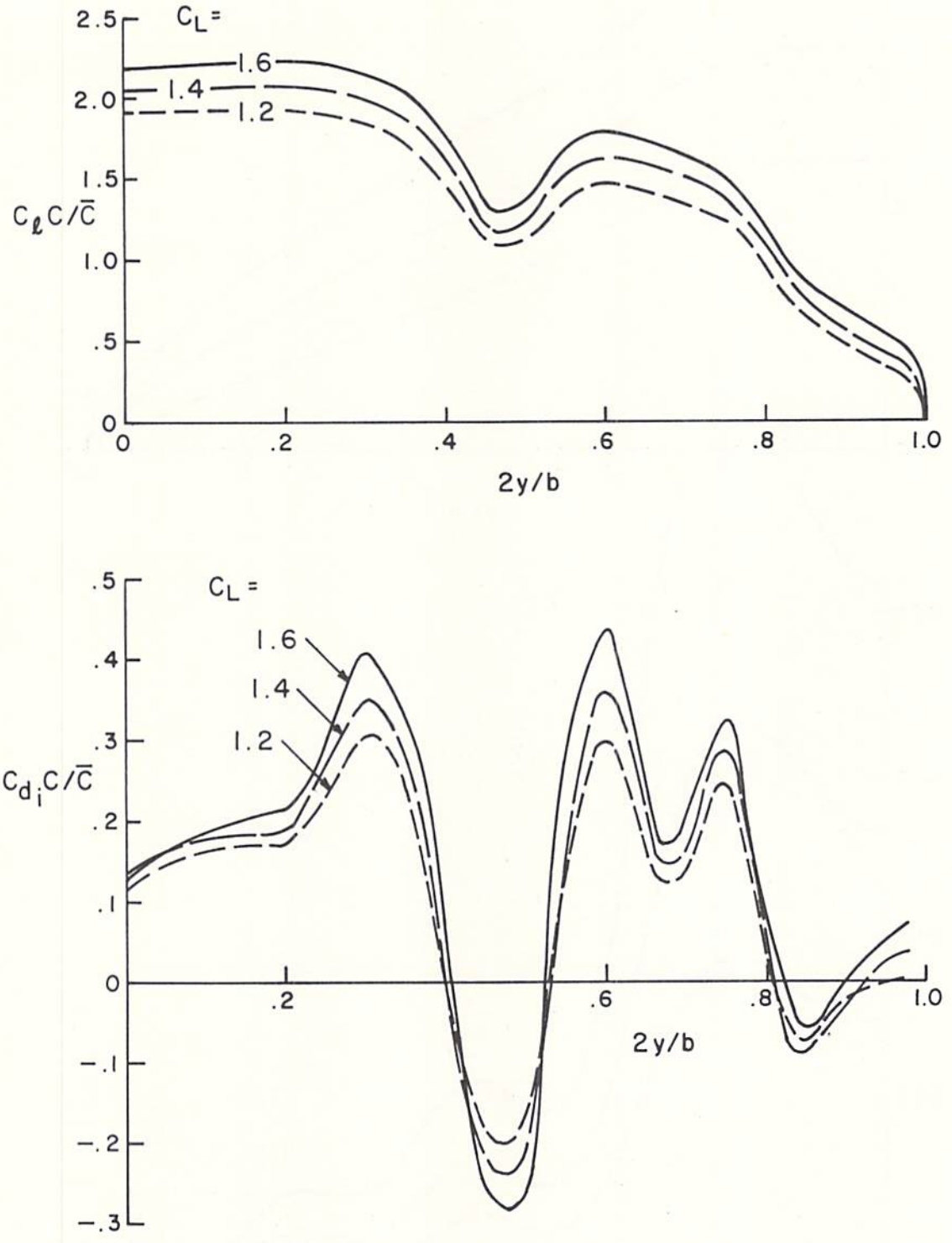

Fig. 3-7. Spanwise lift and drag distributions. L-1011 aircraft, landing configuration, $\delta_f = 42^\circ$.

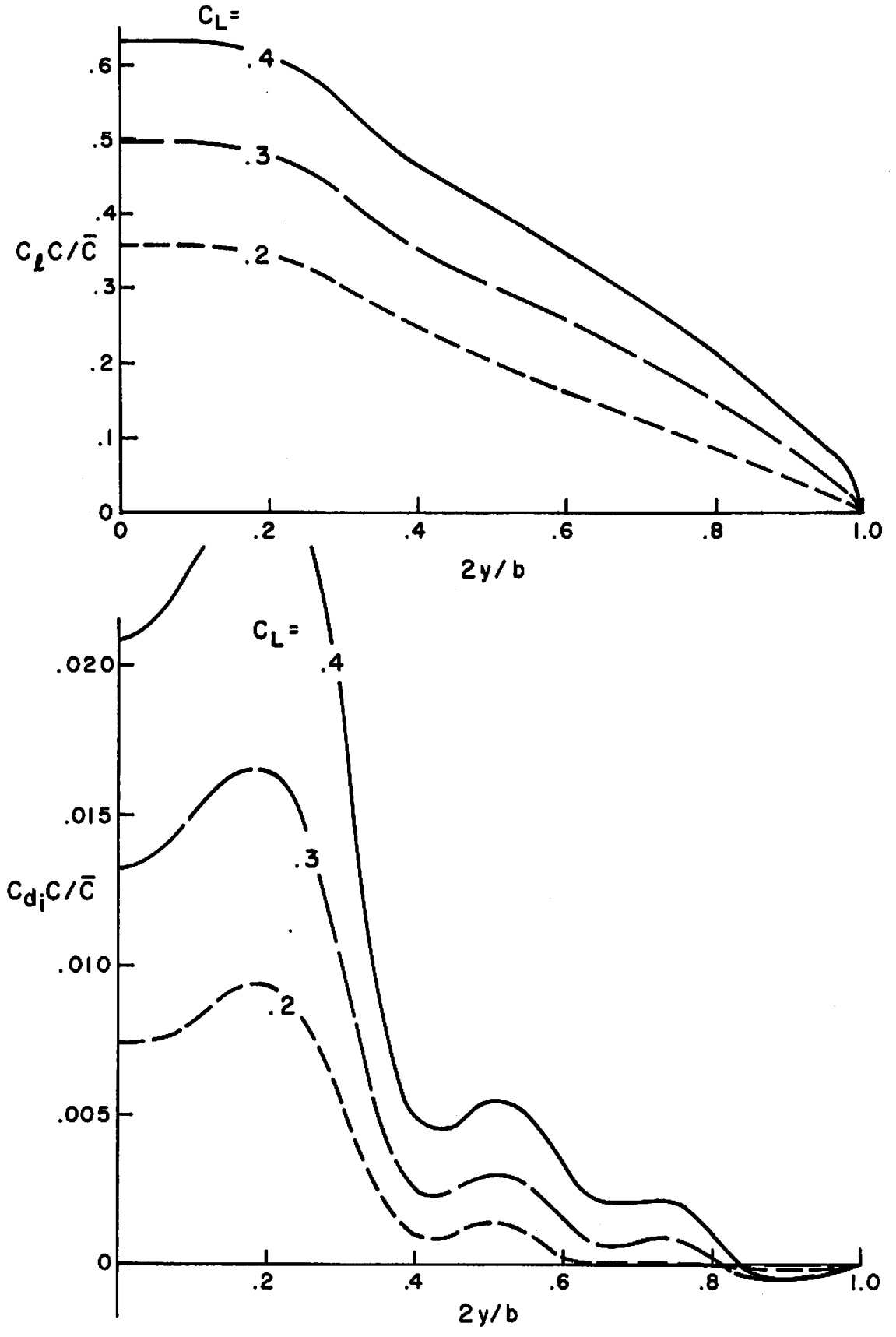

Fig. 3-8. Spanwise lift and drag distributions. DC-10 aircraft, cruise configuration, $\delta_f = 0^\circ$.

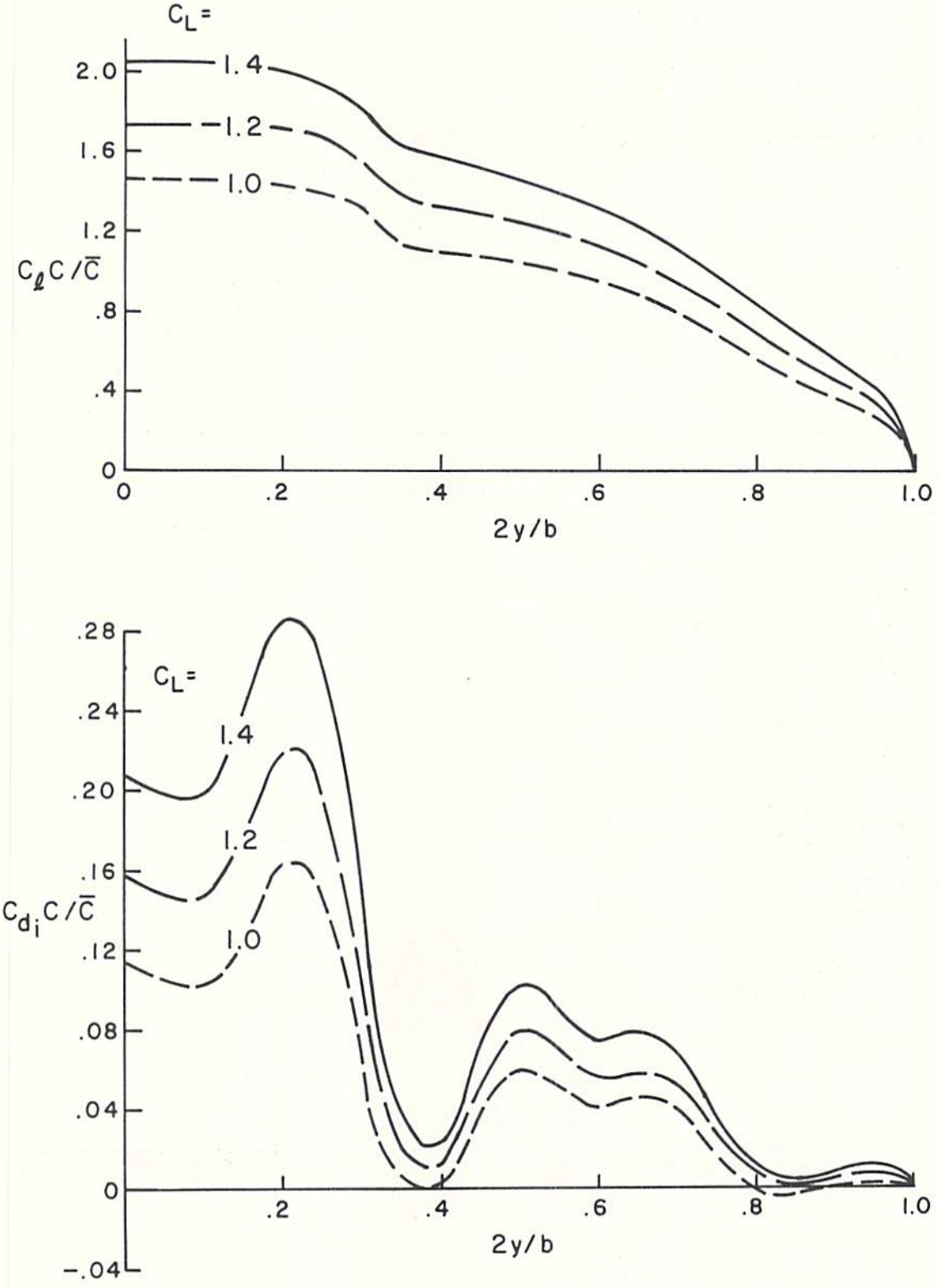

Fig. 3-9. Spanwise lift and drag distribution. DC-10 aircraft, take-off configuration, $\delta_f = 10^o$.

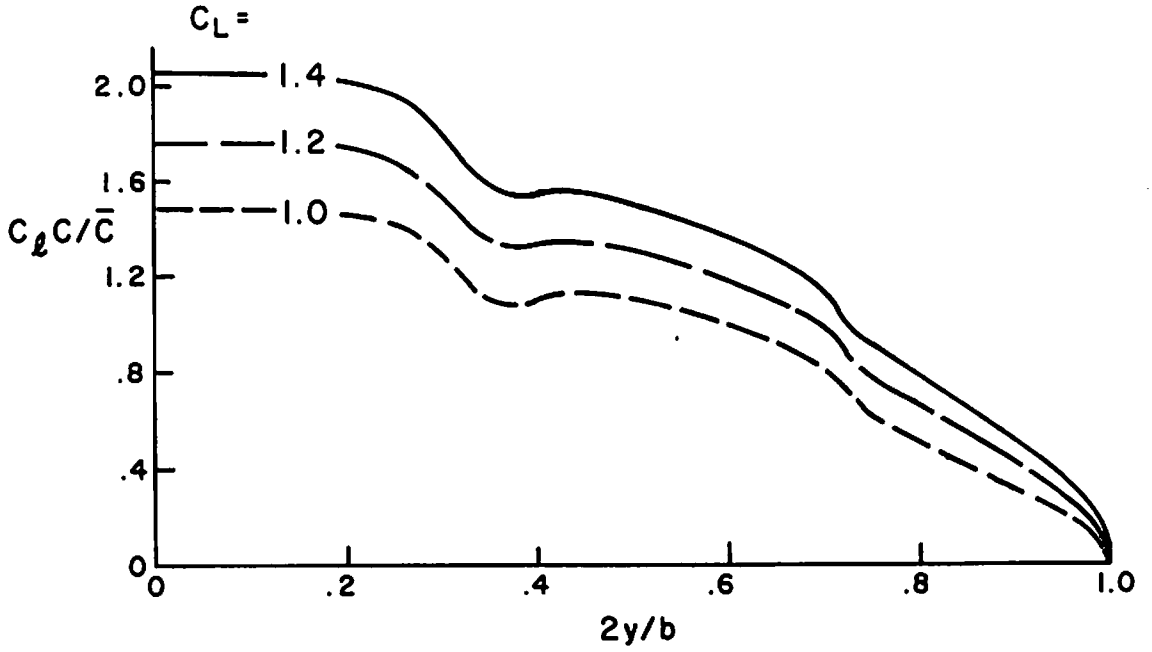

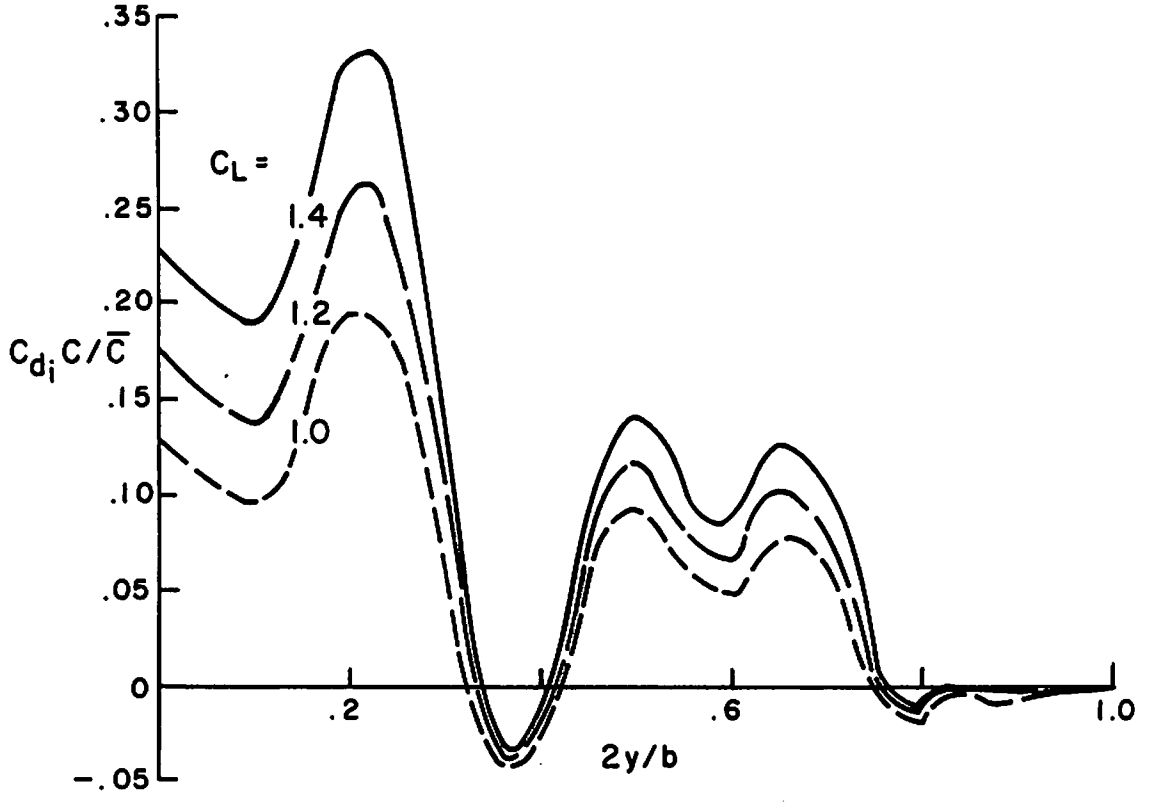

Fig. 3-10. Spanwise lift and drag distributions. DC-10 aircraft, take-off/approach configuration, $\delta_f = 22^\circ$.

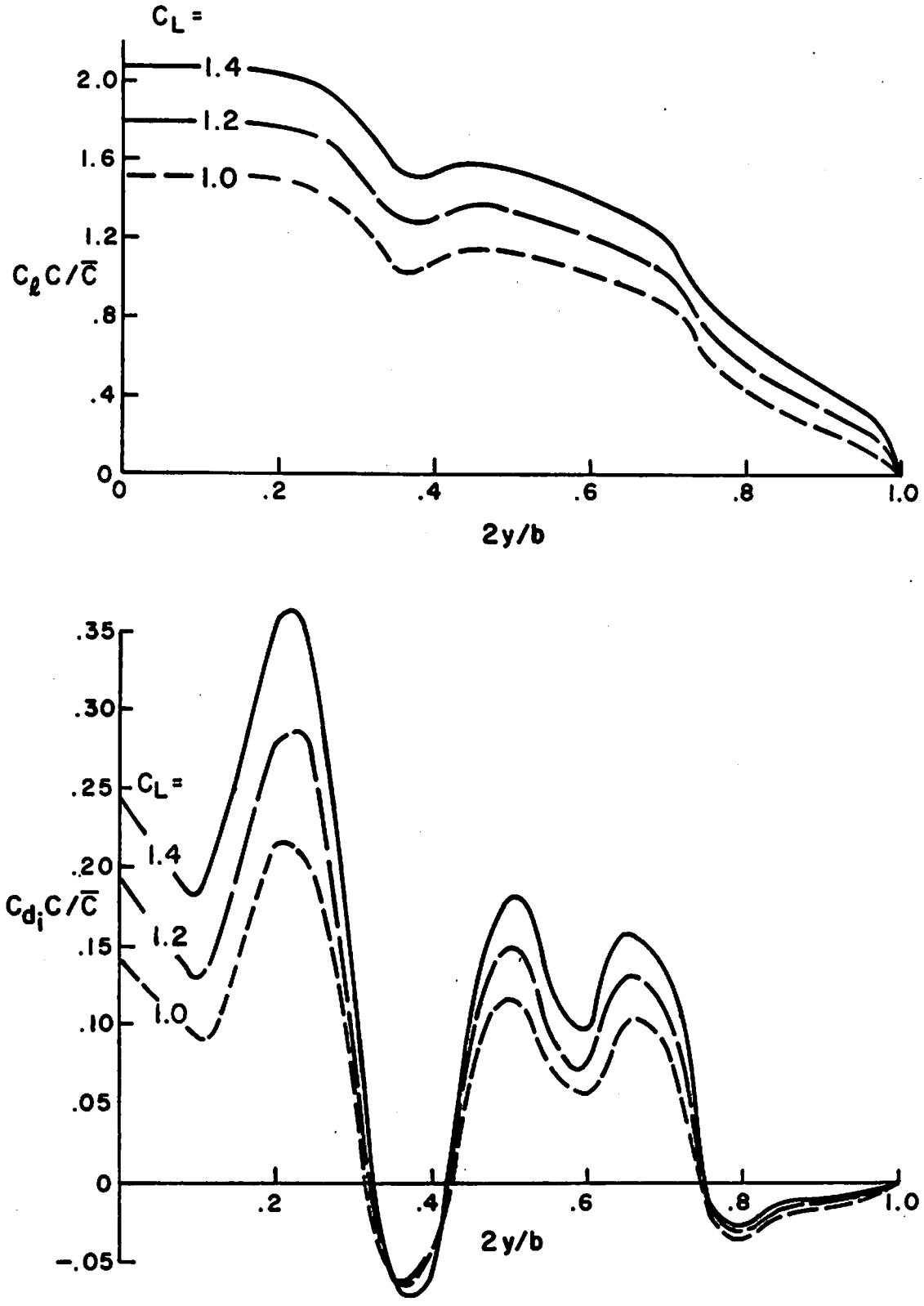

Fig. 3-11. Spanwise lift and drag distributions. DC-10 aircraft, landing configuration, $\delta_f = 35^\circ$.

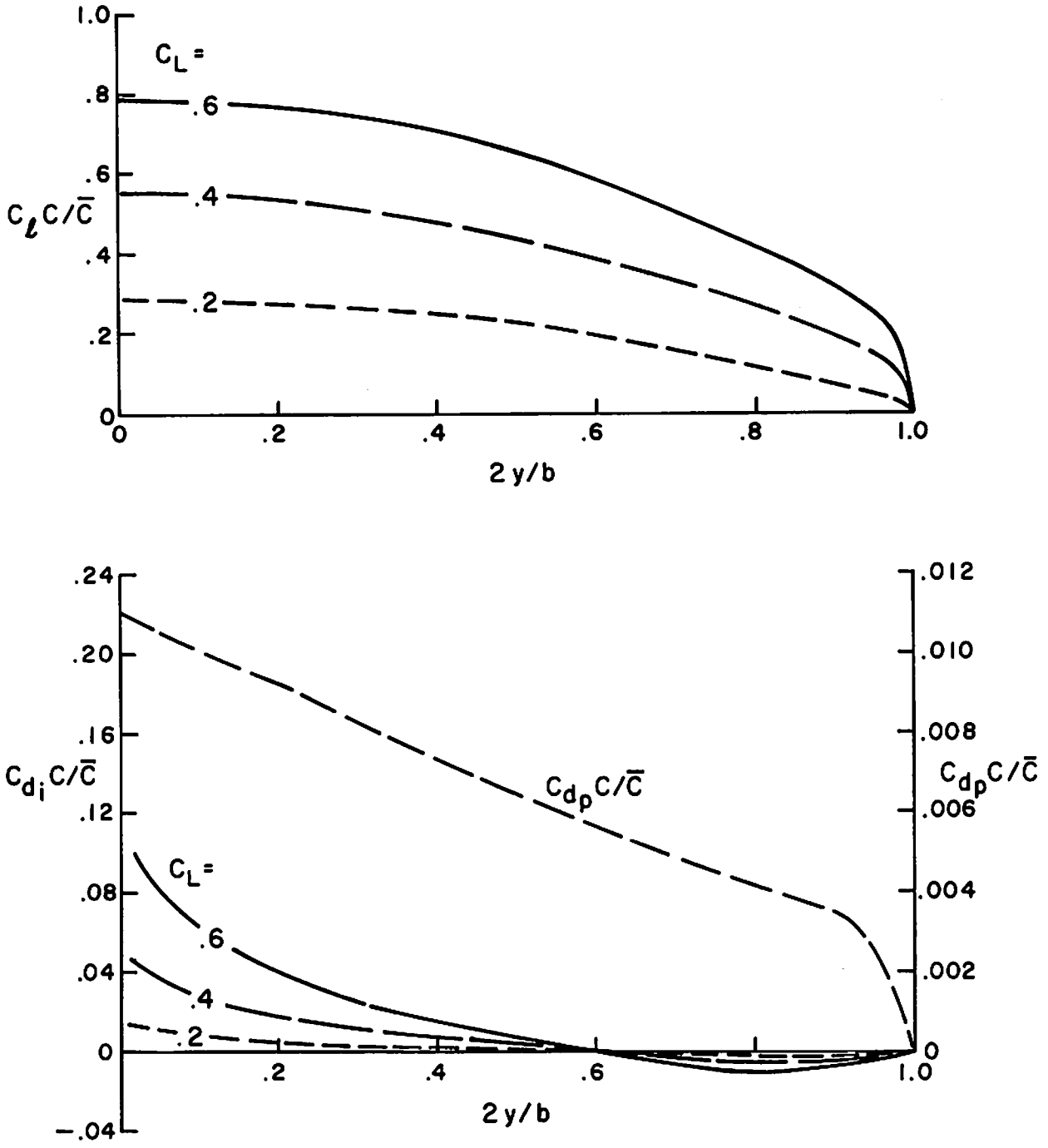

Fig. 3-12. Spanwise lift and drag distributions. 747 aircraft, holding configuration, $\delta_f = 0^o$.

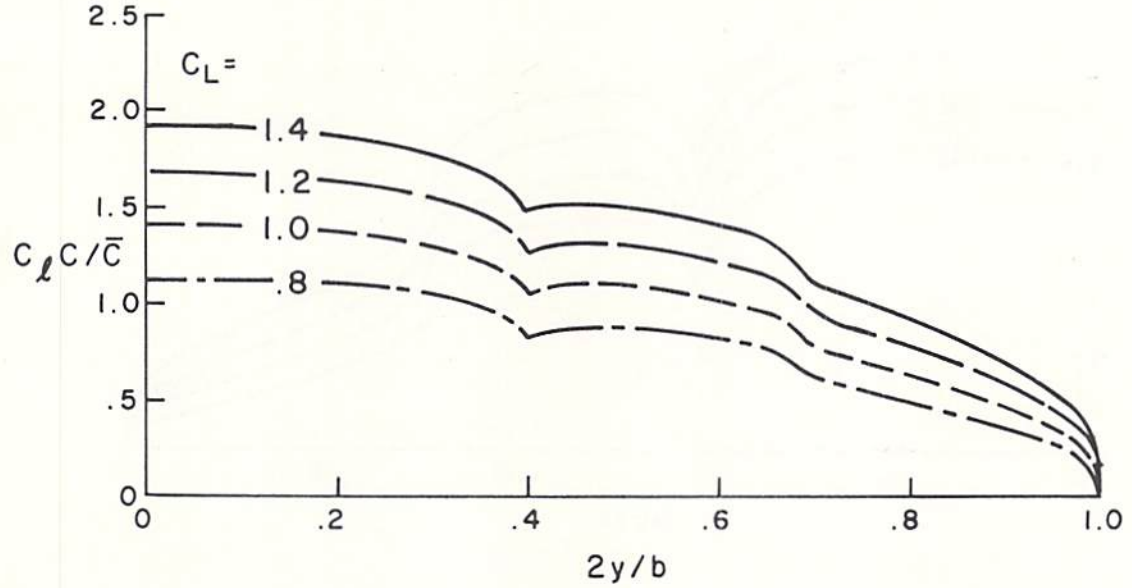

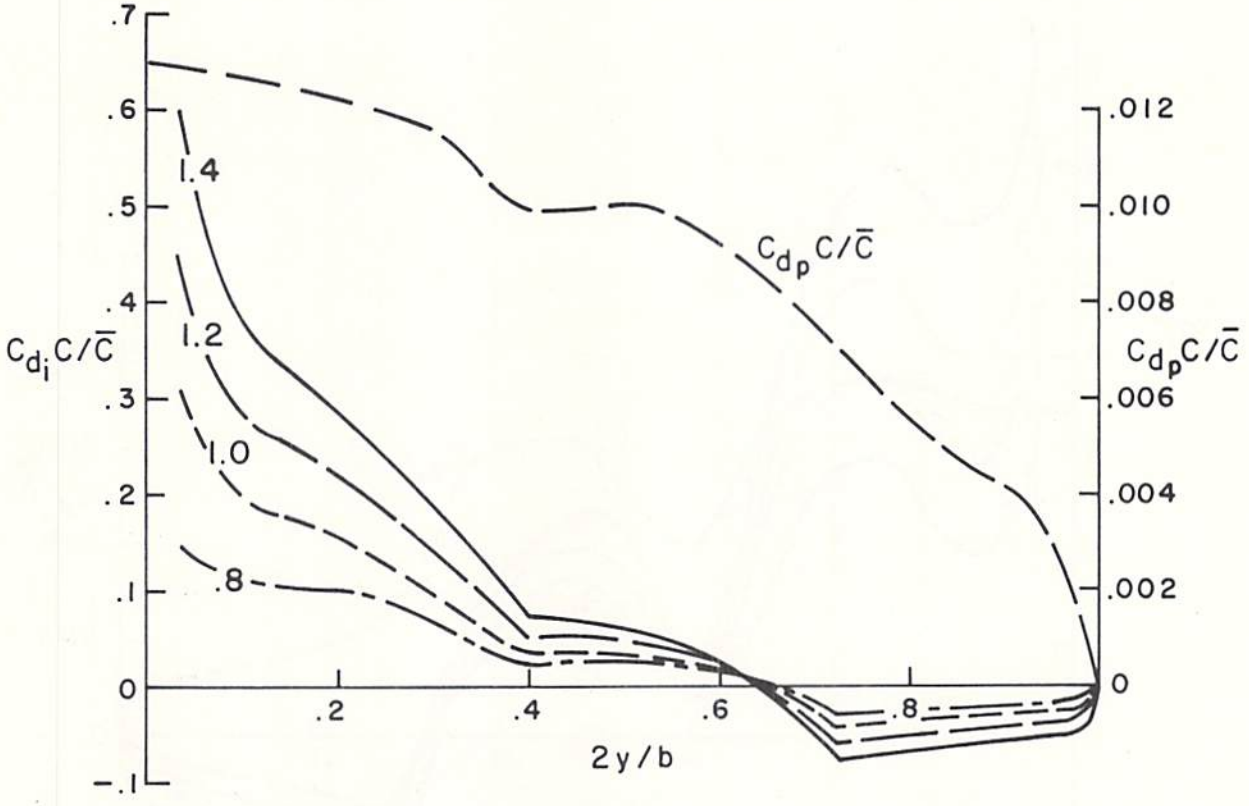

Fig. 3-13. Spanwise lift and drag distributions. 747 aircraft, take-off configuration, $\delta_f = 10^\circ$.

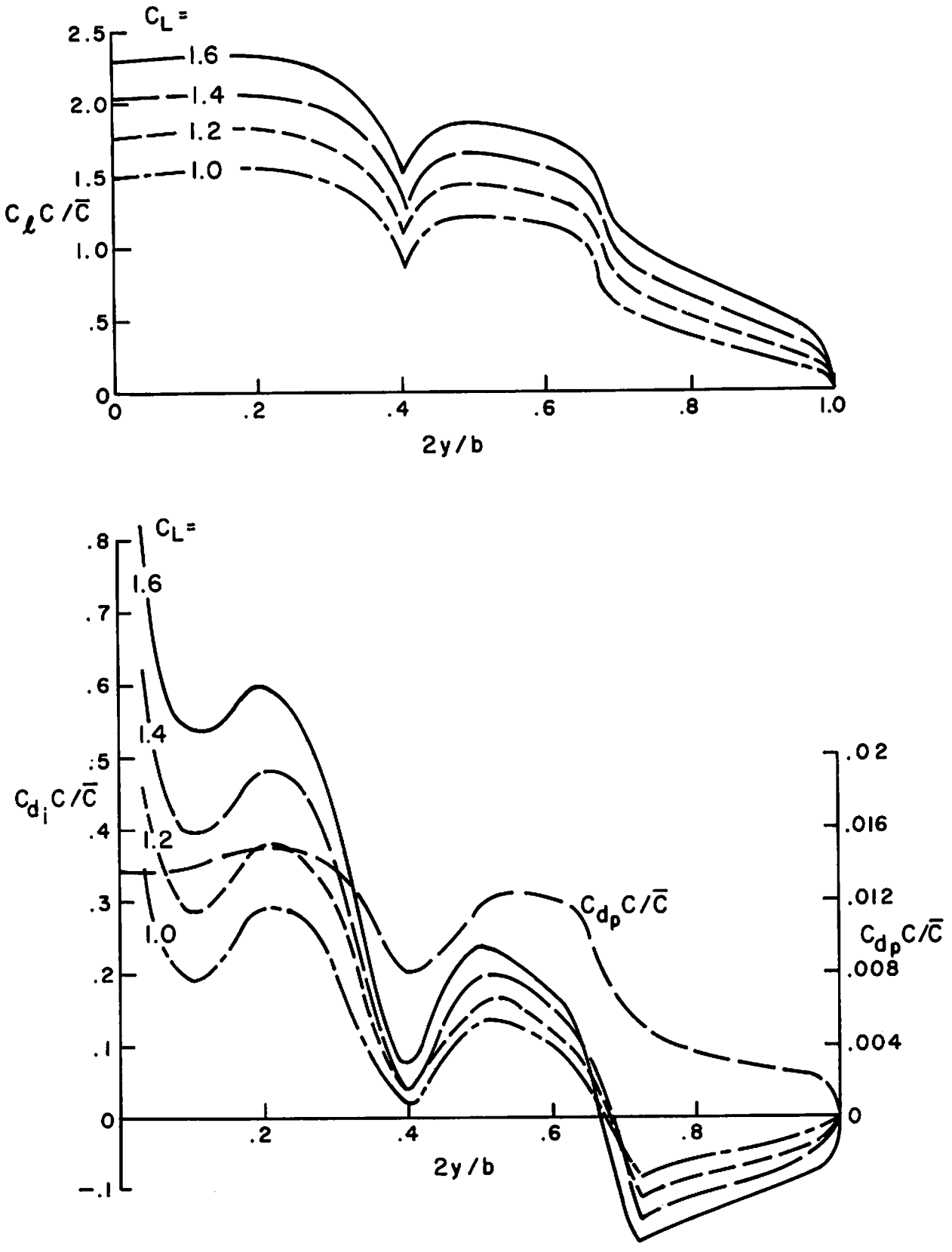

Fig. 3-14. Spanwise lift and drag distributions. 747 aircraft, landing configuration, $\delta_f = 25^\circ$.

lift for $C_L = 0$ and various flap deflections, and another set of curves of "additional" lift as a function of C_L .

For the 727 and 747, the manufacturer supplied camber line, twist, and planform information which was sufficient to carry out the vortex lattice calculation of load distribution mentioned above. In these cases, the planform change due to chordwise extension of the flaps was taken into account. Since the calculation of vortex velocity profiles actually makes use of the spanwise circulation distribution $\Gamma(y)$, the distributions of $c_\ell c/\bar{c}$ were converted during the calculation through the relation

$$\Gamma(y) = \frac{c_\ell c}{\bar{c}} \frac{U_\infty}{2} \bar{c}$$

3.2 Drag distributions

In no case was the manufacturer able or willing to supply drag distribution data. Therefore, it was necessary to make estimations based on the available planform and section information.

The local induced drag is related to the product of the local downwash velocity $w(y)$ and the local circulation $\Gamma(y)$ by

$$c_{d_i}(y) = - \frac{2}{U_\infty^2 c(y)} w(y)\Gamma(y) \tag{27}$$

The distribution $\Gamma(y)$ is already known, and it only remains to evaluate $w(y)$. This is found from lifting line theory for a wing of known circulation distribution through the relation

$$w(y) = - \frac{1}{4\pi} \int_{-s}^{s} \frac{\frac{d\Gamma}{d\eta}\, d\eta}{y - \eta} \tag{28}$$

For the L-1011 and DC-10 aircraft, the calculation of induced drag was carried out by applying Eqs. (27) and (28). In the case of the 727 and 747, the calculation was made by the vortex-lattice program.

None of the aircraft employed airfoil sections for which profile drag data were readily available. It was necessary, therefore,

to select standard NACA sections which closely resembled those actually used on the basis of comparison of profile shapes found on the drawings supplied. Since profile drag coefficients do not vary greatly within one family of airfoil shapes, as long as the thickness is approximately correct, it is felt that this method of estimation was adequate for present purposes. It should be noted that the profile drag curves for the L-1011 and DC-10 are not plotted since the suggested value was taken to be constant across the wingspan. In each case, the manufacturer felt that a value $c_{d_p} = .01$ would be an adequate average value for our purposes.

4. COMPARISON OF CALCULATED VORTEX VELOCITY PROFILES WITH THE NAFEC MEASUREMENTS

4.1 Data selection

For the purposes of making comparisons between calculated vortex velocity profiles and those measured at NAFEC, 53 flyby cases were selected from the total of 232 available for the four aircraft involved. The selected cases are listed in Table 1 wherein a number of the important characteristics of each flyby and the resulting wake are given. (The significance of b' and dh/dt will be discussed in Subsection 4.3.) The relevant aircraft characteristics are given in Table 2.

The basic aim of the data selection was to choose five cases for each flight configuration of each aircraft. In most cases this was possible, although there were some combinations for which only a single run was made and others for which only a few of the runs produced adequate data.

Selection criteria depended on the aircraft involved. For the 727 and 747, the NAFEC data were made available in the form of final project reports issued by FAA (Refs. 14 and 15) in which plots of the wake velocity profiles were given. These profiles were the result of the NAFEC data reduction procedures described in the cited reports. The selection for these aircraft took into primary account the extent of the profiles to each side of the vortex center and the freedom from apparently faulty data acquisition channels. Apparent axial symmetry was also a factor in selection, although it is realized that erroneous values of lateral drift velocity and local probe interference effects at the instrumentation tower can limit the validity of axial symmetry as an indication of "good" data. For the L-1011 and DC-10, A.R.A.P. was provided with a set of plots of sensor response time history for each flyby. Tangential velocity profiles were deduced from these plots by the method described in Ref. 3. This method is essentially equivalent to that used by NAFEC for the 727 and 747 data. Criteria for the selection of L-1011 and DC-10 cases were necessarily less stringent

Table 1. Aircraft and configurations analyzed

Aircraft Conf.	NAFEC Run No.	Weight (lbs×10^{-3})	U_∞ (ft/sec)	C_L	Γ_o (ft^2/sec)	b' (ft)	-dh/dt (ft/sec)
727 H/C	34	133.0	355.8	0.58	2481.7	68.5	5.8
	35	132.0	355.8	0.57	2455.0	68.7	5.7
	36	131.5	346.3	0.60	2389.5	72.2	5.3
	49	130.5	354.7	0.57	2447.4	68.4	5.7
727 L	18	136.0	216.2	1.59	3956.5	72.3	8.7
	45	133.5	216.2	1.56	3891.6	72.1	8.6
	58	131.3	212.8	1.59	3894.2	72.0	8.6
	77	126.0	211.0	1.55	3766.4	72.1	8.3
	106	133.5	211.0	1.64	3956.3	72.6	8.7
727 TO	26	138.0	219.6	1.57	3788.1	75.4	8.0
	40	137.0	245.0	1.25	3472.9	73.2	7.6
	41	136.0	245.0	1.24	3454.5	73.0	7.5
	42	135.0	255.0	1.14	3346.9	71.9	7.4
	53	136.2	216.2	1.59	3761.9	76.1	7.9
747 H/C	45	496.0	329.4	0.70	4001.7	158.1	4.0
	55	593.0	337.8	0.79	4611.0	159.9	4.6
	53	597.0	371.6	0.66	4291.2	157.3	4.3
	68	528.0	591.2	0.23	2742.8	136.8	3.2
	44	498.0	320.9	0.74	4091.2	159.3	4.1
747 L	11	516.0	228.0	1.52	6691.2	142.1	7.5
	26	556.0	270.0	1.16	6339.0	136.5	7.4
	38	530.0	253.0	1.26	6388.9	137.7	7.4
	49	487.0	236.0	1.33	6281.7	138.0	7.2
	51	482.0	245.0	1.23	6019.0	137.3	7.0
747 TO	64	566.0	295.0	0.99	5637.5	143.0	6.3
	43	500.0	273.6	1.02	5303.2	144.8	5.8
	28	552.0	270.3	1.15	5977.1	143.6	6.6
	42	502.0	279.0	0.99	5331.7	141.7	6.0
	29	549.0	275.0	1.10	5930.9	141.4	6.7
DC-10 H/C	20	276.0	506.0	0.28	2947.3	84.1	5.6
DC-10 L	14	283.5	236.0	1.30	5693.7	95.9	9.5
	15	283.0	230.0	1.37	5826.3	96.0	9.7
	16	281.5	230.0	1.36	5787.7	96.1	9.6
	17	280.0	230.0	1.36	5787.7	96.1	9.6

Table 1. (Continued)

Aircraft Conf.	NAFEC Run No.	Weight ($lbs \times 10^{-3}$)	U_∞ (ft/sec)	C_L	Γ_o (ft^2/sec)	b' (ft)	-dh/dt (ft/sec)
DC-10 TO	3	316.7	257.0	1.23	5742.5	97.5	9.4
	4	315.3	262.0	1.18	5628.5	97.2	9.2
	5	314.0	253.0	1.26	5783.9	97.5	9.4
	6	313.0	257.0	1.21	5653.9	97.9	9.2
DC-10 TA	18	277.7	253.0	1.2	5370.9	96.7	8.8
	19	276.7	243.0	1.2	5370.8	96.4	8.9
L-1011 H/C	19	328.0	515.0	0.31	2400.0	113.9	3.4
L-1011 L	2	363.0	240.0	1.57	5818.0	111.6	8.3
	4	356.0	236.0	1.59	5711.0	113.4	8.0
	6	353.0	241.0	1.51	5709.0	110.1	8.3
	7	350.0	235.0	1.57	5687.0	112.4	8.1
	18	329.0	230.0	1.54	5489.0	111.8	7.8
L-1011 TO	14	337.0	282.0	1.05	4651.0	110.3	6.7
	15	360.0	279.0	1.07	4583.0	120.8	6.0
	16	340.0	280.0	1.06	4538.0	114.8	6.3
L-1011 TA	9	345.0	267.0	1.2	4861.0	114.1	6.8
	10	344.0	267.0	1.2	4861.0	113.8	6.8
	11	343.0	268.0	1.19	4879.0	112.6	7.0
	12	341.0	267.0	1.19	4860.0	112.8	6.9

NOTE: H/C - Holding/cruise configuration
L - Landing configuration
TO - Take-off configuration
TA - Take-off/approach configuration

Table 2. Relevant aircraft and test characteristics

Aircraft	Wing Ref. Area (ft^2)	Wing Span (ft)	$\bar{c}$ (ft)	Air Density ($Slugs/ft^3$)
727	1700	108	15.0	.0022
747	5500	196	27.3	.00238
DC-10	3550	155	25.0	.0022
L-1011	3456	155	22.3	.00233

because of the relatively few runs available - 19 for the L-1011 and 20 for the DC-10. Of primary concern in the selection were the clear indication of both downwind and upwind vortex "hits" and the absence of suspect data channels. In addition, an attempt was made to choose cases for which the ambient air was the least turbulent.

It has already been pointed out that with their segmented flaps deployed, these aircraft present complex spanwise load distributions which can result in wake formations having several initial centers of roll up. The application of the extended Betz method to such cases results in a well-defined inviscid vortex velocity profile for each center of roll up, where the vortices so defined are assumed to form independently. In a real wake, of course, from the onset of their formation, the vortices are subject to a number of influences. Primary among these are the mutually induced motions of the centers themselves and the interactions of the vortex flow fields, both with each other and with the ambient atmosphere. Under these conditions, turbulent interactions may very well result in substantial redistribution of vorticity in the wake. It is reasonable to suppose, therefore, that at the time of measurement, the vortices which may have begun to form as a result of a specific complex load distribution may have, in fact, interacted to the point that their individual identification as a "tip" vortex or a particular "interior" vortex is no longer possible. These interactions may result both in the formation of new velocity profiles, brought on by the merging of vortex centers, and in the early dissipation of some vortices due to mutually induced instabilities. The method of presenting the velocity profiles computed for each case and their comparison with the NAFEC measurements takes into account the foregoing considerations.

4.2 Comparison of computed and measured velocity profiles

The results of the velocity profile calculations and their comparison with the NAFEC measurements are shown in Figs. 4-1 through 4-14, and in Appendix Figs. A-1 through A-39.

Figures 4-1 through 4-14 give the results for one case of each aircraft in each flight configuration. Each figure has two parts, "a" and "b." Part "a" presents the calculated profiles of both swirl or tangential velocity and axial velocity for all vortices that resulted from well-defined minima of $|d\Gamma/dy|$. In some cases, an attempt was made to limit the number of vortex concentrations resulting from a complex Γ distribution by designing the computation to recognize only those minima of $|d\Gamma/dy|$ that would result in vortices of strength $\Delta\Gamma \geq 0.1\Gamma_o$. The profiles were calculated both with and without the effects of distributed wing drag. In this part of each figure, the vortices are located at the appropriate computed value of $\bar{y}$ and their strengths are given. Part "b" of each figure presents a comparison of the profiles measured at NAFEC with the computed profile from part "a" that gives the best match. The interior vortices in these figures are designated by number, starting with 1 for the innermost vortex and proceeding out toward the wing tip. In the appendix figures, only the positive vortices are compared with the measurements.

Some details of the results for each aircraft will now be reviewed. (The aircraft are taken in order of increasing wing spans.)

Boeing 727

In the holding configuration (Figs. 4-1a and 4-1b) the data are in good agreement with the calculated profile, although the data for this case are of limited radial extent. As might be expected, whatever core there might have been was too small to be resolved by the measurements. As will be seen to be typical for tip vortices calculated by this method, there is little effect due to distributed drag except for a small region of axial velocity excess near the center.

The computation for the take-off configuration (Figs. 4-2a and 4-2b) shows four interior vortices, two strong positive ones (2 and 4) and two much weaker negative ones (1 and 3). Vortex

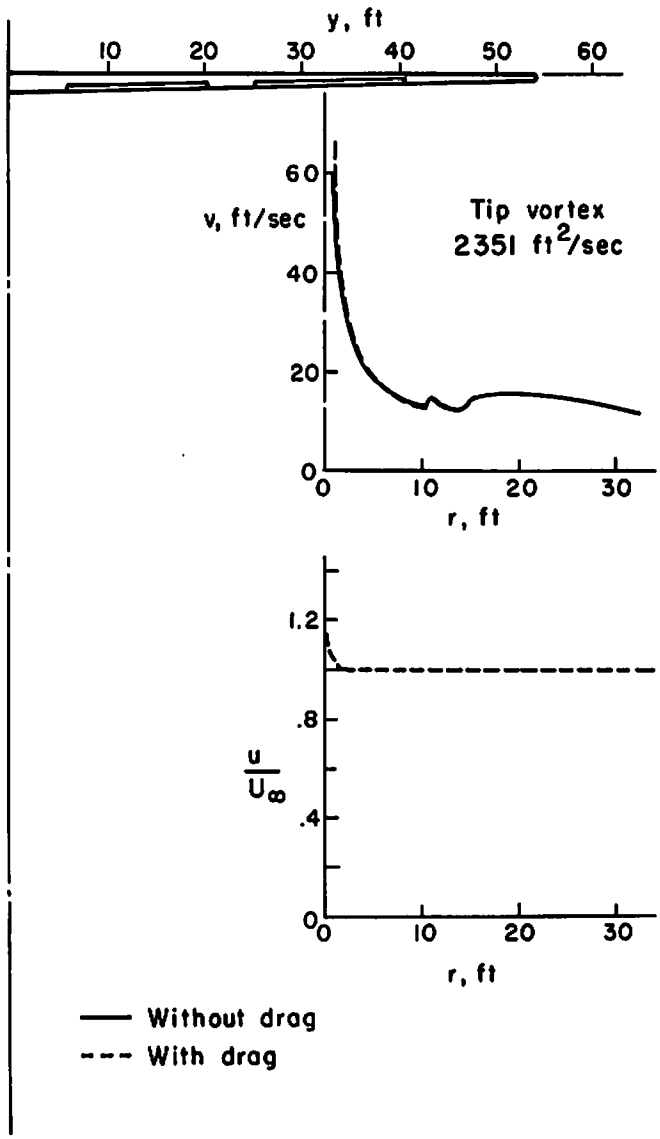

Fig. 4-1a. Computed swirl velocity profiles for a 727 aircraft in holding configuration ($\delta_f = 0^o$). NAFEC Run 49

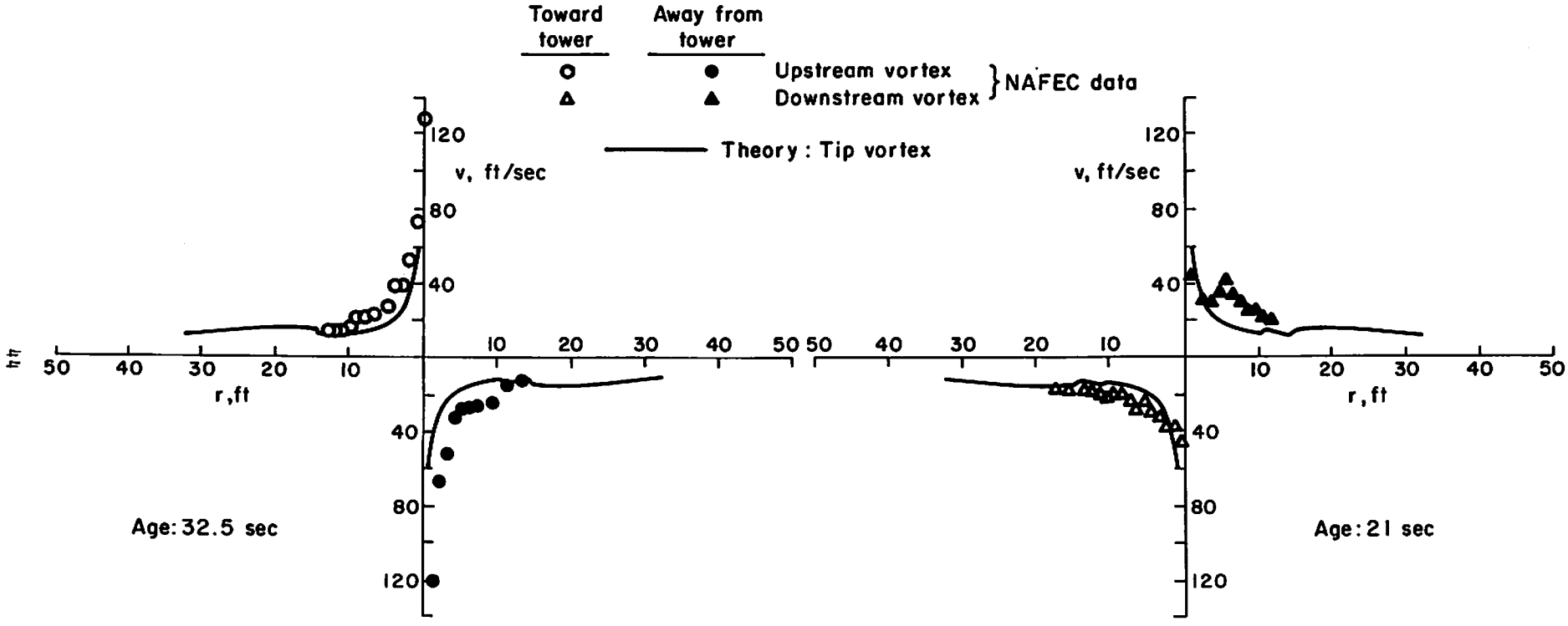

Fig. 4-1b. Comparison of measured and computed swirl velocity profiles for a 727 aircraft in holding configuration ($\delta_f = 0^0$). NAFEC Run 49

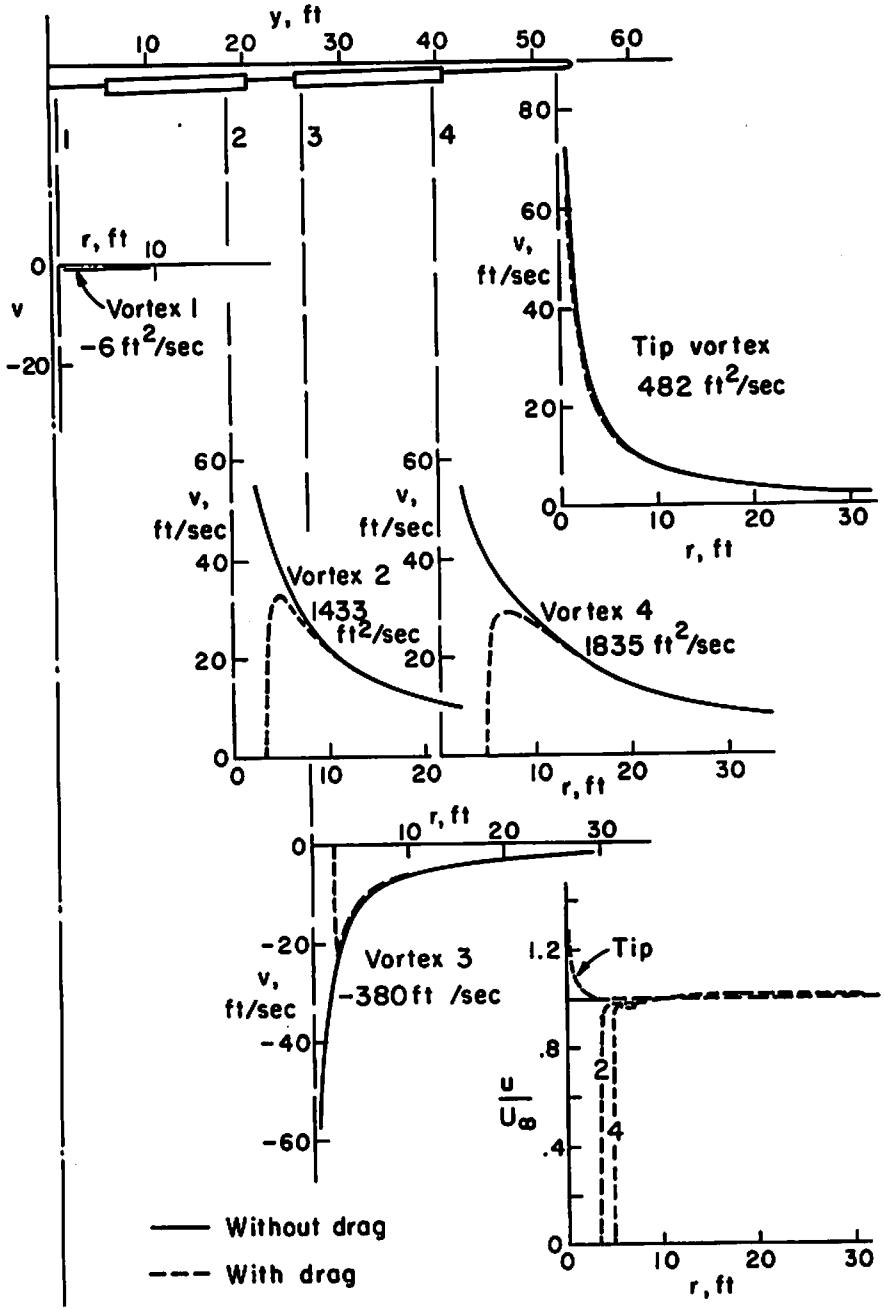

Fig. 4-2a. Computed swirl velocity profiles for a 727 aircraft in take-off configuration ($\delta_f = 25^\circ$). NAFEC Run 40.

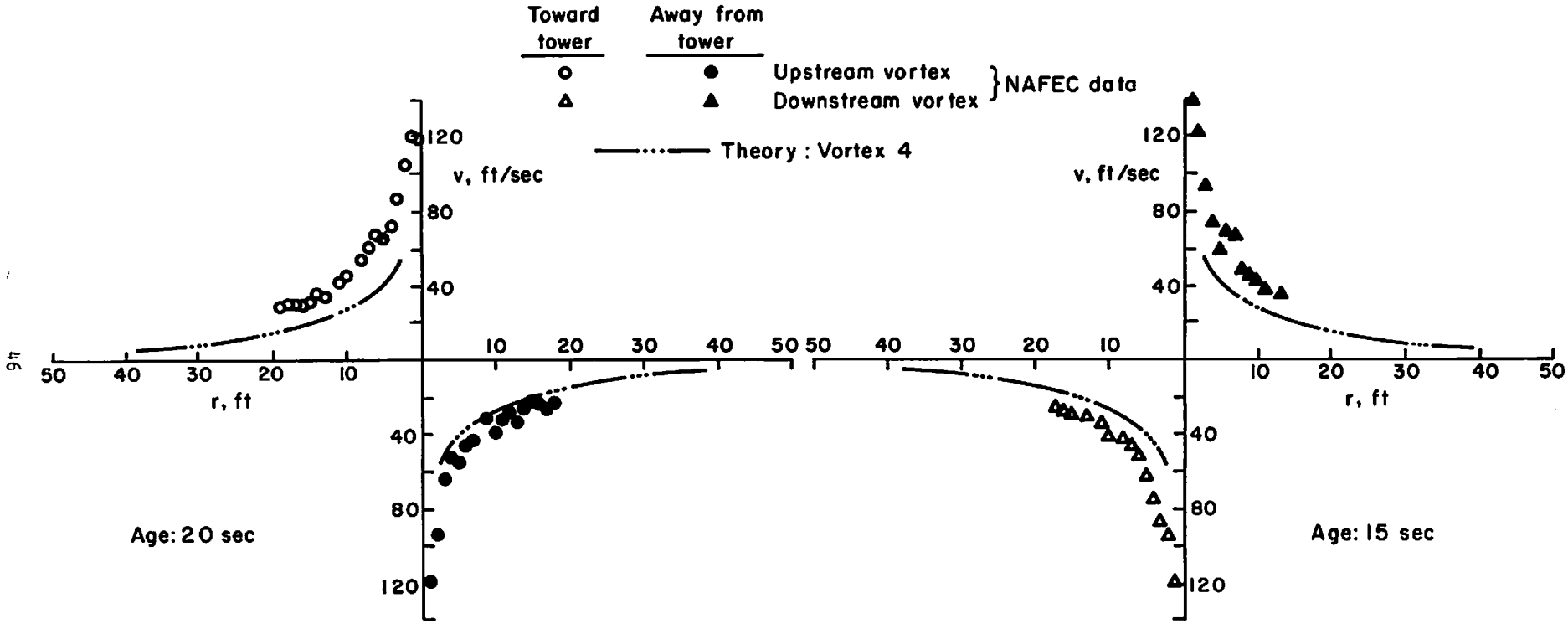

Fig. 4-2b. Comparison of measured and computed swirl velocity profiles for a 727 aircraft in take-off configuration ($\delta_f = 25^o$). NAFEC Run 40

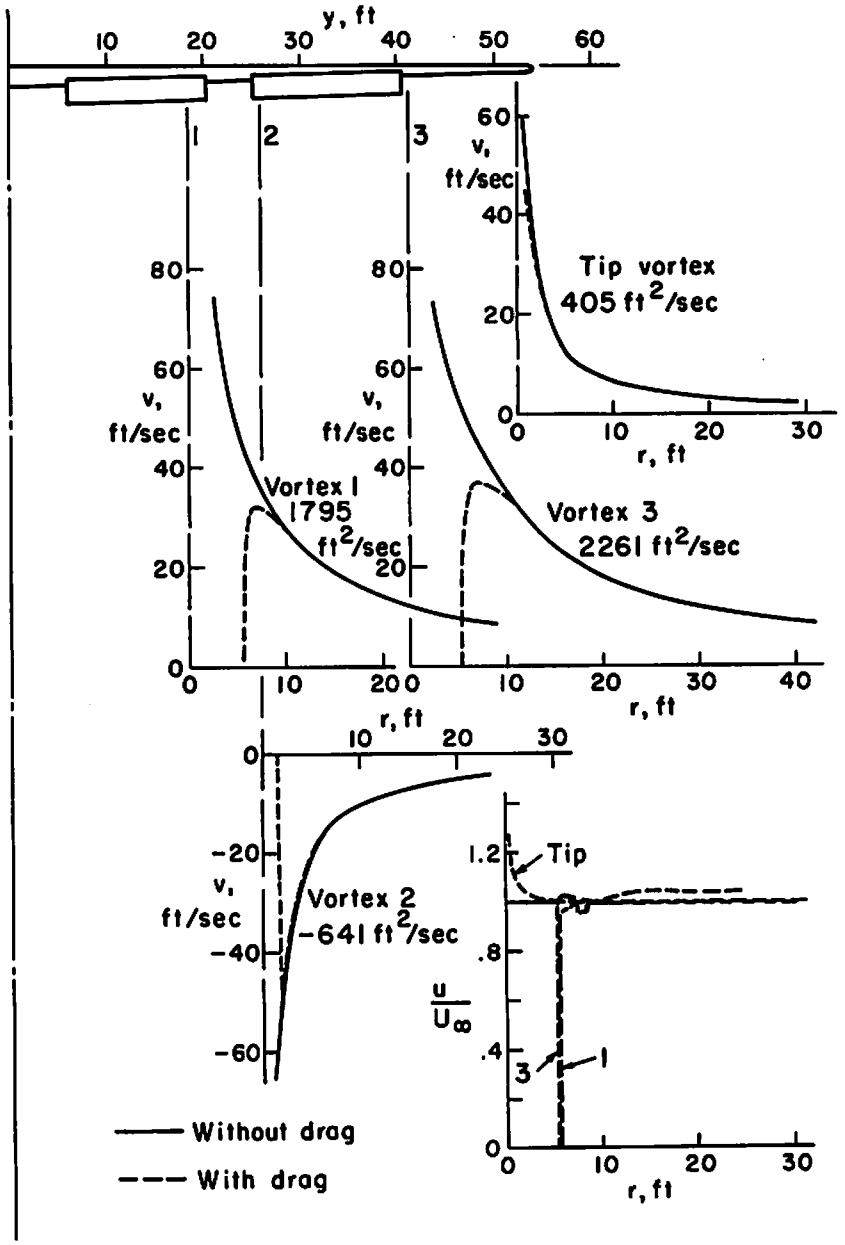

Fig. 4-3a. Computed swirl velocity profiles for a 727 aircraft in landing configuration ($\delta_f = 40^o$). NAFEC Run 18

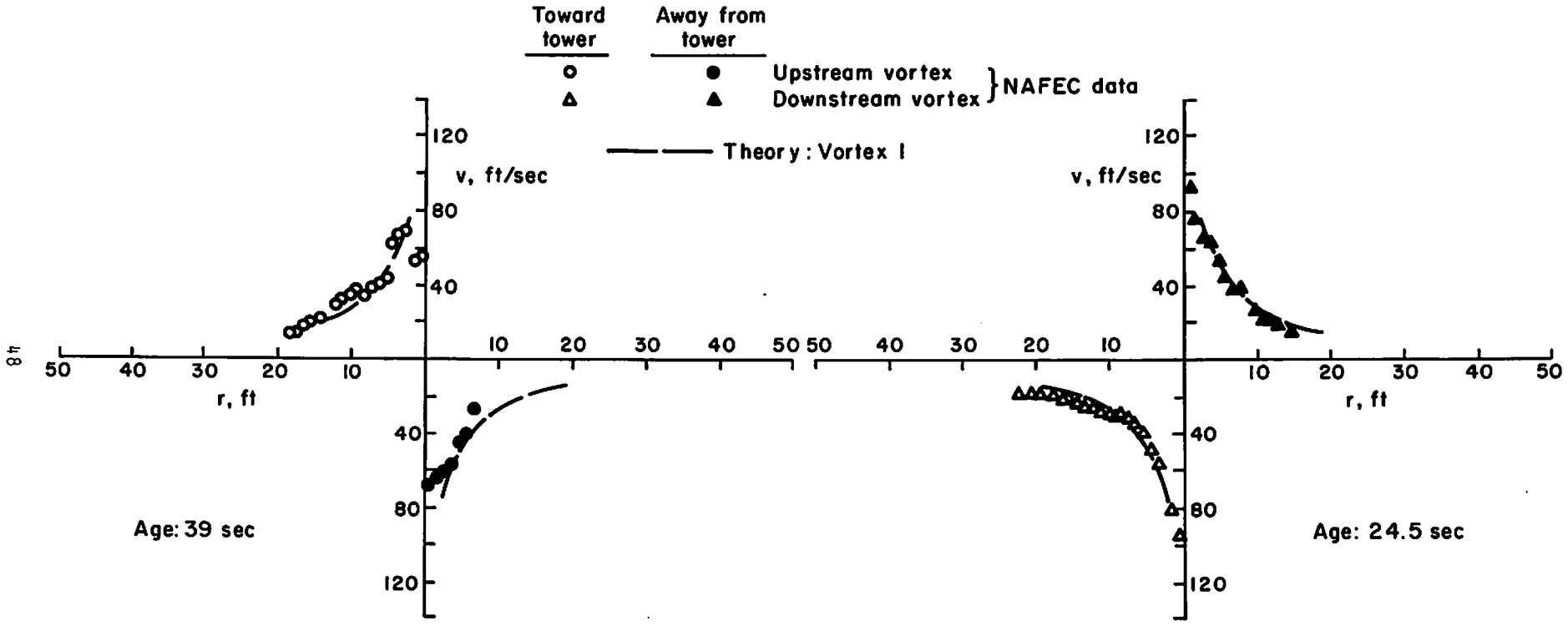

Fig. 4-3b. Comparison of measured and computed swirl velocity profiles for a 727 aircraft in landing configuration ($\delta_f = 40^\circ$). NAFEC Run 18

No. 1, in fact, was computed in the absence of the $0.1\Gamma_o$ limitation mentioned earlier and can be considered negligible.* The predominant vortices are Nos. 2 and 4, those emanating from the outboard ends of each flap segment. As shown in Fig. 4-2b, the stronger of the two, No. 4, while it gives the best match with the data, still falls below the measured velocities throughout the profile. This suggests that what was actually measured may have been a merged combination of two or more of the vortices shed for this configuration. It should also be noted at this point that the apparently large cores computed for the profiles with drag are a result of the way in which the effect of drag is included in the inviscid analysis (Sect. 2). In an actual vortex, the central region of the velocity profiles is "filled in" by the action of turbulent transport. Because of the consequent radial inflow of fluid toward the center, the resulting core might be expected to be considerably smaller than the computed inviscid core.

For the landing configuration (Fig. 4-3a), the pattern of shed vortices is the same as that for take-off, except that the inner negative vortex has now been neglected. It is seen, too, that the interior vortices are now relatively stronger compared to the tip vortex. In the case shown (Fig. 4-3b), the inner of the two positive flap vortices, No. 1, gives a good match with the data. In spite of this good agreement, however, it cannot be said with certainty that the measured profile is actually that of vortex No. 1. As long as there are other vortices in the system of comparable strength, the possibility of significant merging exists and the uncertainty as to the exact identity of the measured profile remains. In this connection, it may be significant that Barber, et al. (Ref. 16), observed apparent merging of flap and tip vortices in flow visualization studies of a 727 wake after 40 seconds.

*The definition of the Γ distribution at the inboard end of the inboard flap, i.e., near the wing root, is somewhat arbitrary, since the presence of the fuselage is always neglected in this analysis. For this reason, this innermost or "fuselage" vortex is usually neglected.

Lockheed L-1011

The limited data for the single run of this aircraft in holding or cruise configuration (Fig. 4-4b) appear to agree well with the Betz theory. As might be expected, there is no measurable core and the region of significant swirl is no more than 10 feet in diameter.

For the take-off configuration case illustrated (Fig. 4-5a), four vortices are computed. Here, vortex No. 2 is quite weak and was apparently computed as a result of a slight irregularity in the Γ distribution near the midpoint of the outboard flap. It is likely that the vorticity contributing to this vortex would, in a real wake, become a part of vortex No. 3. Nevertheless, this computed wake still contains three concentrations of comparable strength. The data (Fig. 4-5b) agree best with the strongest of the three, the tip vortex, although a merged profile may be suspected on the basis of the apparently larger circulation exhibited by the measurements. There is, however, no significant core. The marked irregularity near the center of the profile of vortex No. 3 is a result of the computational technique and does not represent a profile feature that would be expected to occur in an actual vortex. Several other examples of irregularities of this kind are contained in the remaining data.

For the somewhat greater flap deflection of the take-off/approach configuration (Fig. 4-6a), there are four strong positive vortices and a somewhat weaker negative one. In this case, vortex No. 4 would appear to have resulted computationally in much the same way as vortex No. 2 for the take-off case. In Fig. 4-6b, the data are compared with the tip vortex primarily because of the high peak velocities. It is clear, however, that even vortex No. 1, the strongest in terms of circulation, does not represent the total circulation of the measured profile. Here, again, merging of vortices may be suspected. The data in this case do indicate a core of measurable size.

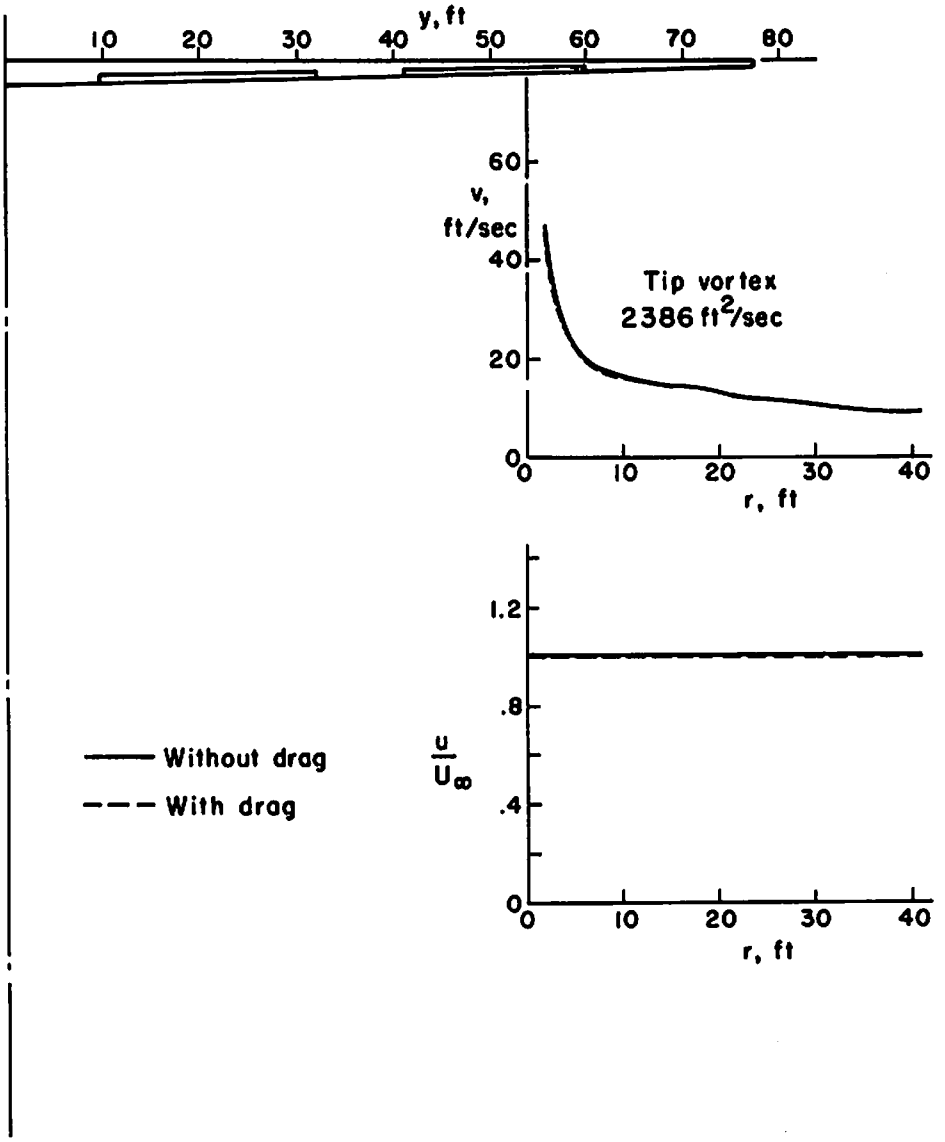

Fig. 4-4a. Computed swirl velocity profiles for a L-1011 aircraft in cruise configuration ($\delta_f = 0^o$). NAFEC Run 19

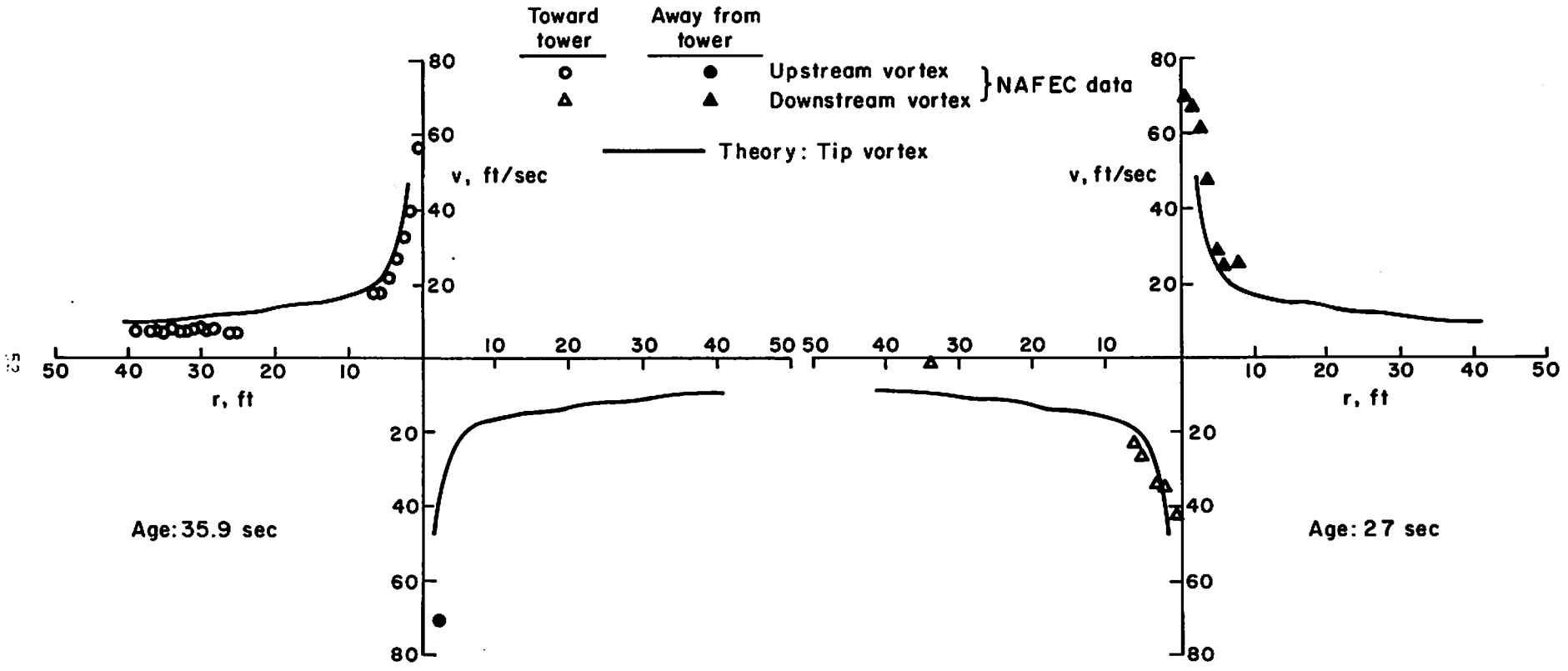

Fig. 4-4b. Comparison of measured and computed swirl velocity profiles for a L-1011 aircraft in cruise configuration ($\delta_f = 0^o$). NAFEC Run 19

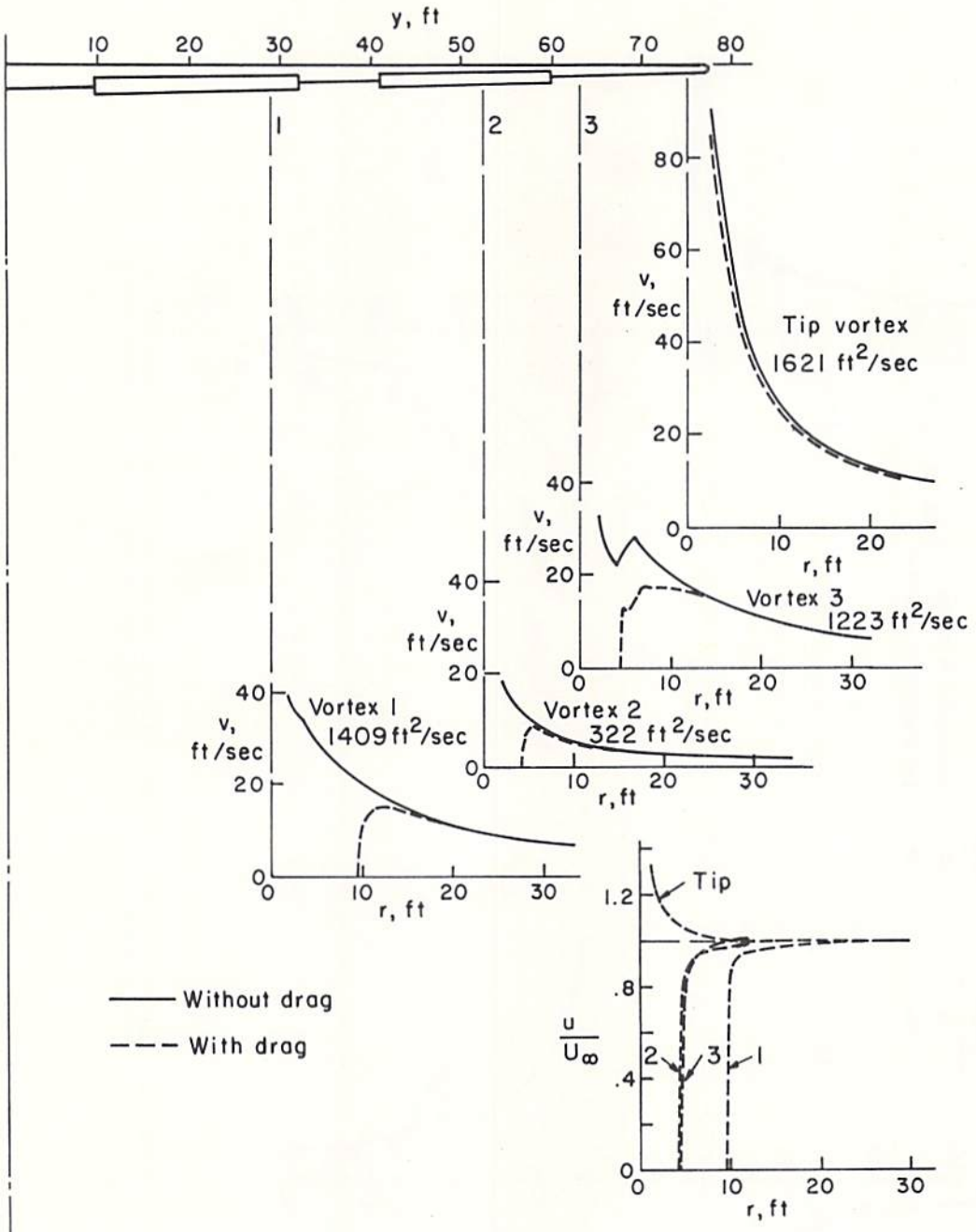

Fig. 4-5a. Computed swirl velocity profiles for a L-1011 aircraft in take-off configuration ($\delta_f = 10^o$). NAFEC Run 14

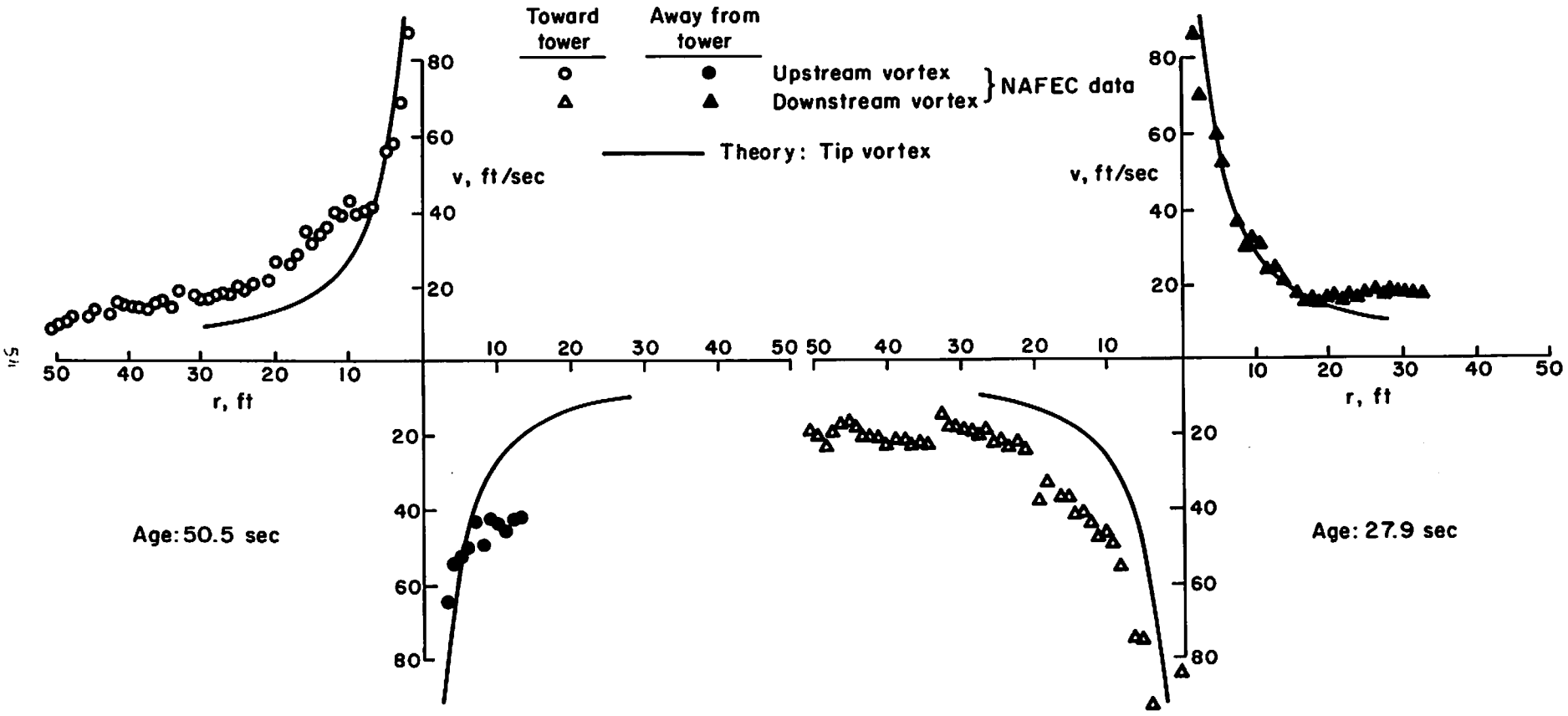

Fig. 4-5b. Comparison of measured and computed swirl velocity profiles for a L-1011 aircraft in take-off configuration ($\delta_f = 10^o$). NAFEC Run 14

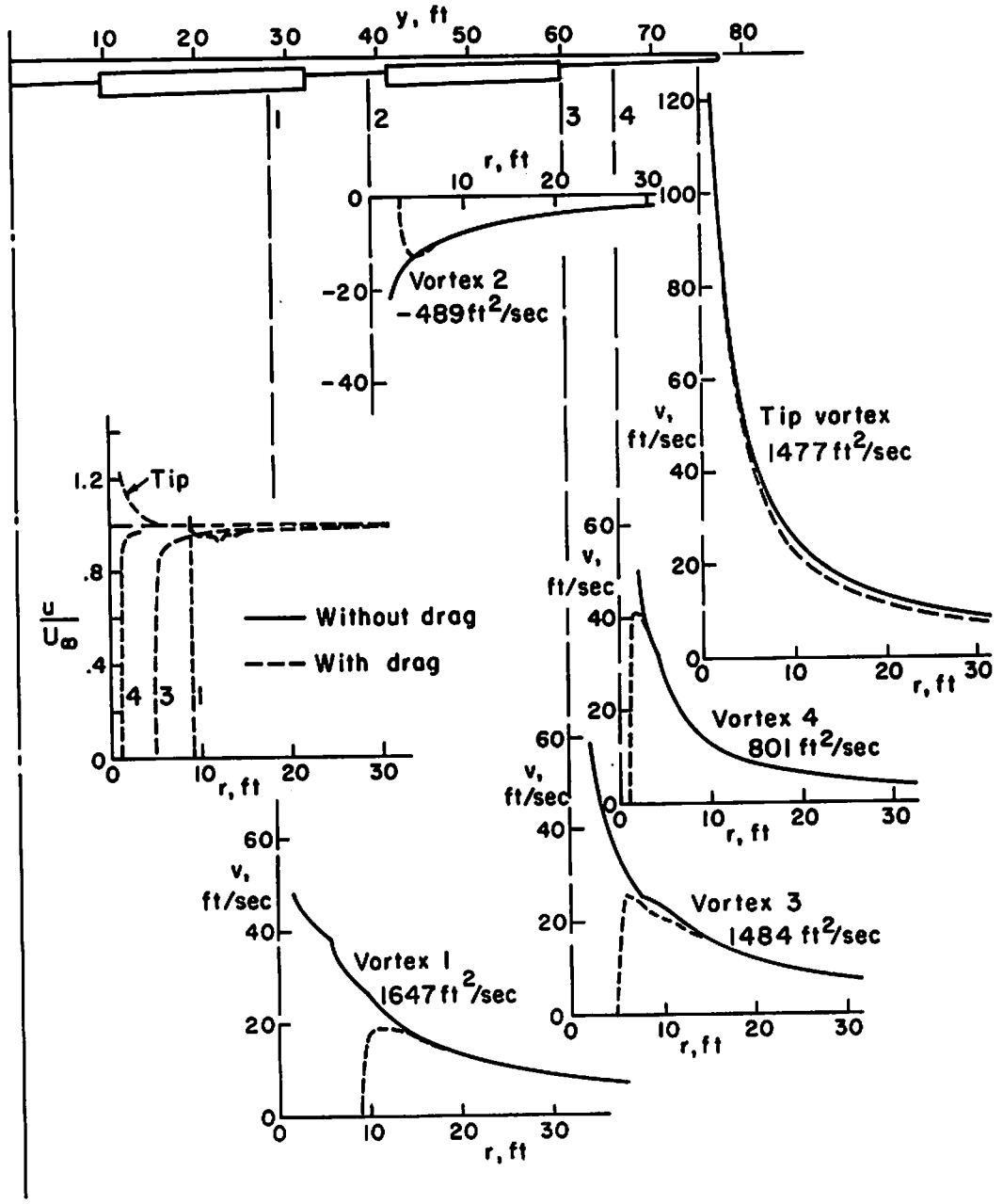

Fig. 4-6a. Computed swirl velocity profiles for a L-1011 aircraft in take-off/approach configuration ($\delta_f = 25^o$). NAFEC Run 10

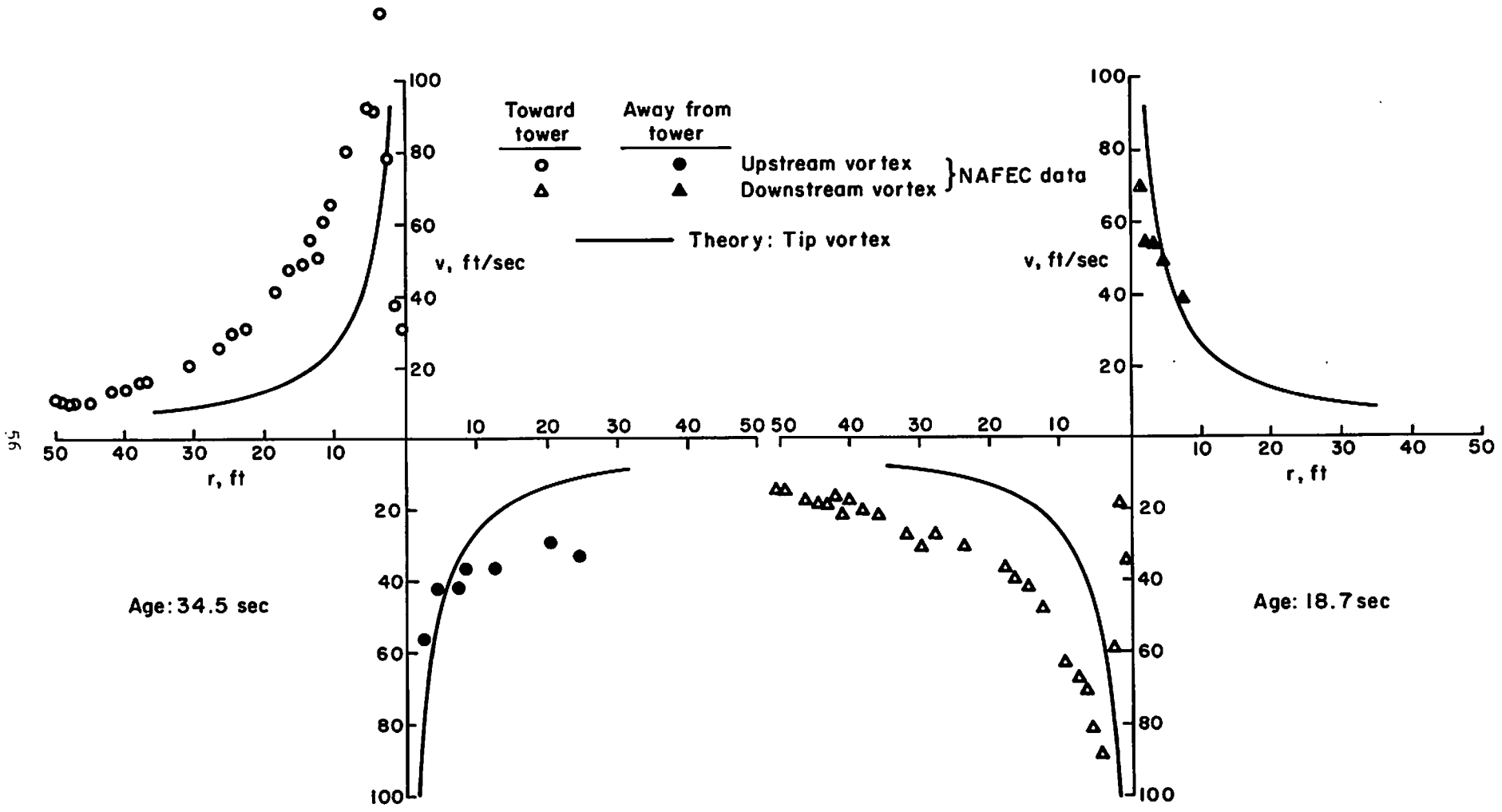

Fig. 4-6b. Comparison of measured and computed swirl velocity profiles for a L-1011 aircraft in take-off/approach configuration ($\delta_f = 25^\circ$). NAFEC Run 10

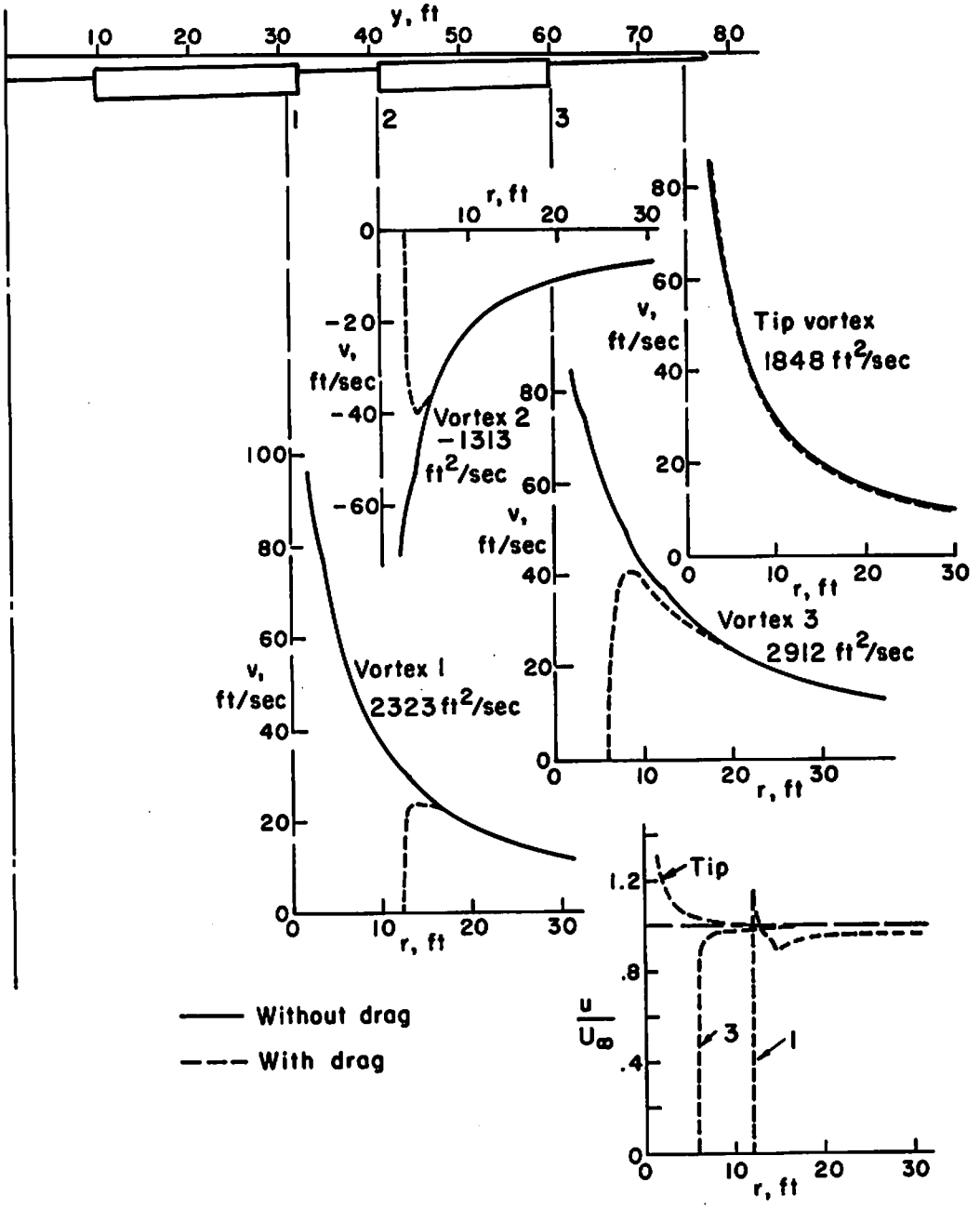

Fig. 4-7a. Computed swirl velocity profiles for a L-1011 aircraft in landing configuration ($\delta_f = 42^o$). NAFEC Run 4

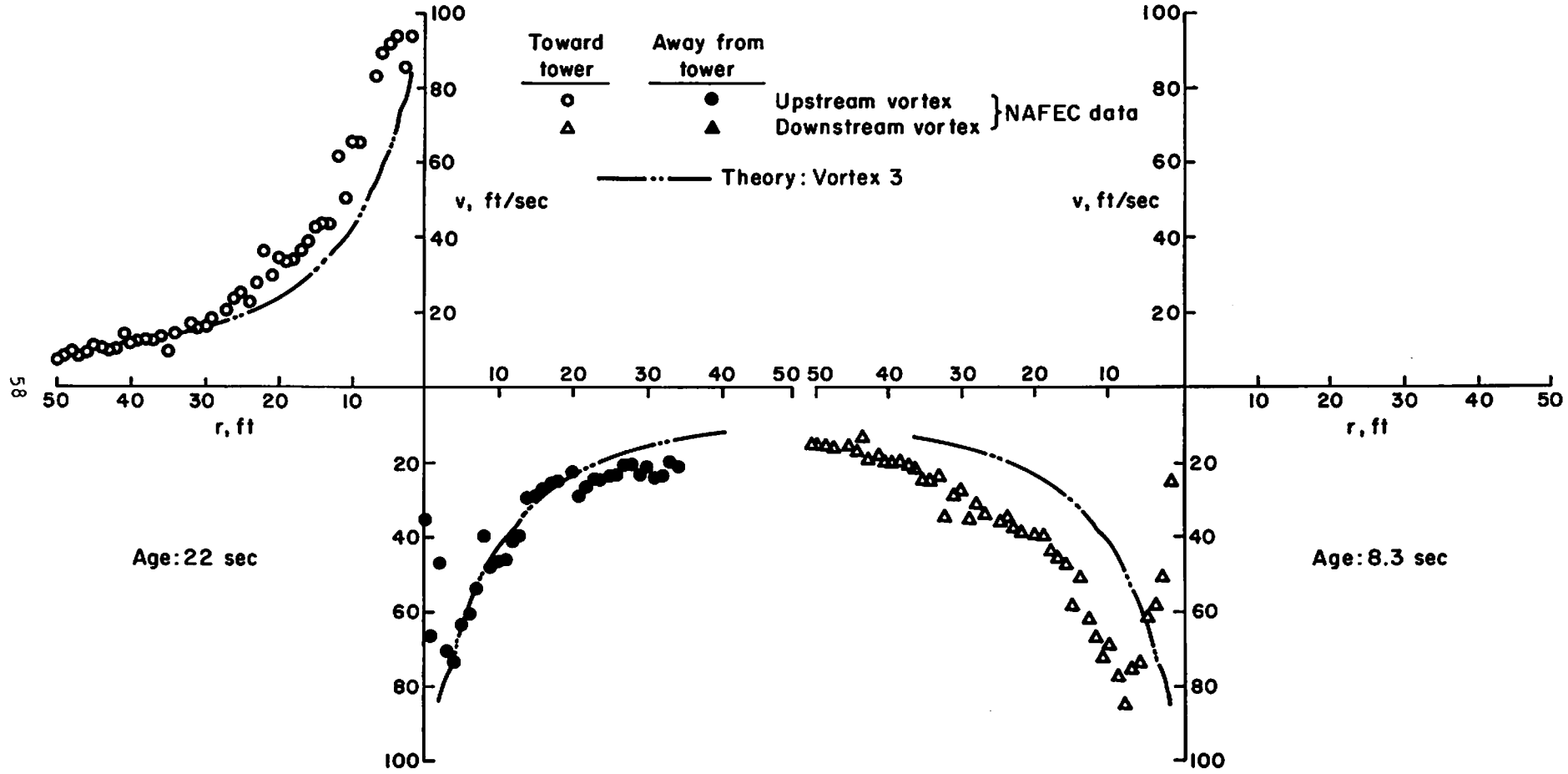

Fig. 4-7b. Comparison of measured and computed swirl velocity profiles for a L-1011 aircraft in landing configuration ($\delta_f = 42^0$). NAFEC Run 4

With flaps fully deployed for landing, the L-1011 load distribution results in four strong vorticity concentrations (Fig. 4-7a). The strongest, vortex No. 3, appears to agree well with the data (Fig. 4-7b), especially for the upwind vortex. Since the downwind vortex in this case passed near or above the top of the instrumentation tower, the location of its center may have been misjudged in the data reduction. A shift of five to ten feet would bring the measured half-profile into satisfactory agreement with the computed profile of vortex No. 3. It is possible, in this case, that vortices Nos. 1 and 2, being of opposite sign and both relatively strong, may have tended to neutralize each other, leaving vortex No. 3 as the dominant one. The data for this case show definite signs of a core of perhaps five to ten feet in diameter.

McDonnell Douglas DC-10

The results for the DC-10 are generally similar to those for the L-1011, which may not be surprising in view of the geometrical similarities of the two aircraft. What differences there are appear to be a result of slight differences in the detailed shapes of the loading curves.

In the cruise configuration (Fig. 4-8a), a very flat profile is noted, and the computation cannot resolve a high swirl region near the center. The data are consistent with this result (Fig. 4-8b), although increased swirl velocities are found within about five feet of the center.

For take-off (Fig. 4-9a), the results are remarkably similar to those for the L-1011 (Fig. 4-5a), even to the presence of a weak vortex No. 2 and the same relative strengths of all the vortices. In both cases, the data appear to agree best with the tip vortex (Figs. 4-5b and 4-9b), although the measurements indicate a profile of greater circulation, perhaps the result of vortex merging. Coincidentally, the vortex ages for these two cases are also quite similar.

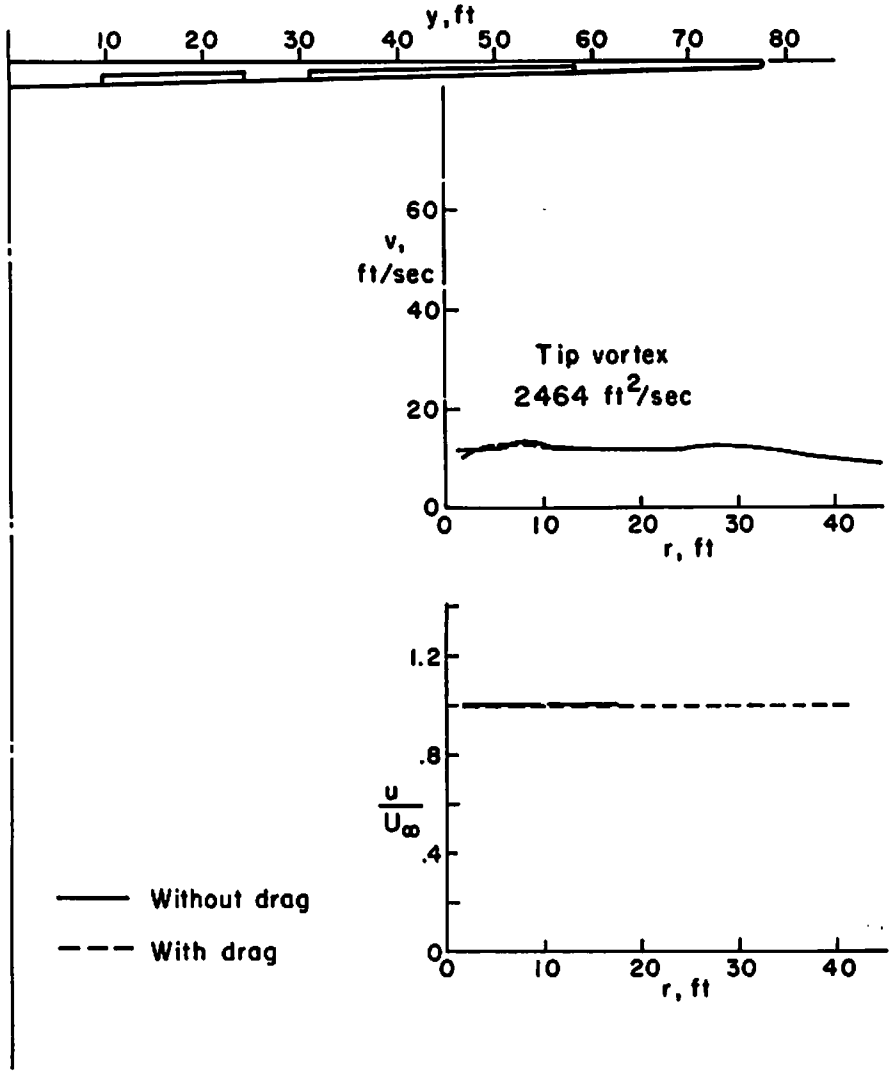

Fig. 4-8a. Computed swirl velocity profiles for a DC-10 aircraft in cruise configuration ($\delta_f = 0^o$). NAFEC Run 20

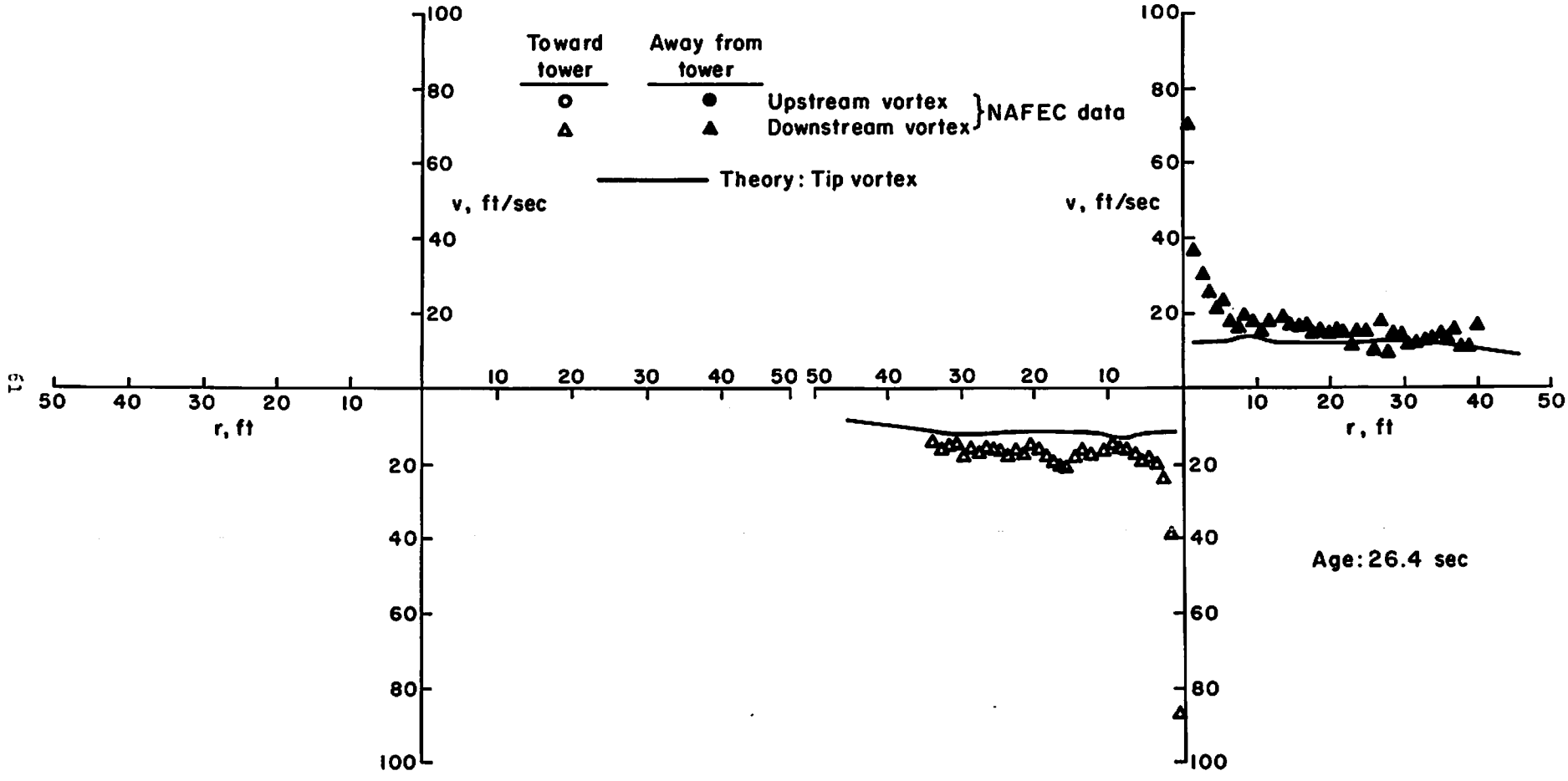

Fig. 4-8b. Comparison of measured and computed swirl velocity profiles for a DC-10 aircraft in cruise configuration ($\delta_f = 0^o$). NAFEC Run 20

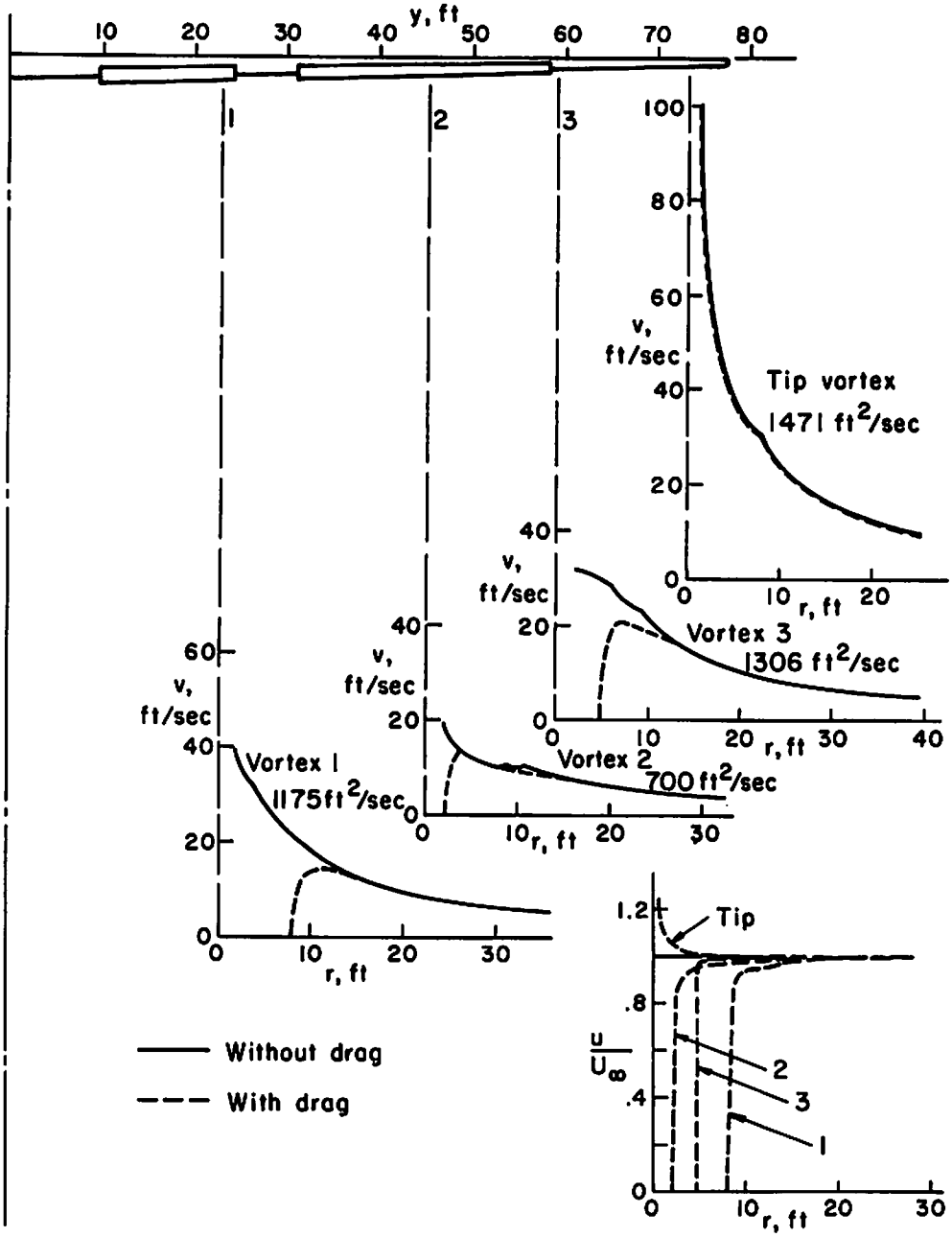

Fig. 4-9a. Computed swirl velocity profiles for a DC-10 aircraft in take-off configuration ($\delta_f = 10^o$). NAFEC Run 6

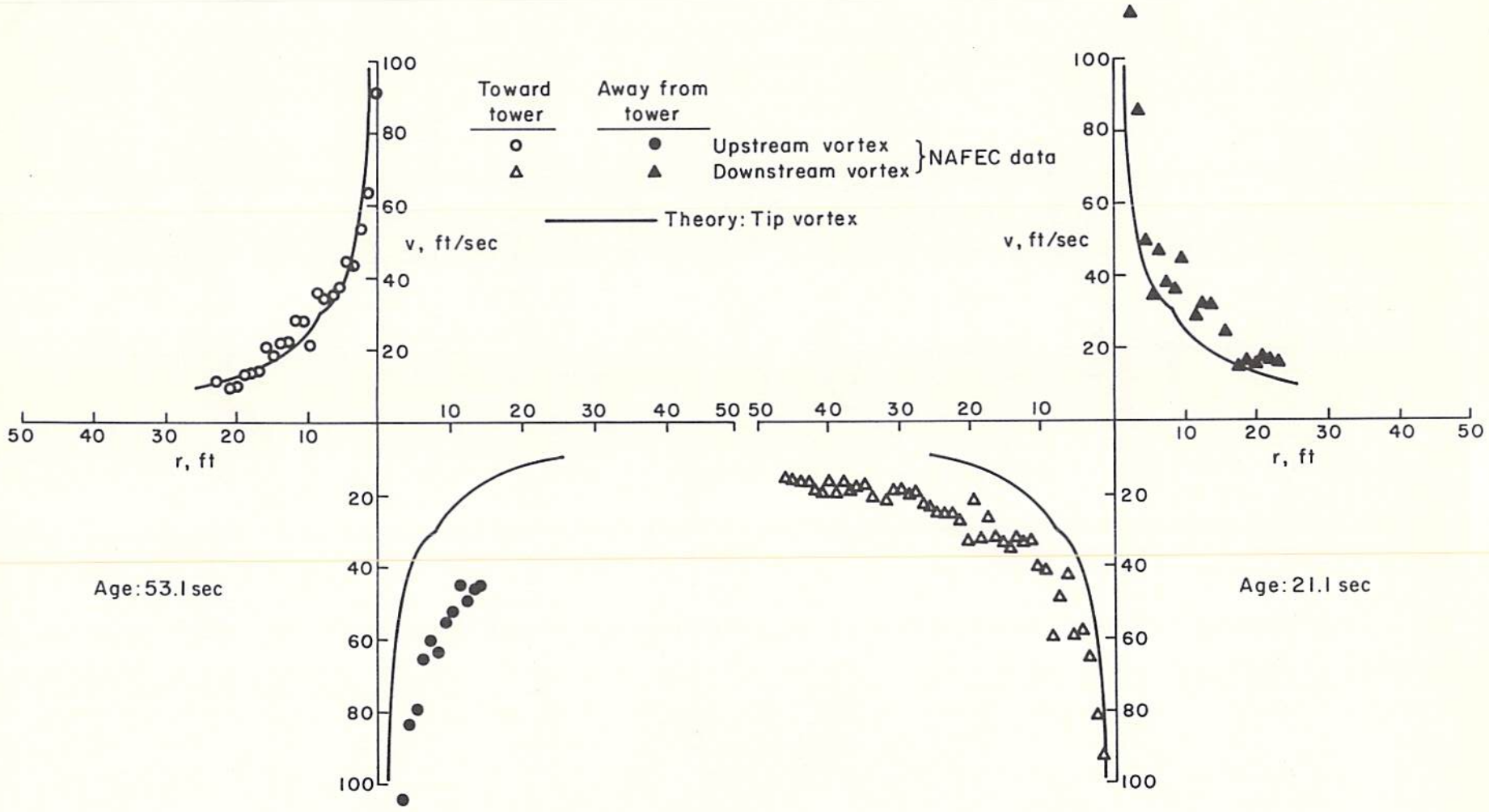

Fig. 4-9b. Comparison of measured and computed swirl velocity profiles for a DC-10 aircraft in take-off configuration ($\delta_f = 10^\circ$). NAFEC Run 6

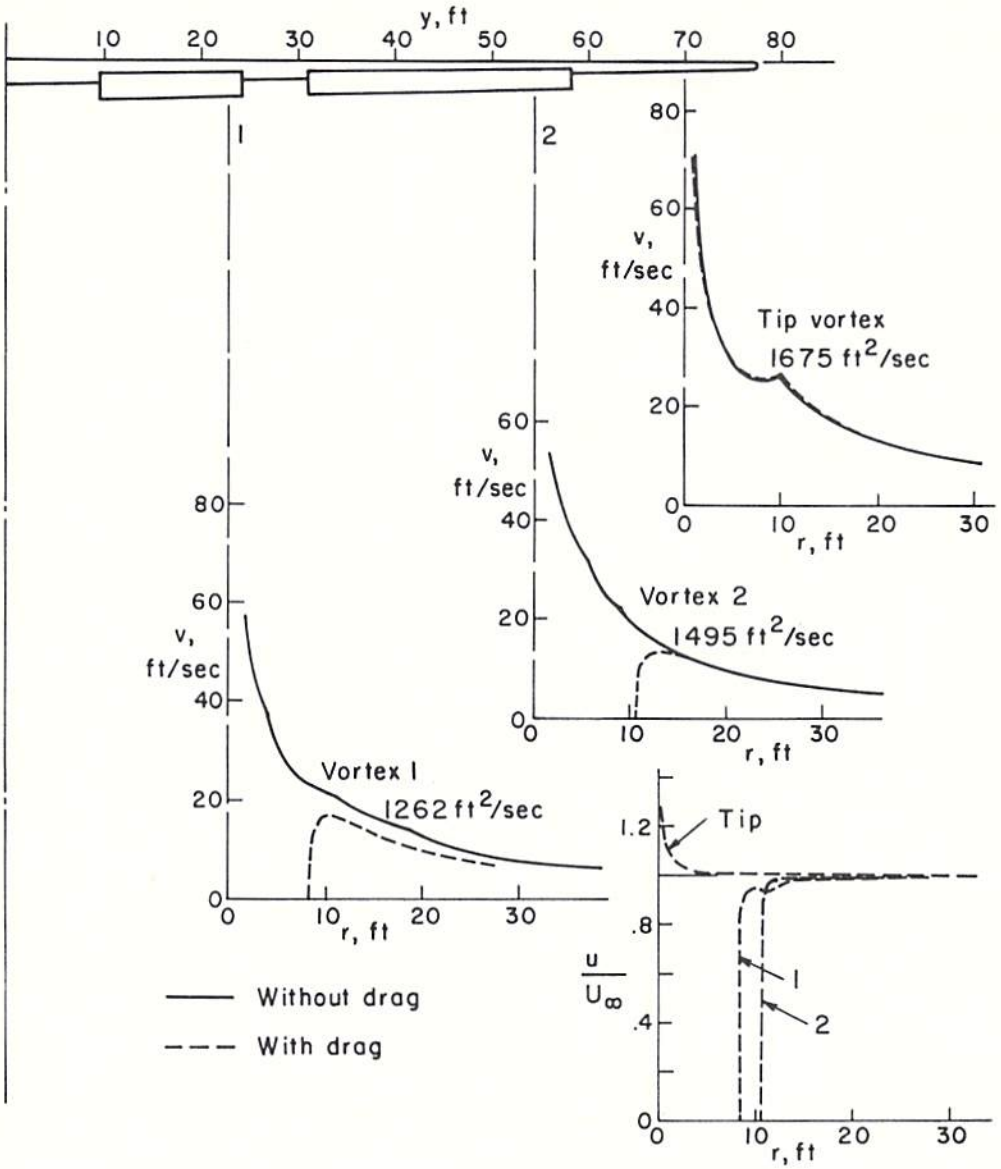

Fig. 4-10a. Computed swirl velocity profiles for a DC-10 aircraft in take-off/approach configuration ($\delta_f = 22^o$). NAFEC Run 18

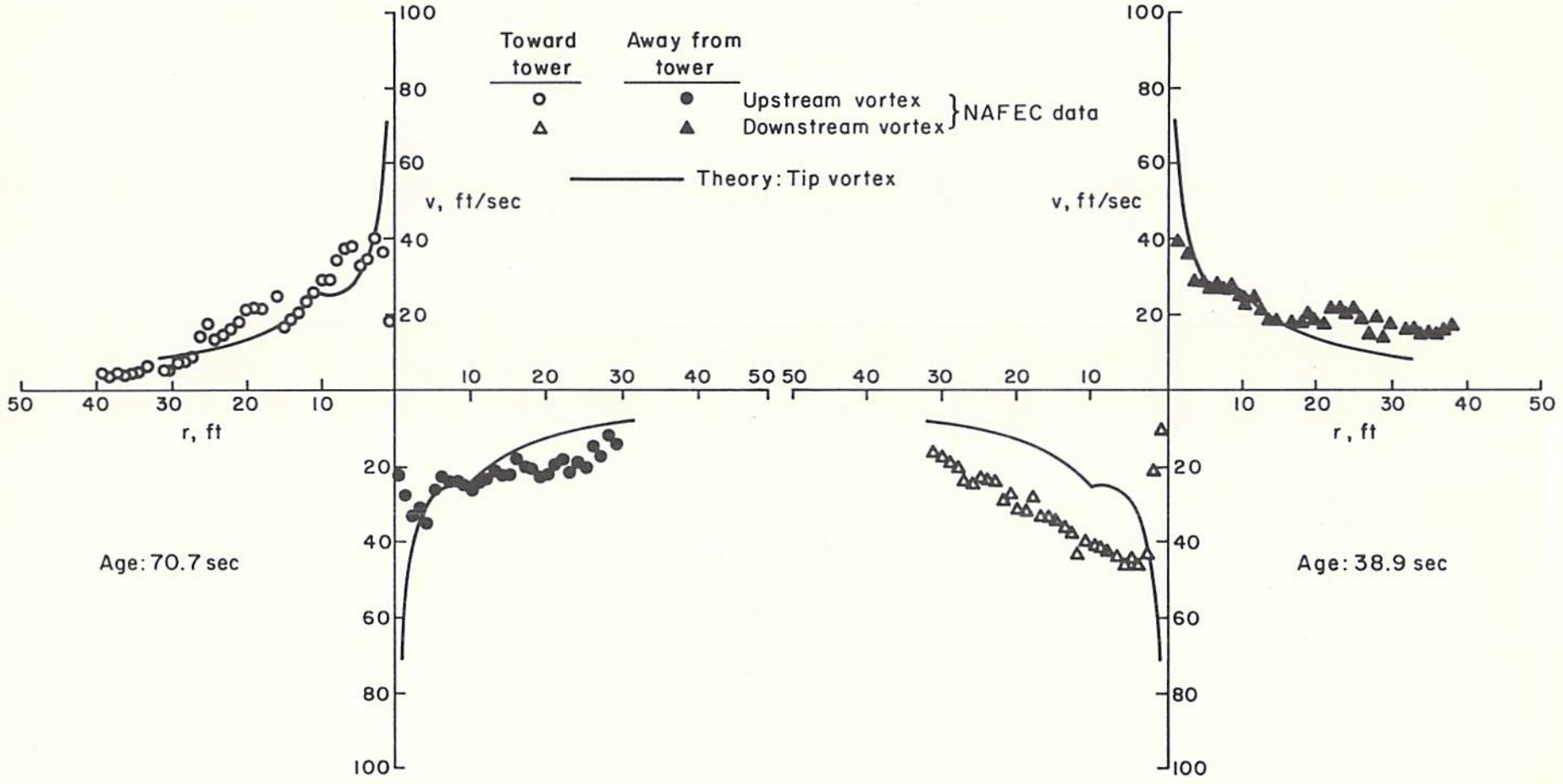

Fig. 4-10b. Comparison of measured and computed swirl velocity profiles for a DC-10 aircraft in take-off/approach configuration ($\delta_f = 22^o$). NAFEC Run 18

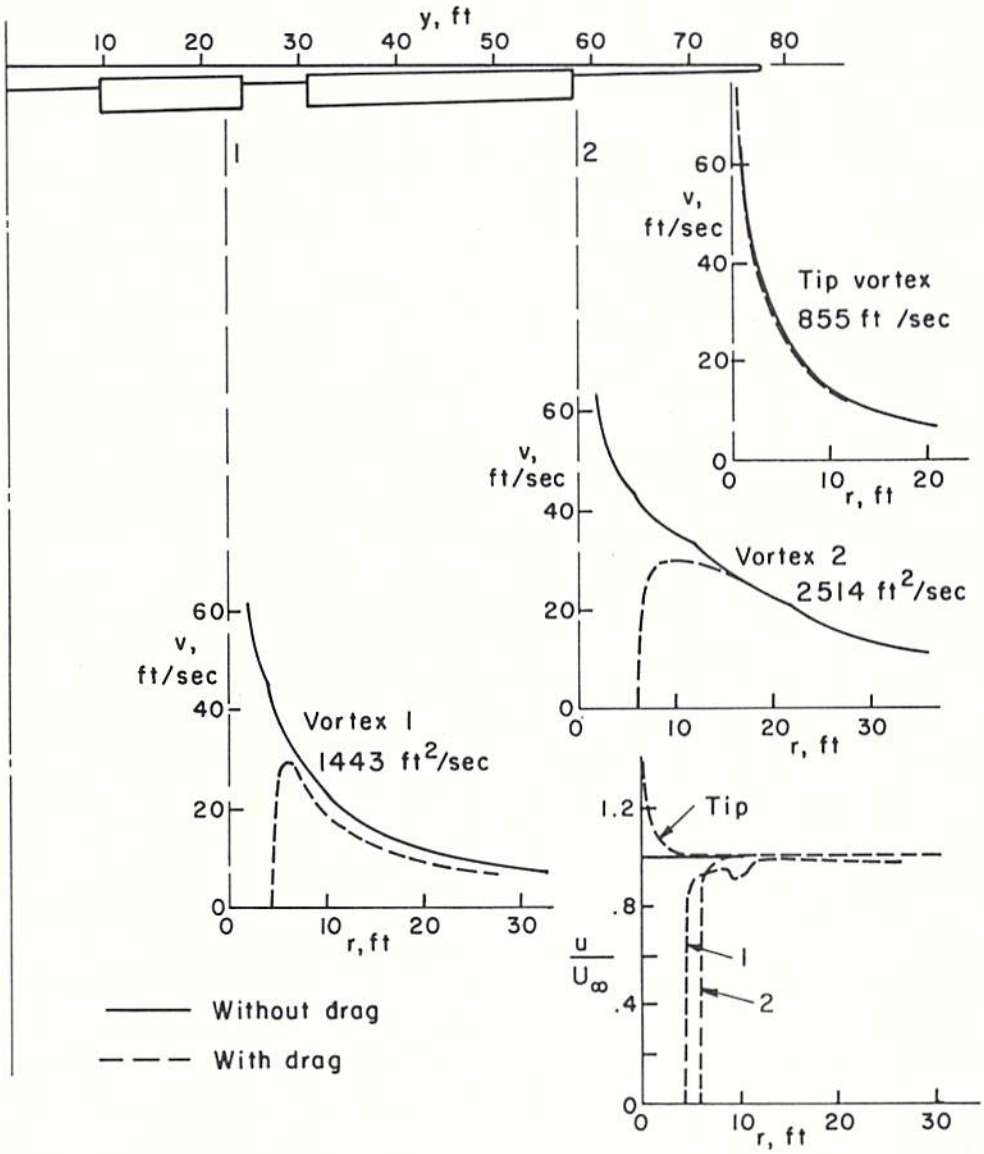

Fig. 4-11a. Computed swirl velocity profiles for a DC-10 aircraft in landing configuration ($\delta_f = 35^o$). NAFEC Run 15

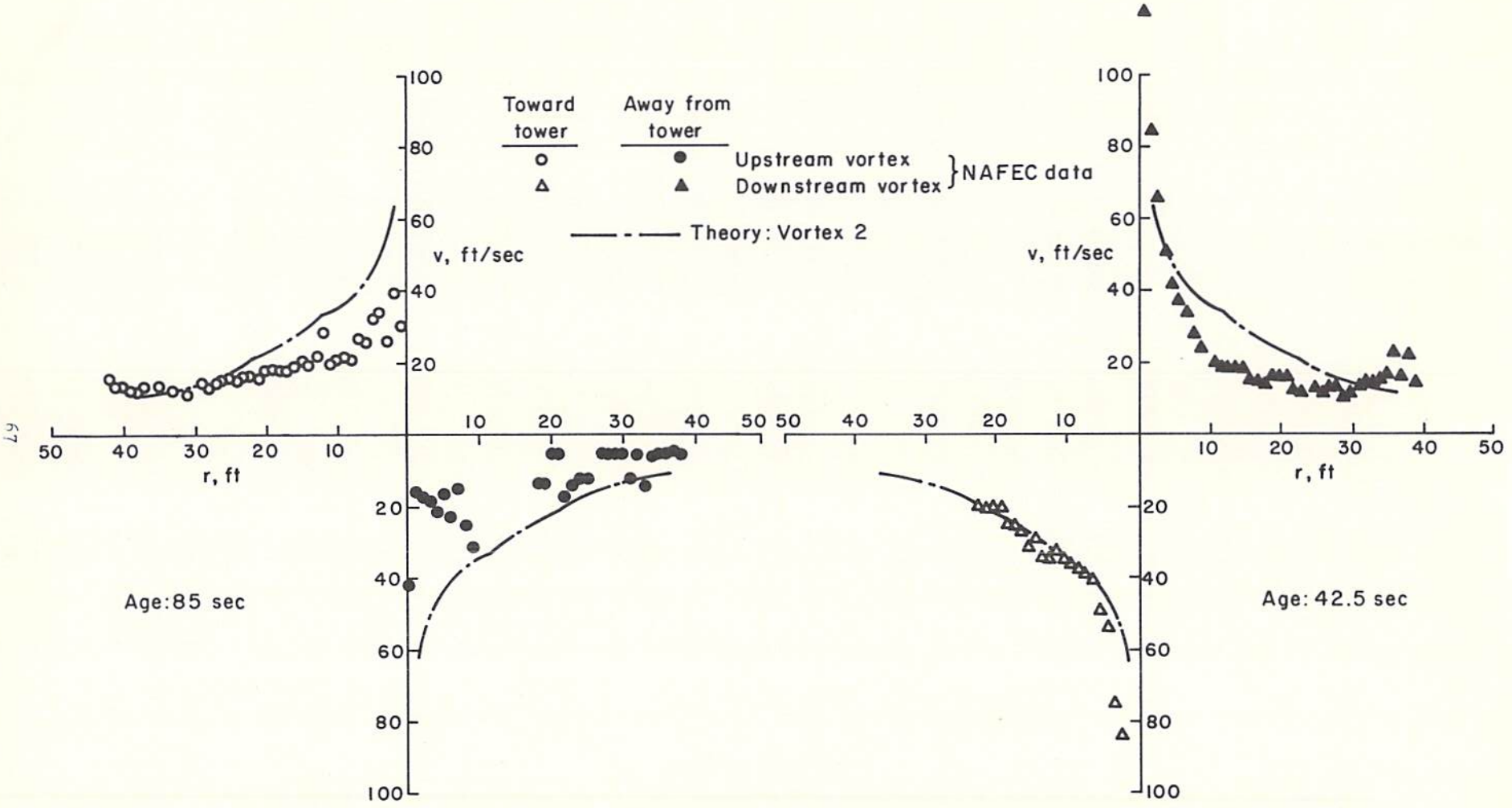

Fig. 4-11b. Comparison of measured and computed swirl velocity profiles for a DC-10 aircraft in landing configuration ($\delta_f = 35^o$). NAFEC Run 15

With the flaps further extended for the take-off/approach configuration (Fig. 4-10a), the DC-10 shows the three major vortices that might be expected, one from the outboard end of each flap segment and one from the tip. They are all of comparable strength. In this case, the data also agree best with the tip vortex, although, once again, there is some indication of merged vortices, especially in the case of the downwind vortex (Fig. 4-10b).

In the landing configuration (Fig. 4-11a), the expected pattern is continued, with the major concentration, vortex No. 2, emanating from the outboard flap segment. A portion of the data agree very well with vortex No. 2, while there is some ambiguity for the remainder (Fig. 4-11b). Portions of the measured profile for this case are marked by considerable scatter.

At this point it is of interest to mention that the NAFEC data for the L-1011 and DC-10 included several instances of apparent multiple-vortex "hits" at the instrumentation tower. Heretofore, in the analysis of data for the aircraft discussed in Ref. 3 (DC-7, DC-9, and C-141), there was seldom if ever any indication of more than a single pair of vorticity concentrations intercepting the tower. For both the L-1011 and DC-10, however, there are a number of instances where the upwind vortex appears to be a multiple vortex at some stage of merging. The characteristic sensor time histories show two distinct peaks at approximately the same altitude, and there is a very marked increase in the field of influence as this pattern passes the tower. (The two peaks in this case are distinguishable from and should not be confused with the twin peaks that are indicative of a "core penetration" for a single vortex.) The most pronounced cases of this kind were observed in the data for the DC-10 in take-off configuration. For take-off/approach and landing, the same effect was noted but it was less pronounced, perhaps an indication that merging had proceeded further in these cases. The most distinctive aspect of this observation is that there was never any clear indication of similar multiple concentrations near the downwind vortex. This may mean

either that the vortices which ultimately appear to merge on the upwind side of the wake were not within range when the downwind side passed the tower, or that there actually was some asymmetry in the wakes of these aircraft under the conditions of these observations. An example of apparent asymmetry was found for NAFEC run 16, with the DC-10 in landing configuration. A possible interpretation of the data for this case is illustrated schematically in Fig. 4-15. It is seen that within a fairly short time interval, three vorticity concentrations passed the tower at different altitudes on the upwind side of the wake. The lateral spacing of the vortices in this figure is based on the times of intercept and the approximate ambient wind speed indicated by the velocity time histories at $t = 0$. Naturally, asymmetry of the kind illustrated could be the result of atmospheric interactions. A careful study of flow visualization pictures for this case might clarify this point.

Boeing 747

The computed tip vortex for this aircraft in holding configuration is in excellent agreement with the measured profile as shown in Fig. 4-12b.

In take-off configuration (Fig. 4-13a), the computed tip vortex is far stronger than either flap vortex, and it shows the best agreement with the data (Fig. 4-13b). There is an indication, however, of even greater circulation in the measured profiles, which may mean that some merging has taken place.

In landing configuration, five vortices result from the calculation for this load distribution (Fig. 4-14a). The innermost, however, is weak and can be neglected as discussed earlier. The predominant vortex is No. 4, and it is seen to give the best agreement with the measurements (Fig. 4-14b). In the case of the downwind vortex, it appears that better agreement would result if the center of the measured profile were moved five to ten feet lower. The measured profiles for this aircraft in landing configuration

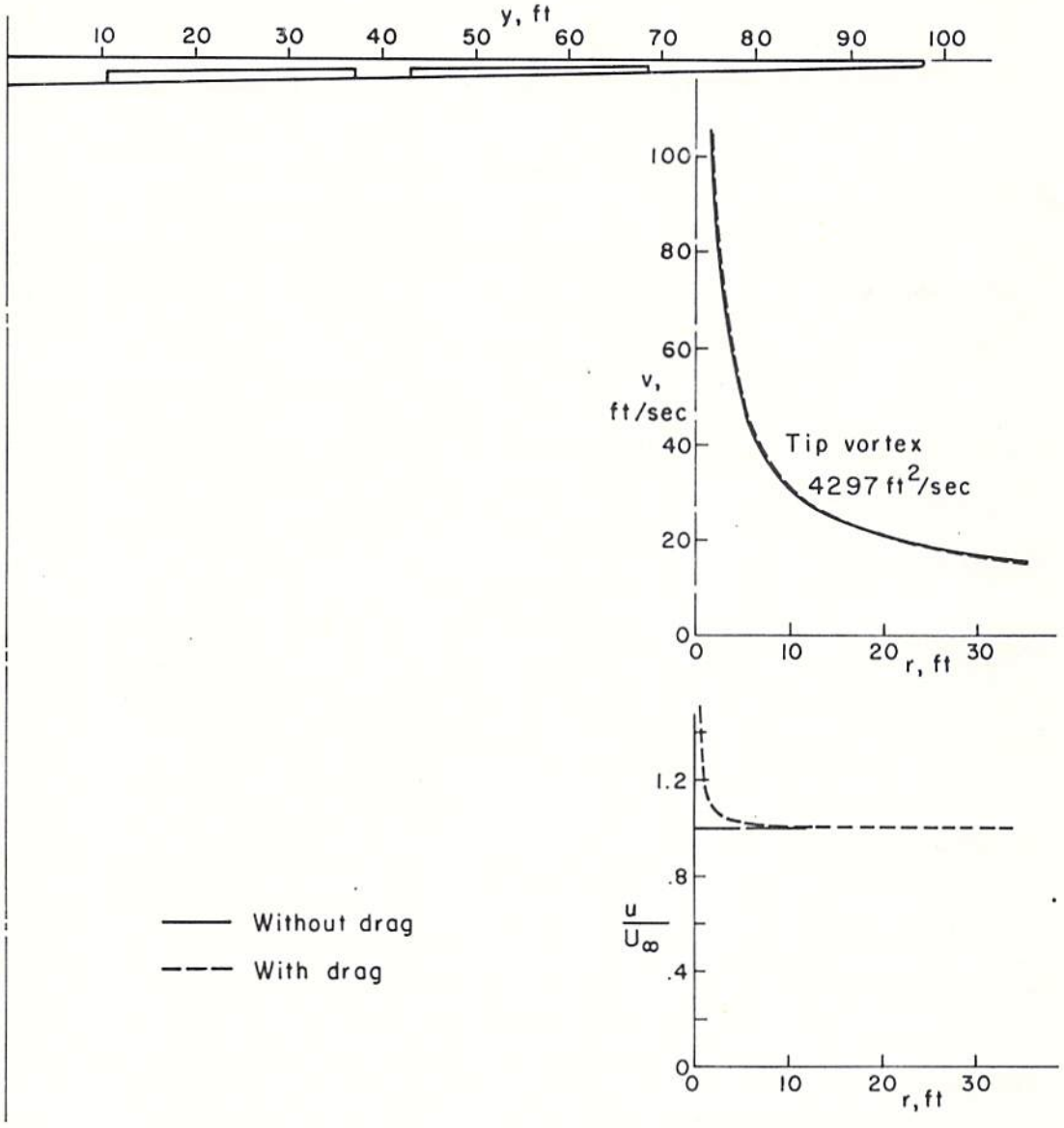

Fig. 4-12a. Computed swirl velocity profiles for a 747 aircraft in holding configuration ($\delta_f = 0^o$). NAFEC Run 45

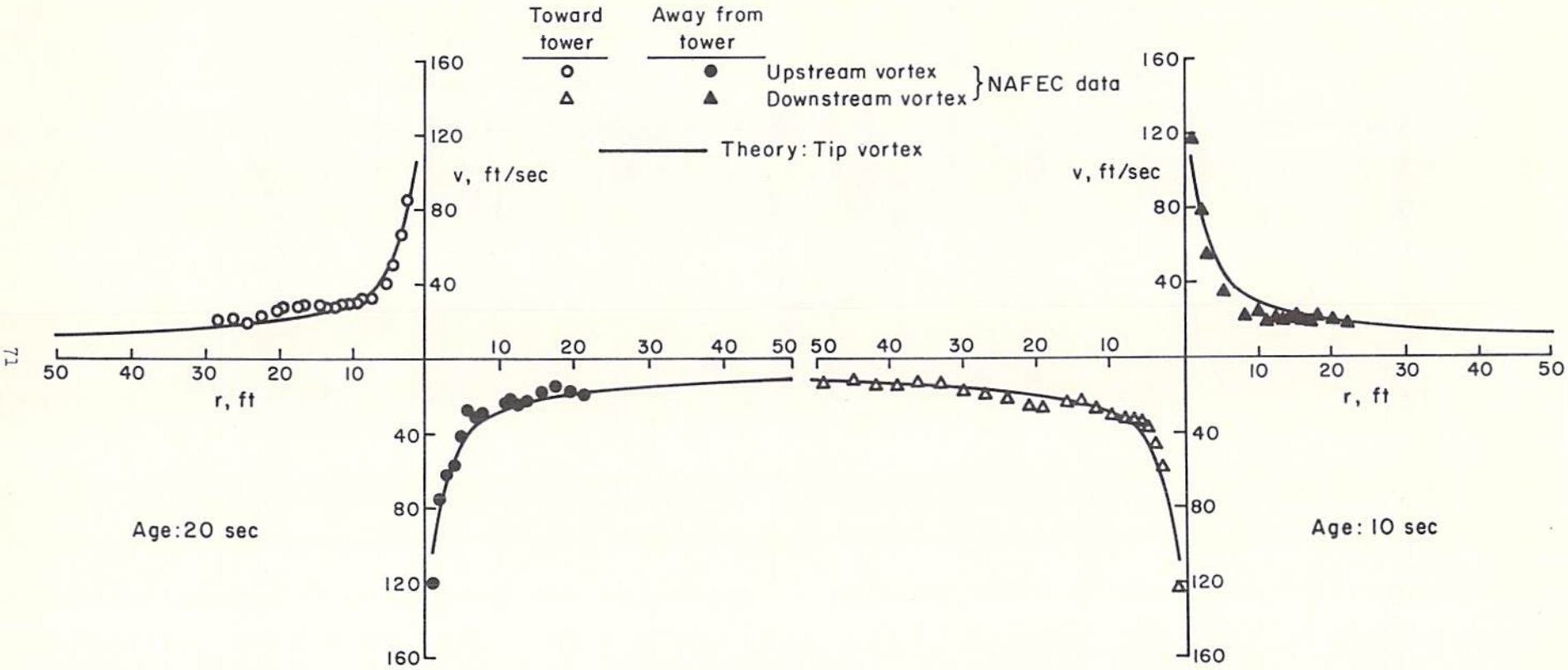

Fig. 4-12b. Comparison of measured and computed swirl velocity profiles for a 747 aircraft in holding configuration ($\delta_f = 0^o$). NAFEC Run 45

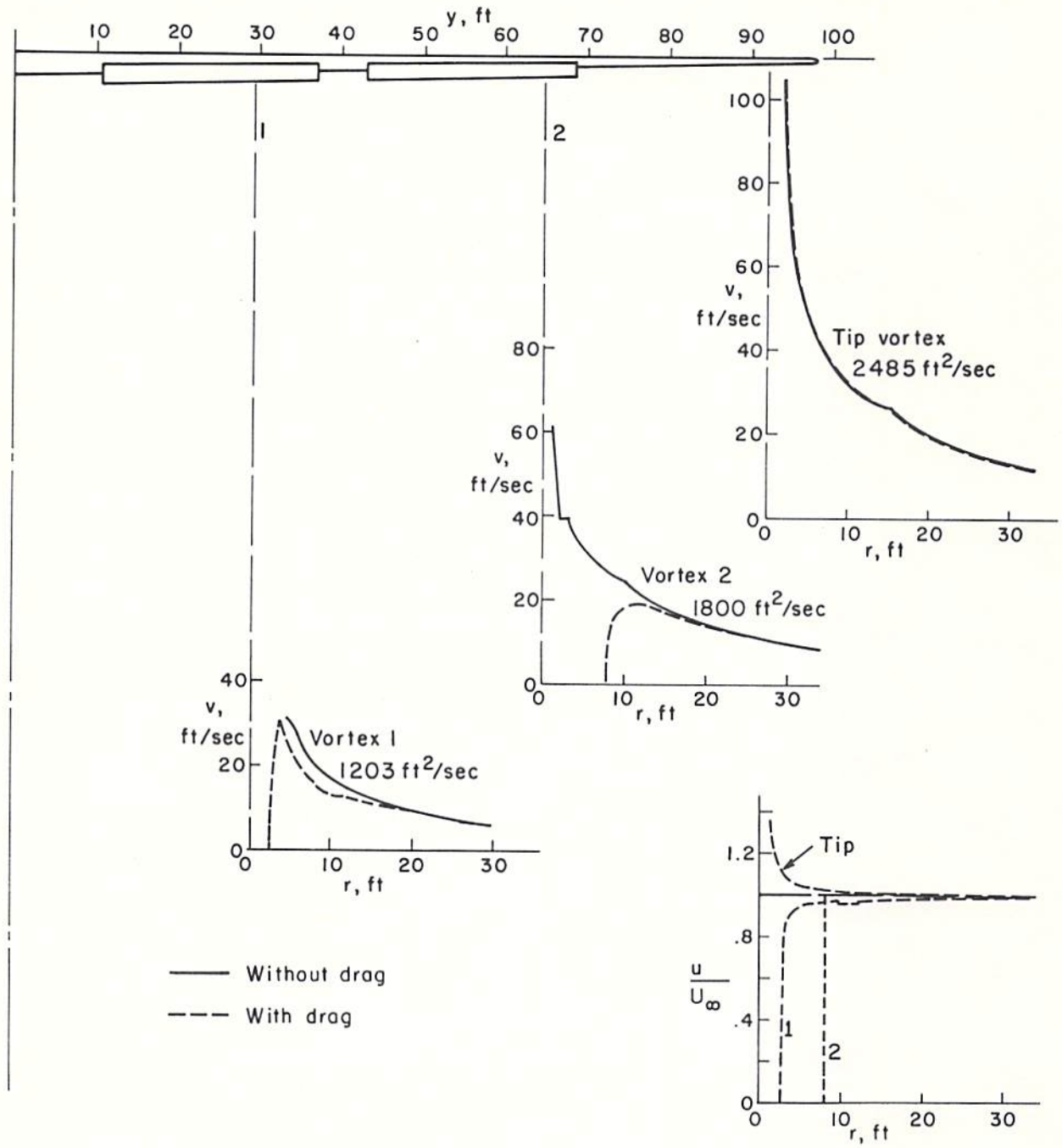

Fig. 4-13a. Computed swirl velocity profiles for a 747 aircraft in take-off configuration ($\delta_f = 10^o$). NAFEC Run 43

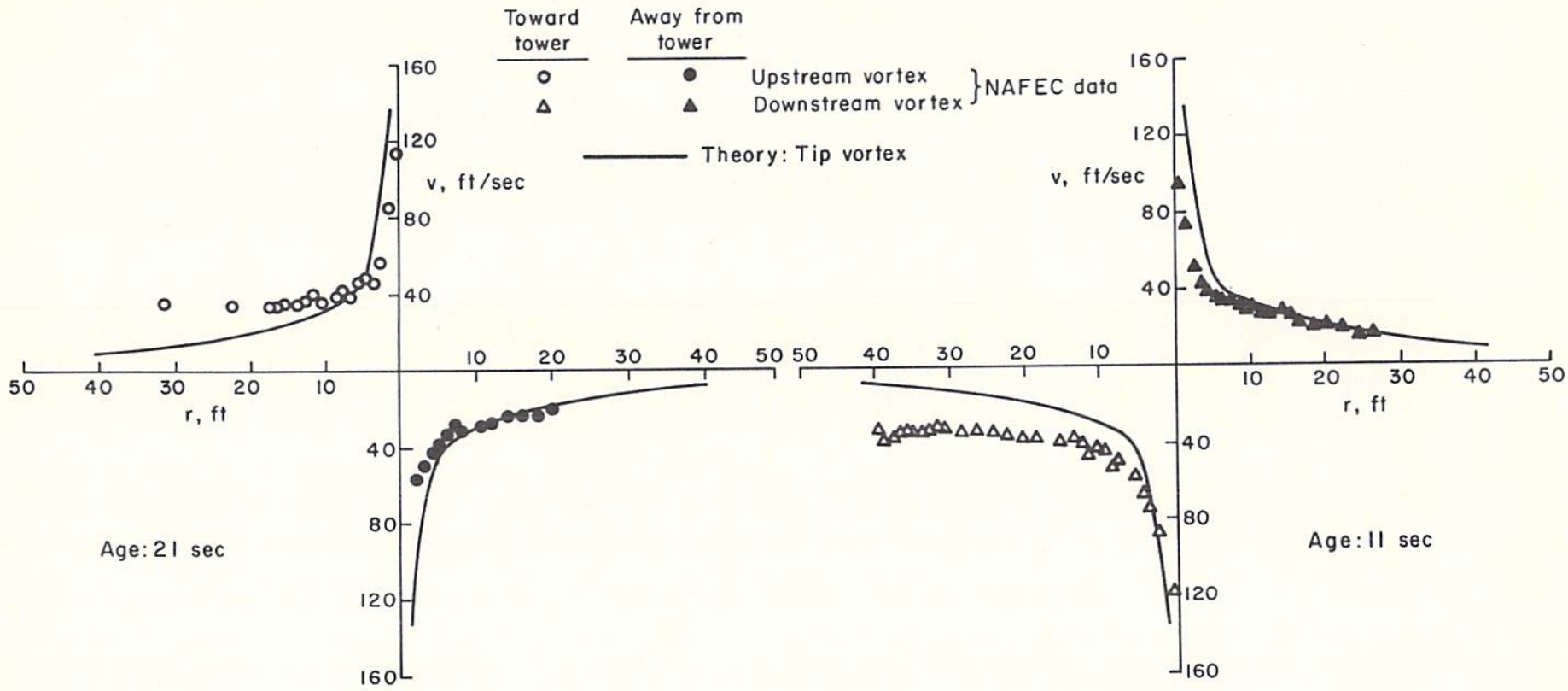

Fig. 4-13b. Comparison of measured and computed swirl velocity profiles for a 747 aircraft in take-off configuration ($\delta_f = 10^o$). NAFEC Run 43

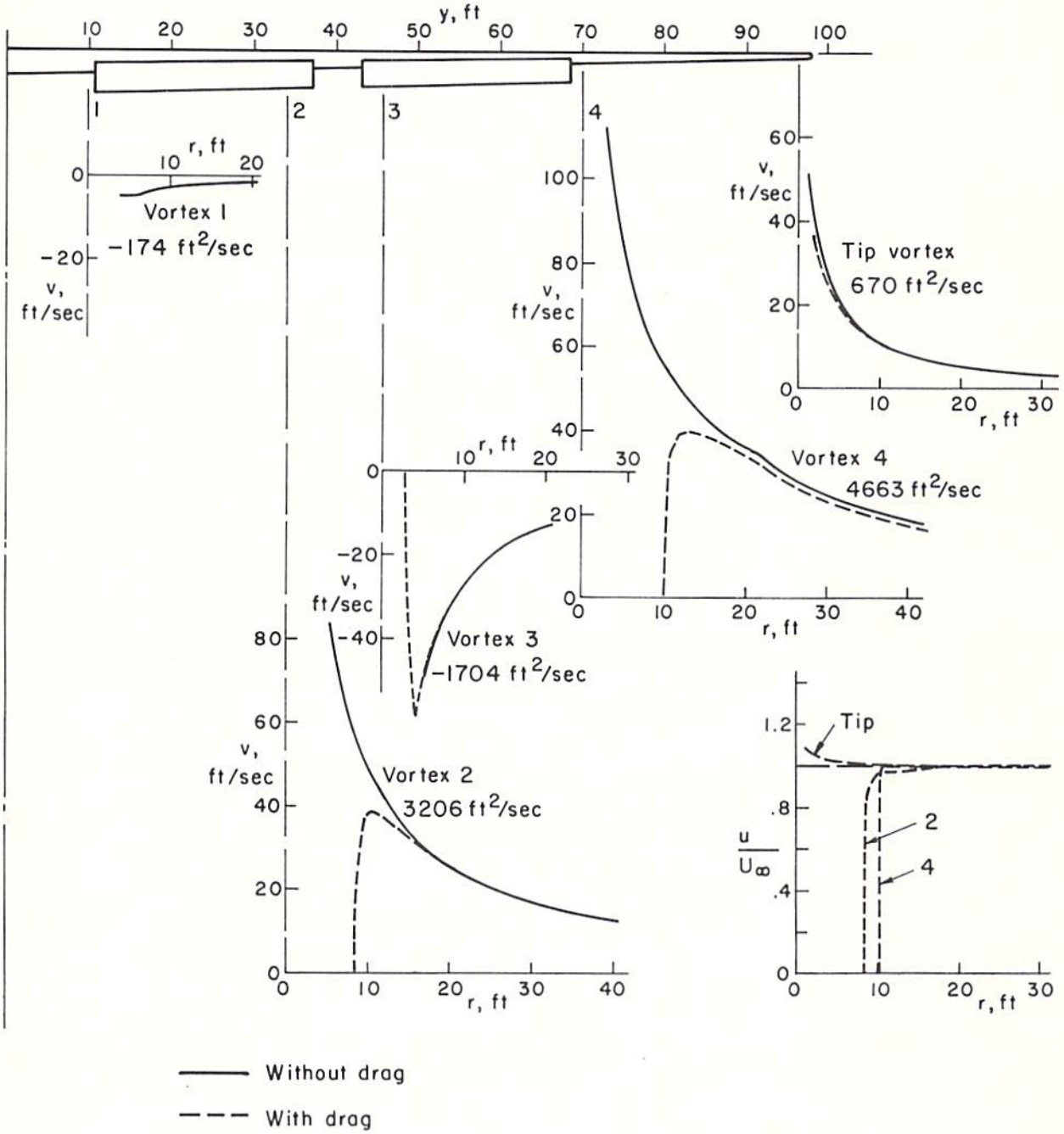

Fig. 4-14a. Computed swirl velocity profiles for a 747 aircraft in landing configuration ($\delta_f = 25^o$). NAFEC Run 26

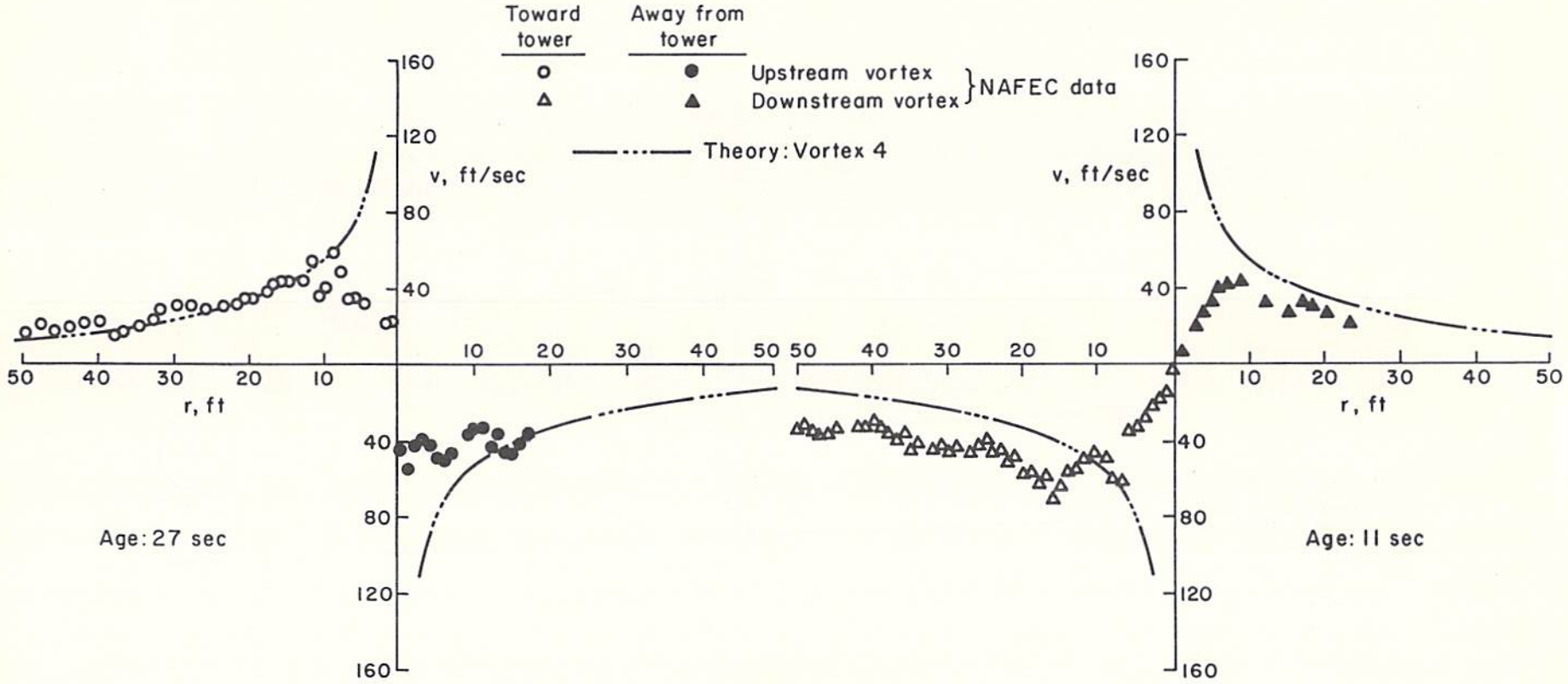

Fig. 4-14b. Comparison of measured and computed swirl velocity profiles for a 747 aircraft in landing configuration ($\delta_f = 25^\circ$). NAFEC Run 26

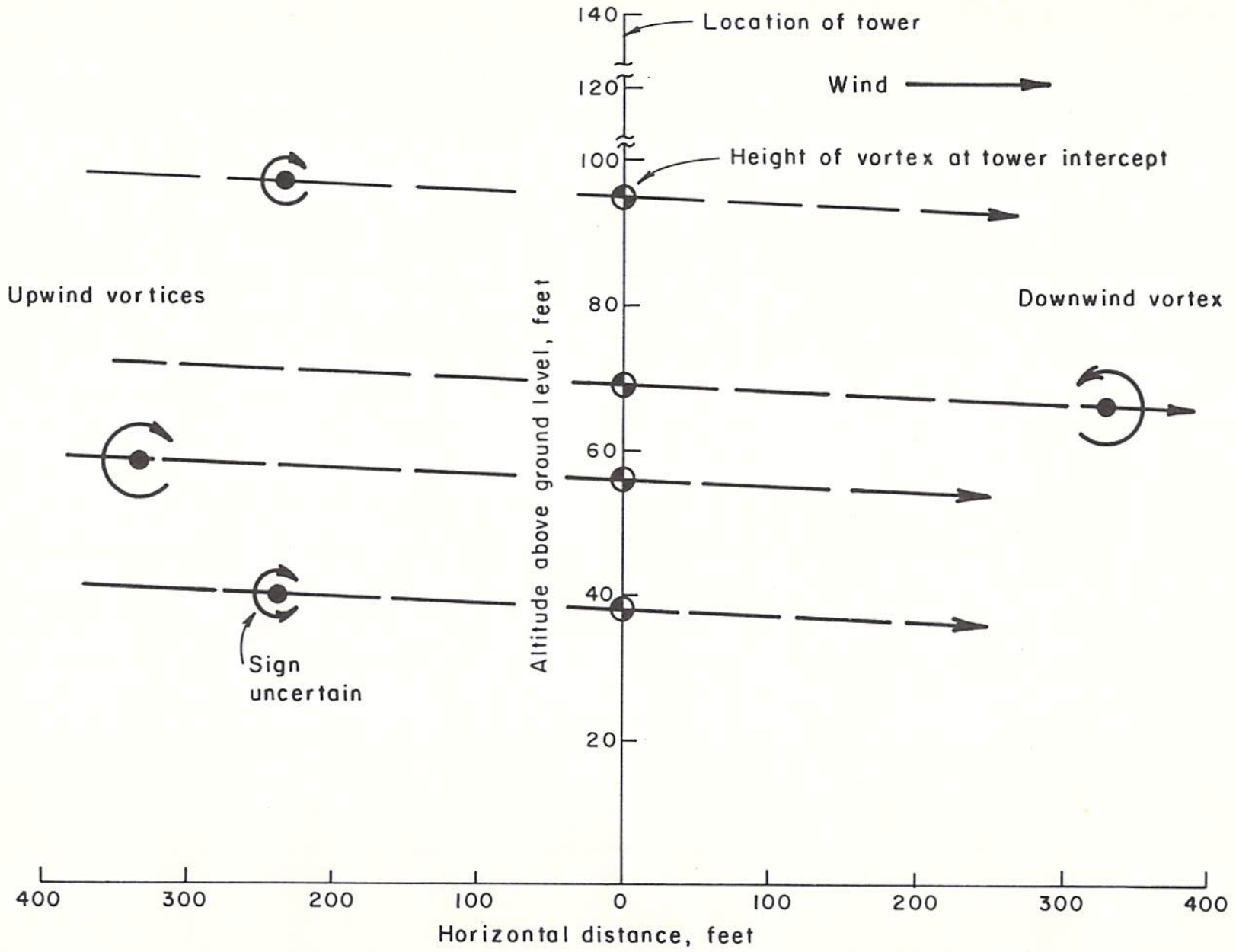

Fig. 4-15. Illustration of multiple vortices in wake of DC-10 aircraft in landing configuration. NAFEC Run 16

are the only ones of all those examined in this study which exhibit large viscous cores. In the present case, the core is over 20 feet in diameter. Some cases for the L-1011 and DC-10 in landing configuration showed measurable cores, but these were less than ten feet in diameter.

4.3 Vortex merging and its effect on wake descent rate

As has been illustrated in the foregoing review, there is mounting evidence that the multiple vortices shed from certain aircraft with flaps deployed do not remain distinct but merge at some distance downstream. Dunham, as cited in Ref. 17, first observed this phenomenon in towing tank experiments where ink was used to mark the flap and tip vortices. In these experiments, merging occurred between 30 and 45 span lengths behind the aircraft. Movies of flight tests with a 727 aircraft where flaps were slowly deployed and the wake was marked by oil vapor also show this phenomenon (Ref. 16). The distance behind the aircraft at which merging occurred, however, was difficult to discern from the movies.

This merging phenomenon has two important consequences. The first is that merging involves rapid turbulent redistribution of the trailed vorticity, which quite effectively ages the wake. This mechanism is now believed to be responsible for the success of the NASA low vortex hazard configuration which has recently been flight tested.

The second consequence is that if this merging process always occurs, the inputs of initial vortex separation and strength for the wake vortex transport predictive model may be directly specified, without having to assume an elliptic load distribution. One cannot say with certainty that all vortices shed from one half of a wing eventually merge, but an investigation into the motion of vortex pairs (see Fig. 2.2, Ref. 7) seems to suggest that for conventional aircraft this might be the case.

Postulating that merging does, in fact, occur fixes the resulting net vortex strength from one half of the wing to be the wing root circulation Γ_o. For the aircraft analyzed in this study Γ_o can be obtained from

$$\frac{2\Gamma_o}{U_\infty \bar{c}} = \left.\frac{c_\ell c}{\bar{c}}\right|_o \tag{29}$$

where the root sectional loading $c_\ell c/\bar{c}|_o$ is shown in Figs. 3-1 through 3-14. The initial separation $2\bar{y}(=b')$ of the merged vortices is obtained from $W = \rho U_\infty \Gamma_o 2\bar{y}$ where W is the weight of the aircraft (see Table 1).

To see how much of an error might be introduced into the initial wake descent velocity dh/dt (see Table 1), we compare the descent velocity of a wake from an elliptically loaded wing to the descent velocity obtained by merging the vortices from the actual load distribution. It is not difficult to show that

$$\frac{dh/dt|_{ellipt}}{dh/dt|_{merged}} = \left(\frac{4C_L}{\pi c_\ell c/\bar{c}|_o}\right)^2 \tag{30}$$

where $c_\ell c/\bar{c}|_o$ is the wing root loading. In the following table Eq. (30) is tabulated for the DC-10 aircraft.

Conf.	C_L	$\left.\frac{dh}{dt}\right\|_{ellipt} \Big/ \left.\frac{dh}{dt}\right\|_{merged}$
H	0.1	0.34
H	0.4	0.65
TO	1.0	0.75
TO	1.4	0.78
L	1.0	0.71
L	1.4	0.74
TA	1.0	0.73
TA	1.4	0.76

As can be seen, the assumption that the wake is that trailed from an elliptically loaded wing may result in appreciable errors in the initial descent velocity.

5. CONCLUSIONS

The object of this study has been to compare measured swirl velocity distributions of the wake vortices of the B-747, B-727, DC-10, and L-1011 with distributions computed from the Betz roll-up method. Swirl velocity distributions from 53 flybys have been analyzed. The aircraft configurations include cruise/holding, landing, take-off, and take-off/approach. The following conclusions have been reached as a result of this effort.

1. The wakes of these aircraft in the holding/cruise configuration, where the wing load distribution is simple, are well described by the Betz method. Comparisons of swirl velocities obtained from flyby measurement with computed velocities are in good agreement for the aircraft analyzed. The effect of distributed wing drag on the inviscid structure of these wakes is small, and while the axial velocity excesses or defects which can result are quite large, the radial extent of this region is small.

2. The wakes of these aircraft in a landing, take-off, or take-off/approach configuration are extremely complicated due to the spanwise segmentation of their flaps. While observation and measurements in the near field have shown that multiple vortices are trailed, analysis of flyby data strongly suggests in most cases that merging of vortices occurs by the time that the vortices intercept the measurement tower. The result of merging is that, ultimately, downstream only one vortex pair can be discerned. Since the merging process is one of turbulent interaction, there is little hope of obtaining vortex structure from the inviscid Betz method. In these cases, an analytic determination of axial and swirl velocity distributions must be obtained from a complete numerical solution of the flow field. Since it has been assumed that interior and tip vortices roll up independently of each other and remain discrete, it is not surprising that agreement between measured swirl velocities and computed distributions is unsatisfactory.

3. The effect of distributed wing drag on the structure of the "interior" vortices, which are part of a multiple pair wake, is at first glance quite significant near the vortex center in that the peak swirl velocities are reduced significantly. Closer inspection reveals that the extent to which the vortex has been de-intensified, in terms of the rolling moment it can induce on an encountering aircraft, is not significant unless the aircraft's wing span is comparable to the size of the modified region. Since the largest drag-modified regions were found to be of the order of twenty feet in diameter, only the smaller general aviation aircraft can benefit from the immediate effects of drag. The large axial velocity deficits which result, however, are important in that they provide a mechanism by which turbulence is generated. The ultimate dissipation of the wake is a result of this turbulent transport.

6. RECOMMENDATIONS

In terms of incorporating the results of this effort into TSC's Wake Vortex Transport Model, a recommendation can be made regarding initial specification of wake vortex strength and separation. If it is assumed that merging of all vortices shed from each half of the wing occurs, initial vortex strength is the wing root circulation Γ_o which may be obtained from Table 1 for the aircraft and configurations investigated in this report. In addition, vortex separation b' and initial descent velocity are tabulated. It is anticipated that improvement in predicted vortex tracks would be obtained by using these descent rates and strengths over those values given by elliptical loading assumptions.

It must be emphasized, however, that the values of wing root circulation, vortex spacing, and initial descent velocities given in this report have been obtained from analytic considerations and may still depart from those of actual aircraft. The reason is that lifting surface theory or vortex-lattice theories which are currently considered to be the most reliable methods of computing wing load distributions are not adequate for wings with slats and flaps deployed. It is, therefore, not surprising that the effect of the fuselage on the wing load distribution is not reliably treated with these methods.

Clearly, the least understood phenomenon in aircraft wake vortex dynamics is turbulent transport. The merging phenomenon illustrates the turbulent vortex-vortex interaction, and it is this process which is believed to be responsible for the low hazard wake now under study by NASA. Other problems appear to be equally important, and these include the interaction of the wake with the turbulent atmosphere and the interaction of the turbulent wake with the ground. The lifespan of an aircraft wake is ultimately determined by turbulent transport, and it is suggested that research be continued in these areas.

APPENDIX FIGURES

A-1 - A-39

Comparisons of calculated
tangential velocity profiles with
measurements made by NAFEC
for 727, L-1011, DC-10 and 747 aircraft.

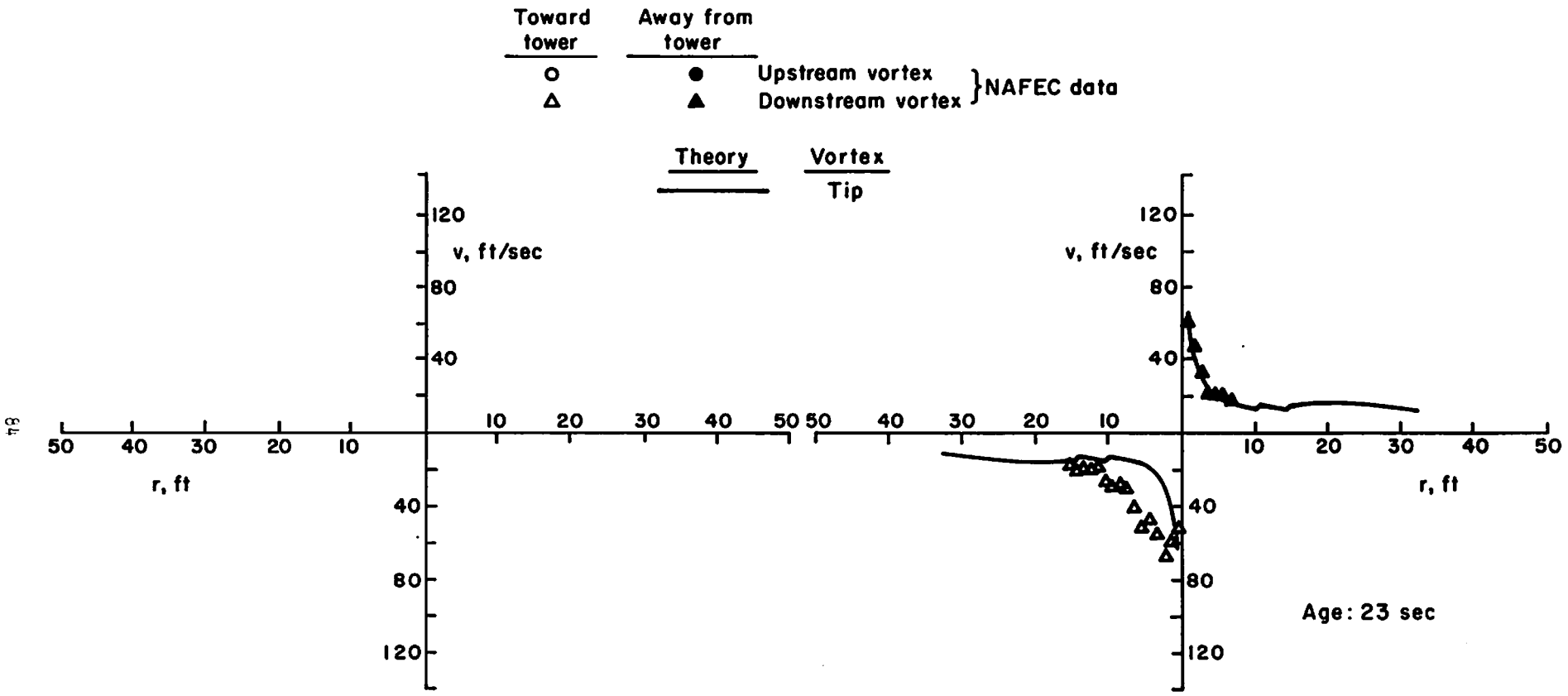

Fig. A-1. 727 Holding. NAFEC Run 34

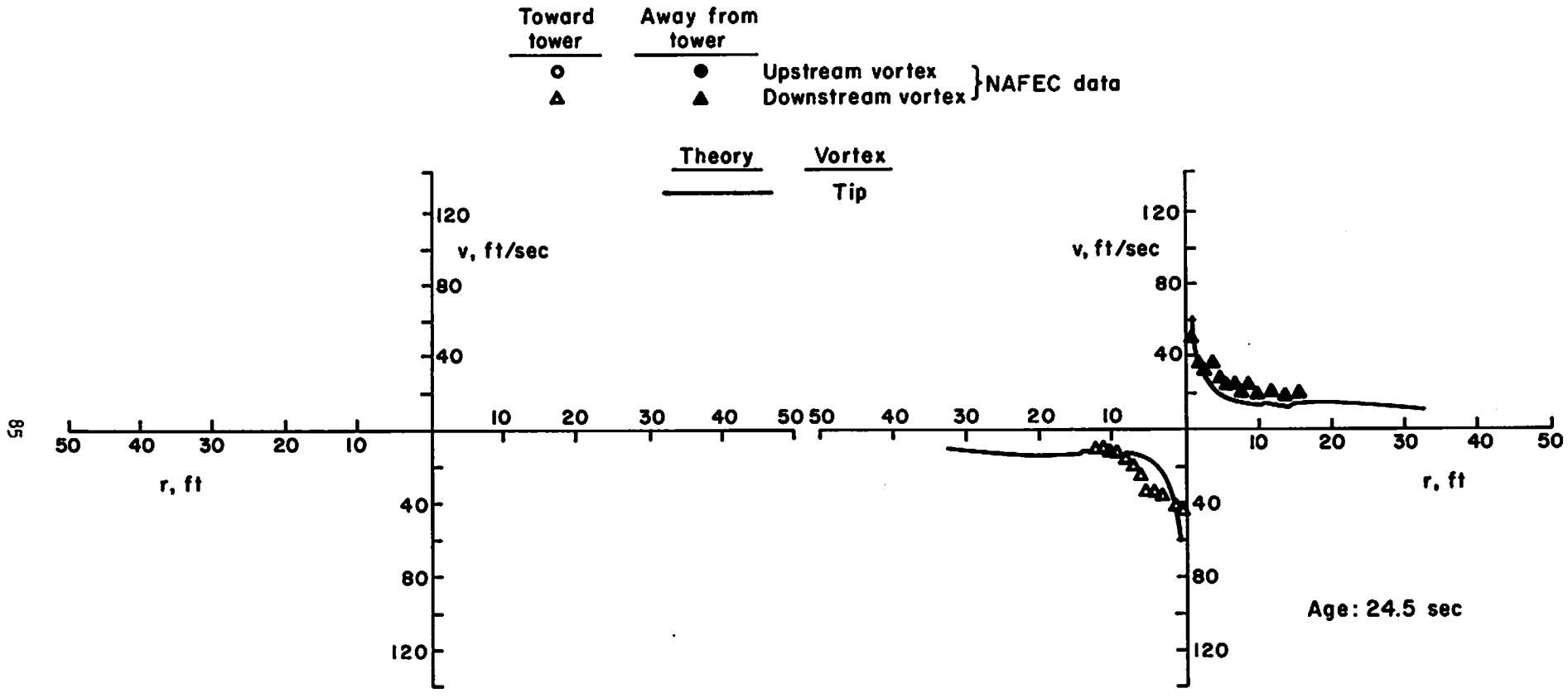

Fig. A-2. 727 Holding. NAFEC Run 35

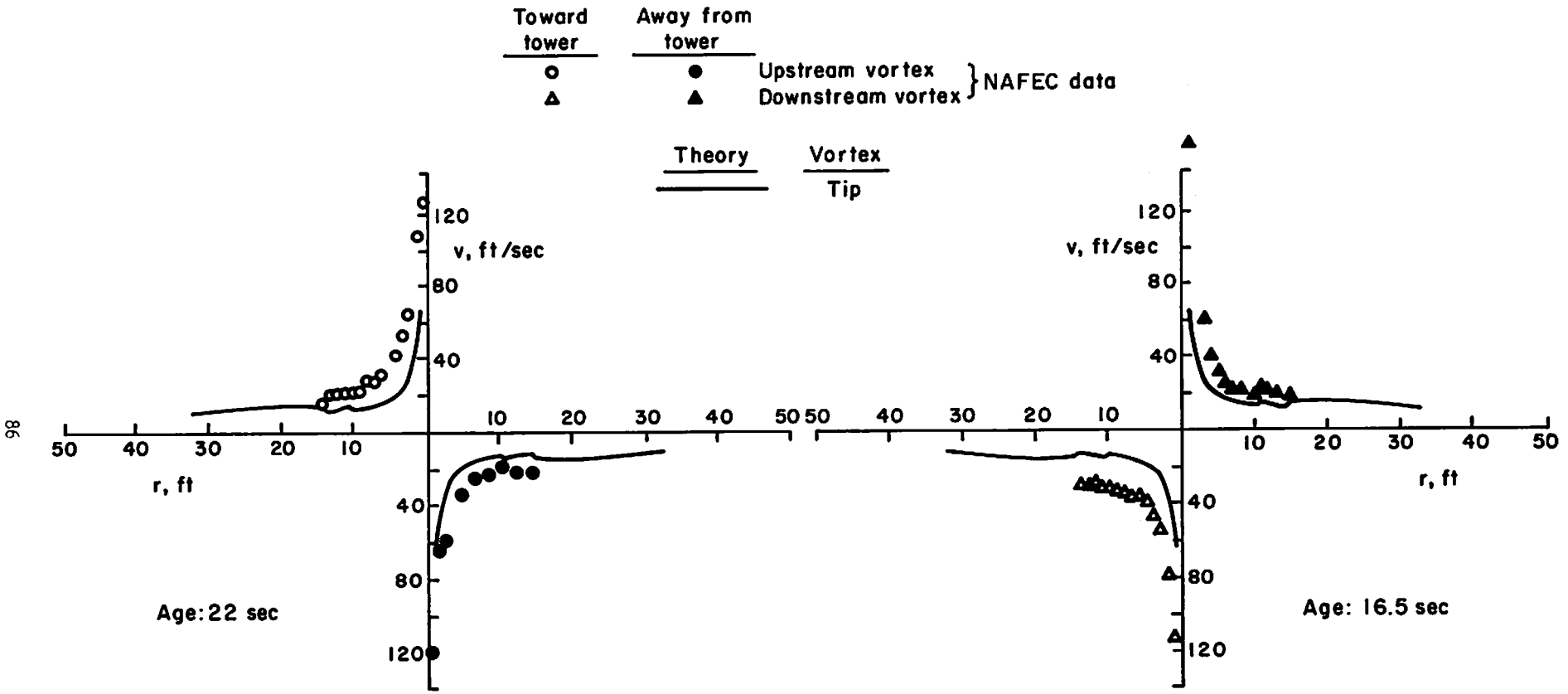

Fig. A-3. 727 Holding. NAFEC Run 36

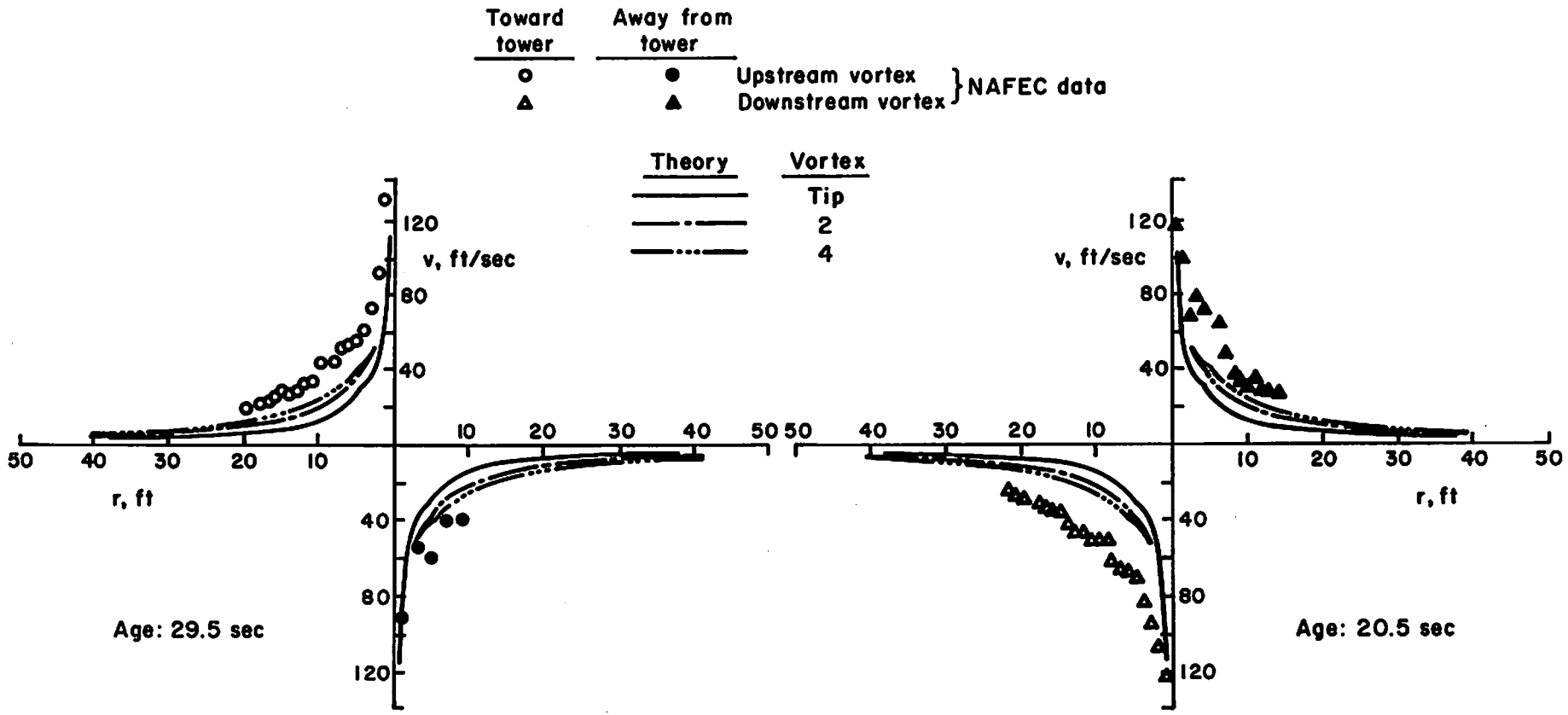

Fig. A-4. 727 Take-off. NAFEC Run 26

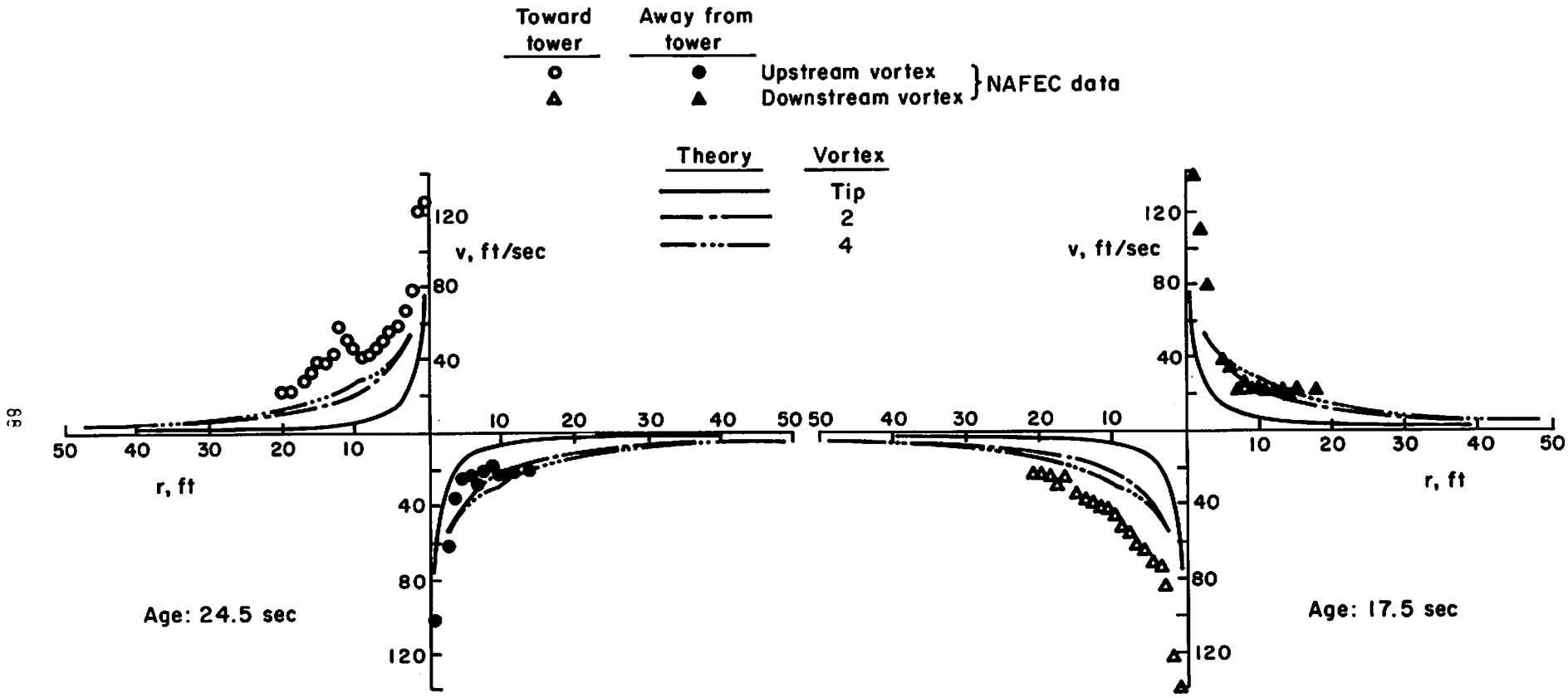

Fig. A-5. 727 Take-off. NAFEC Run 41

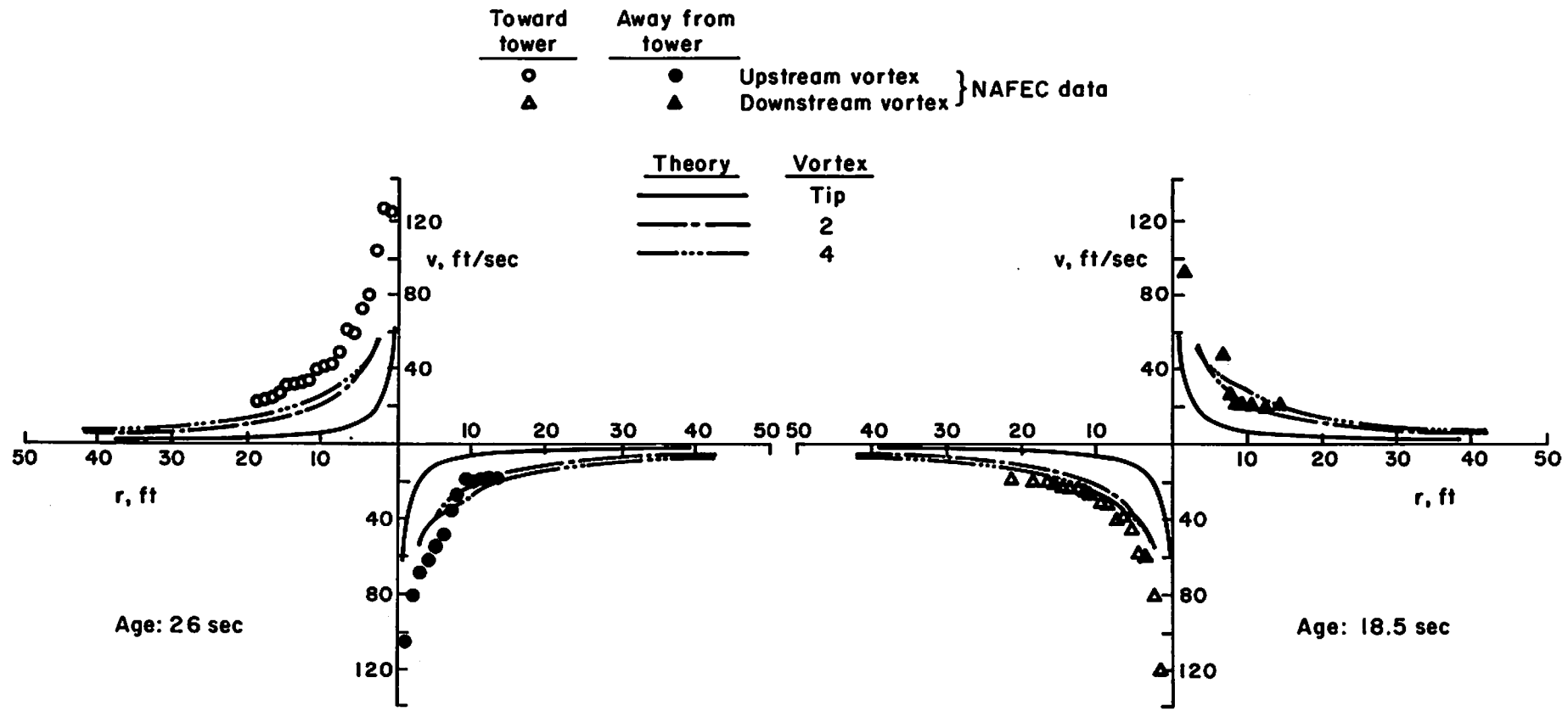

Fig. A-6. 727 Take-off. NAFEC Run 42

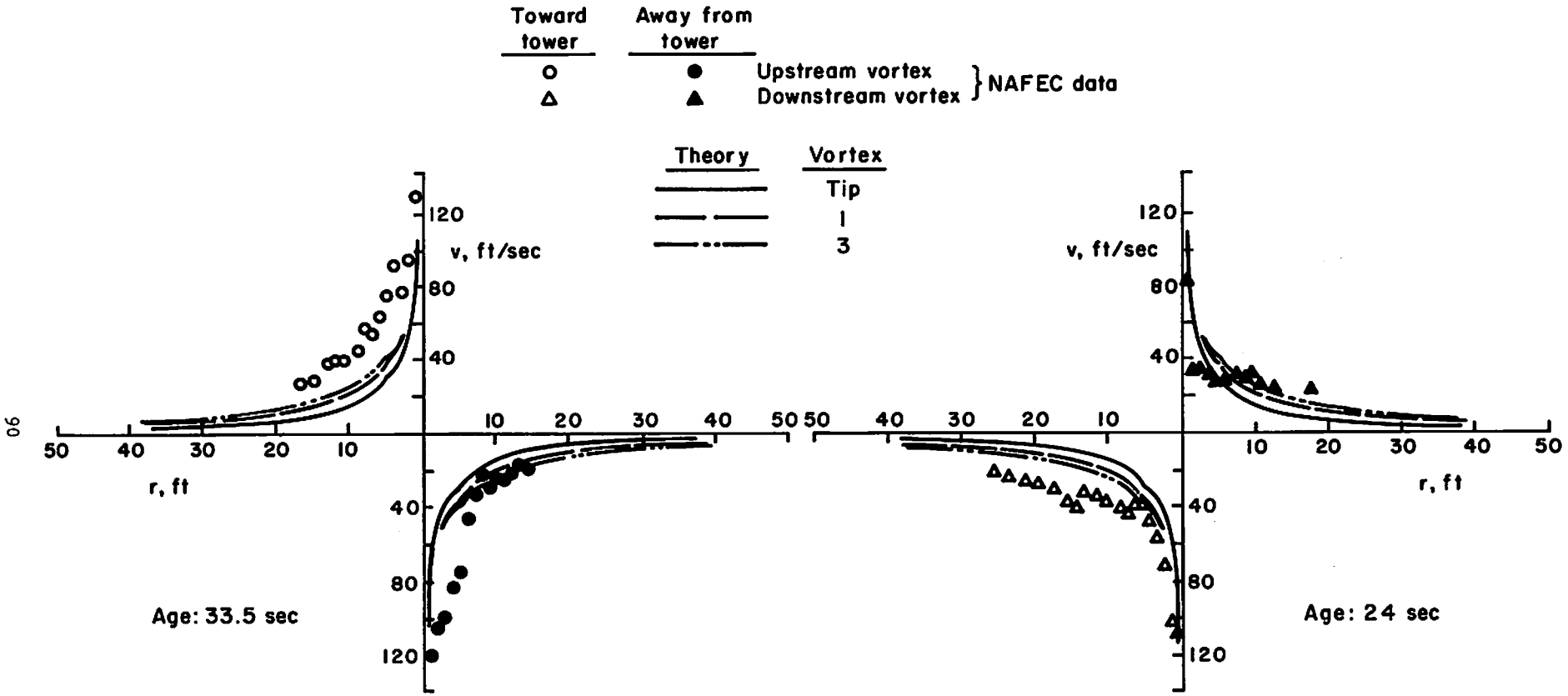

Fig. A-7. 727 Take-off. NAFEC Run 53

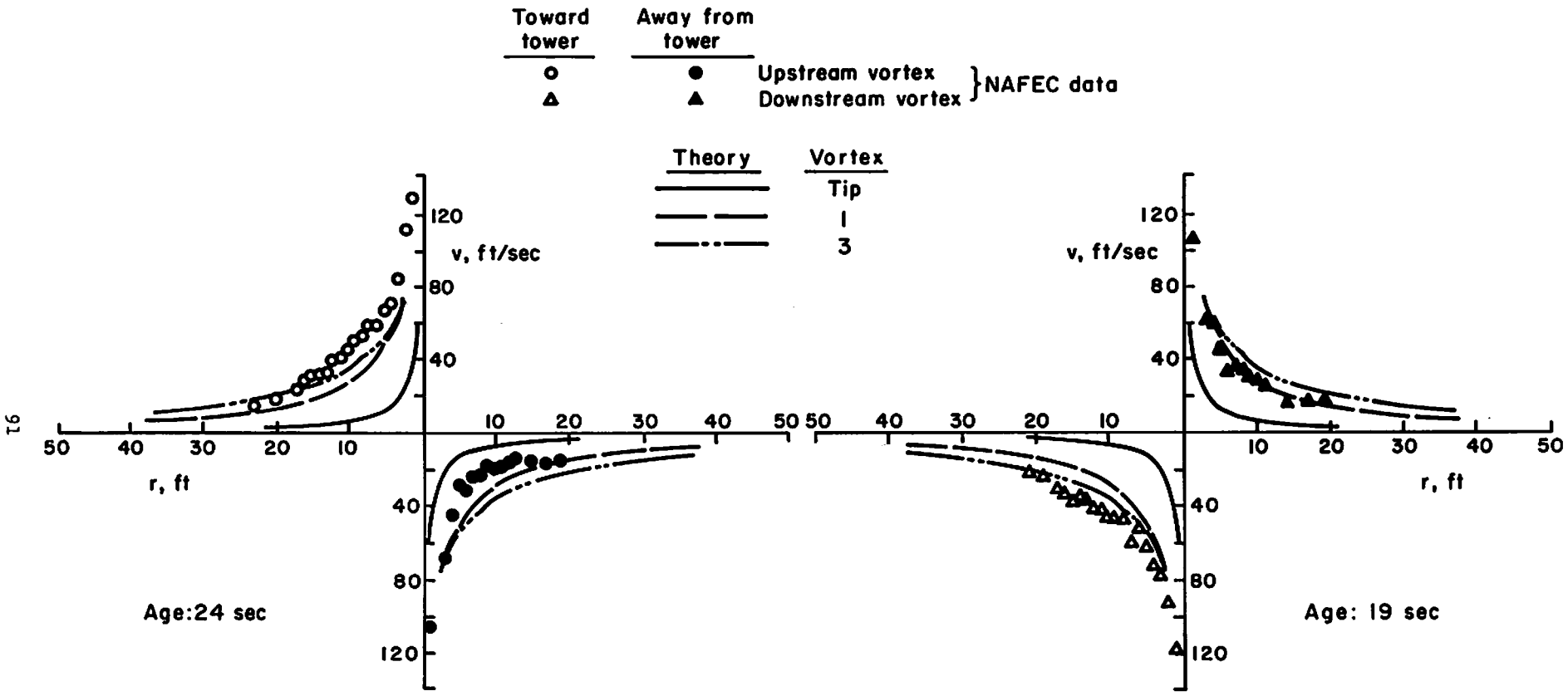

Fig. A-8. 727 Landing. NAFEC Run 45

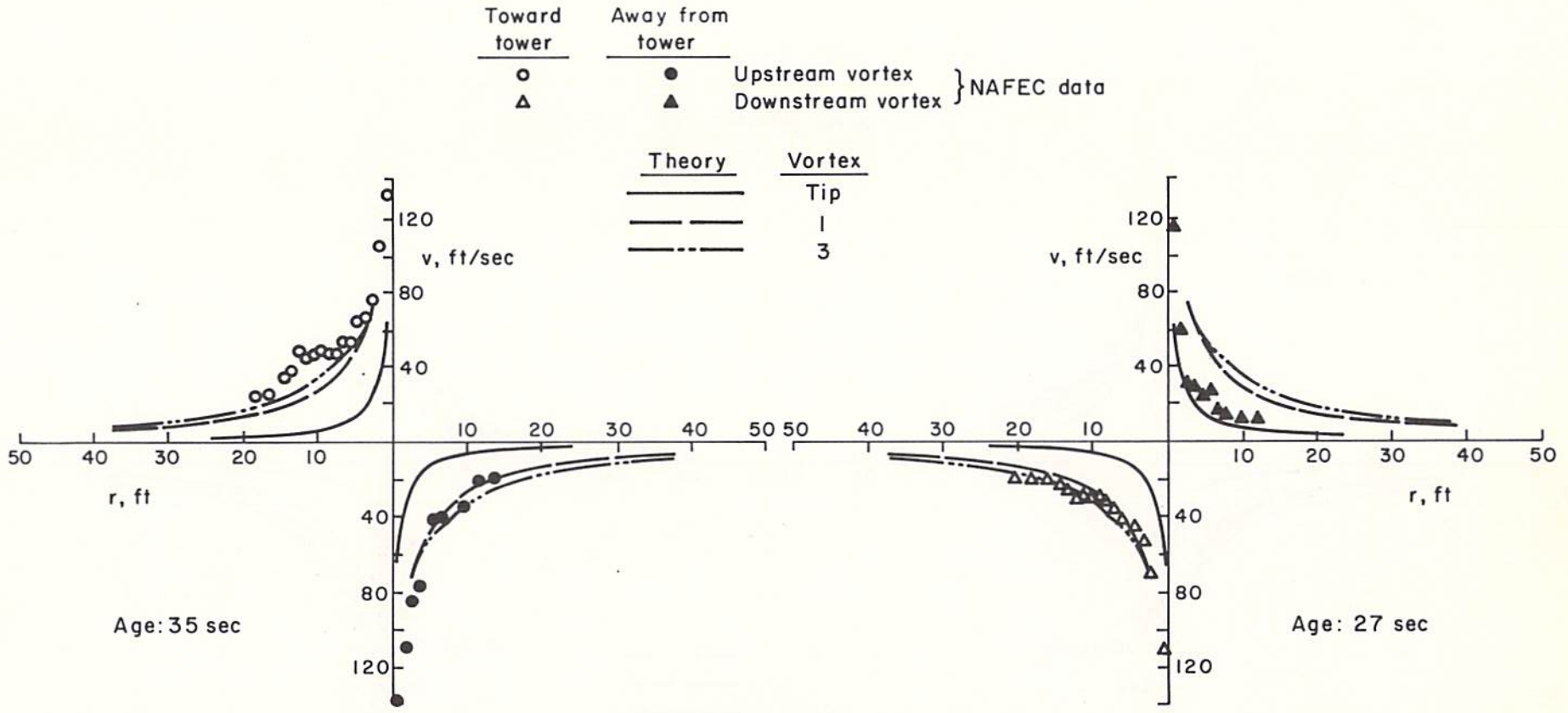

Fig. A-9. 727 Landing. NAFEC Run 58

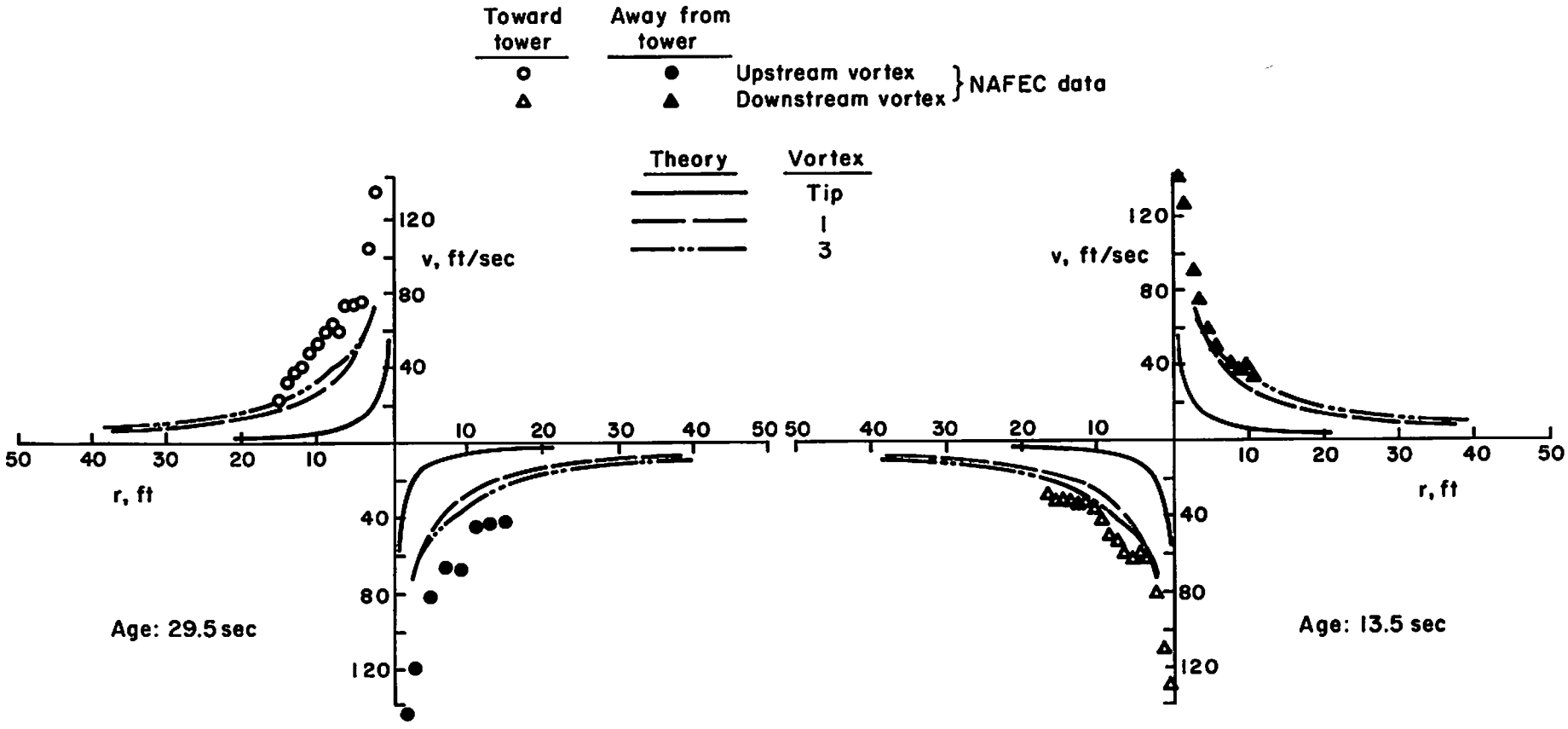

Fig. A-10. 727 Landing. NAFEC Run 77

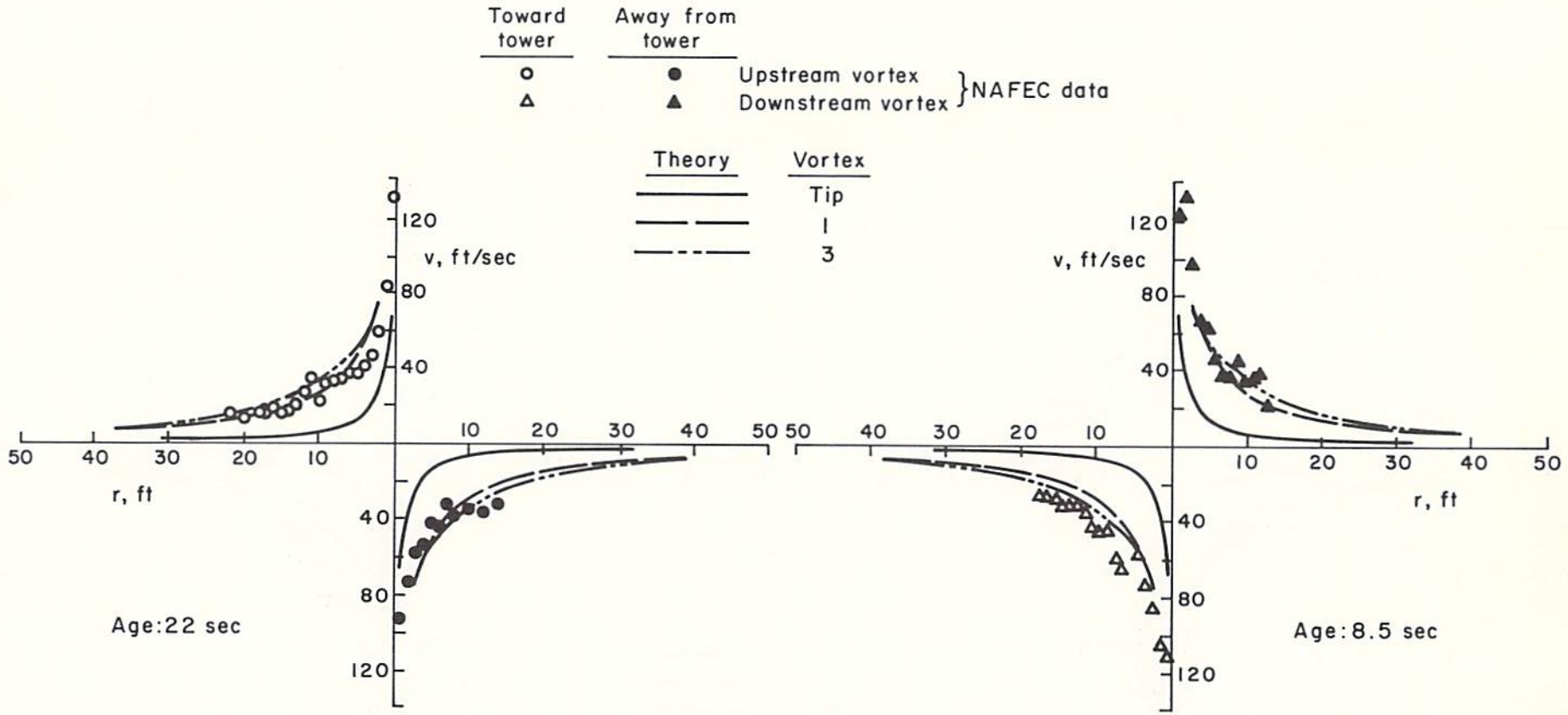

Fig. A-11. 727 Landing. NAFEC Run 106

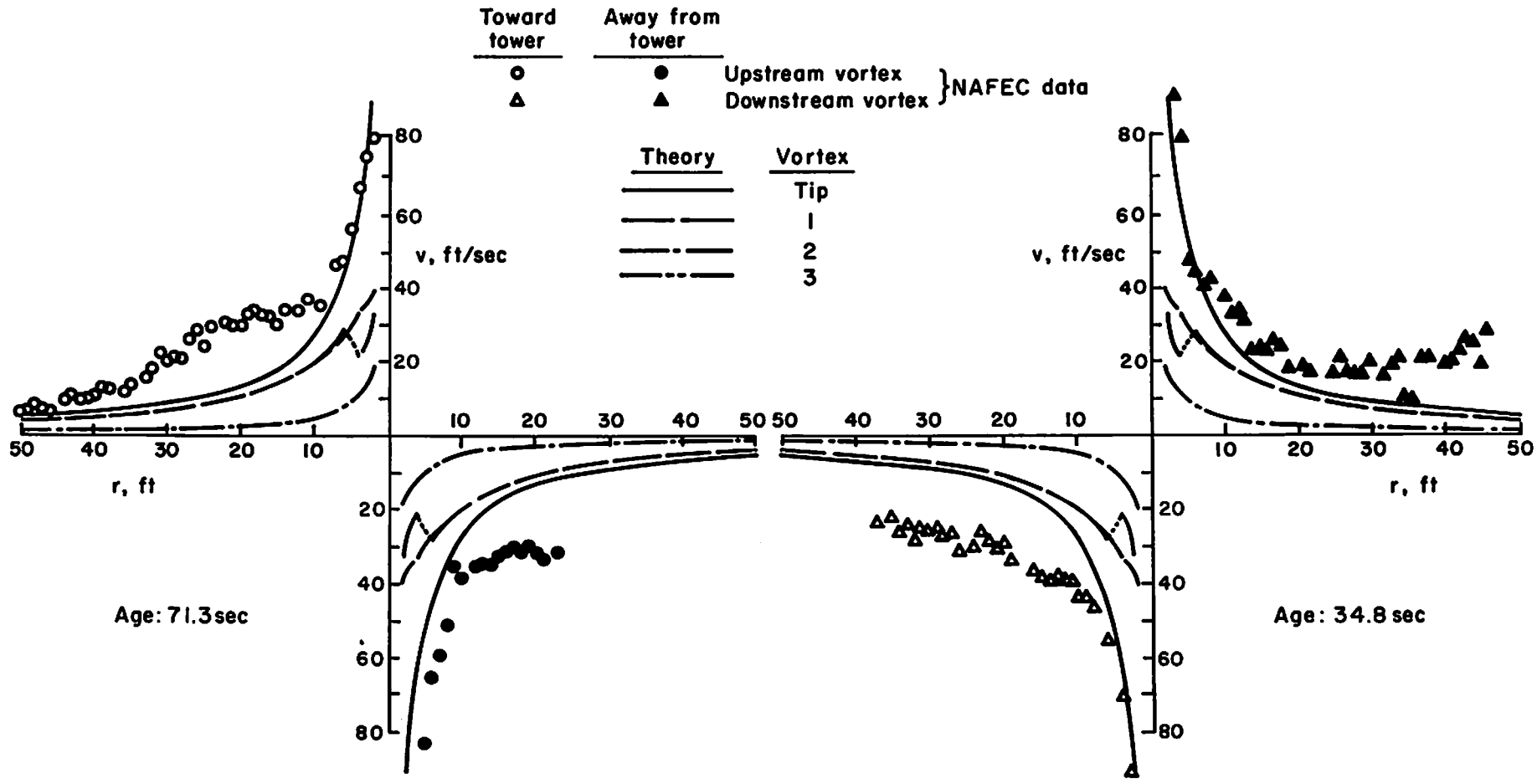

Fig. A-12. L-1011 Take-off. NAFEC Run 15

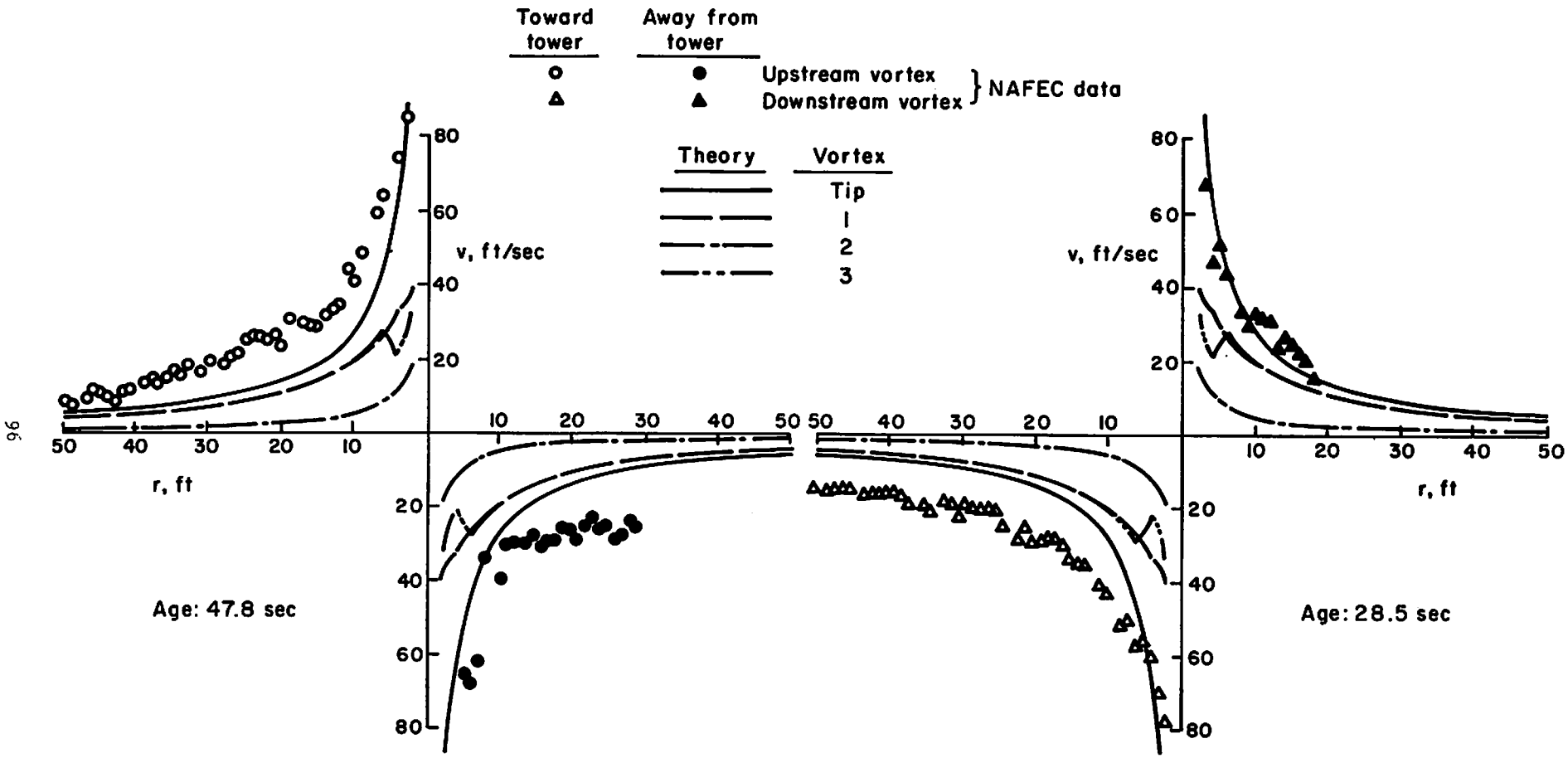

Fig. A-13. L-1011 Take-off. NAFEC Run 16

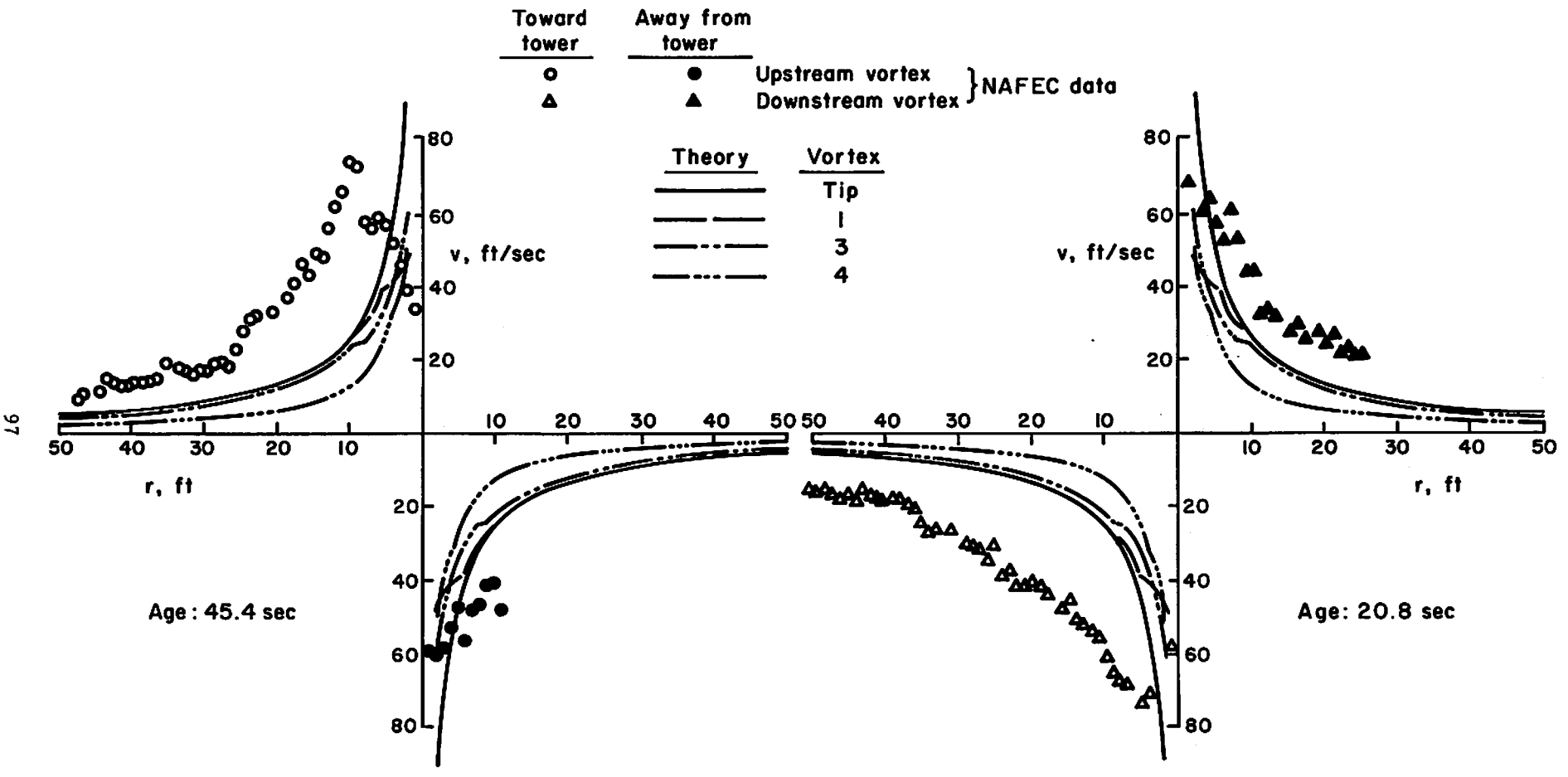

Fig. A-14. L-1011 Take-off/Approach. NAFEC Run 9

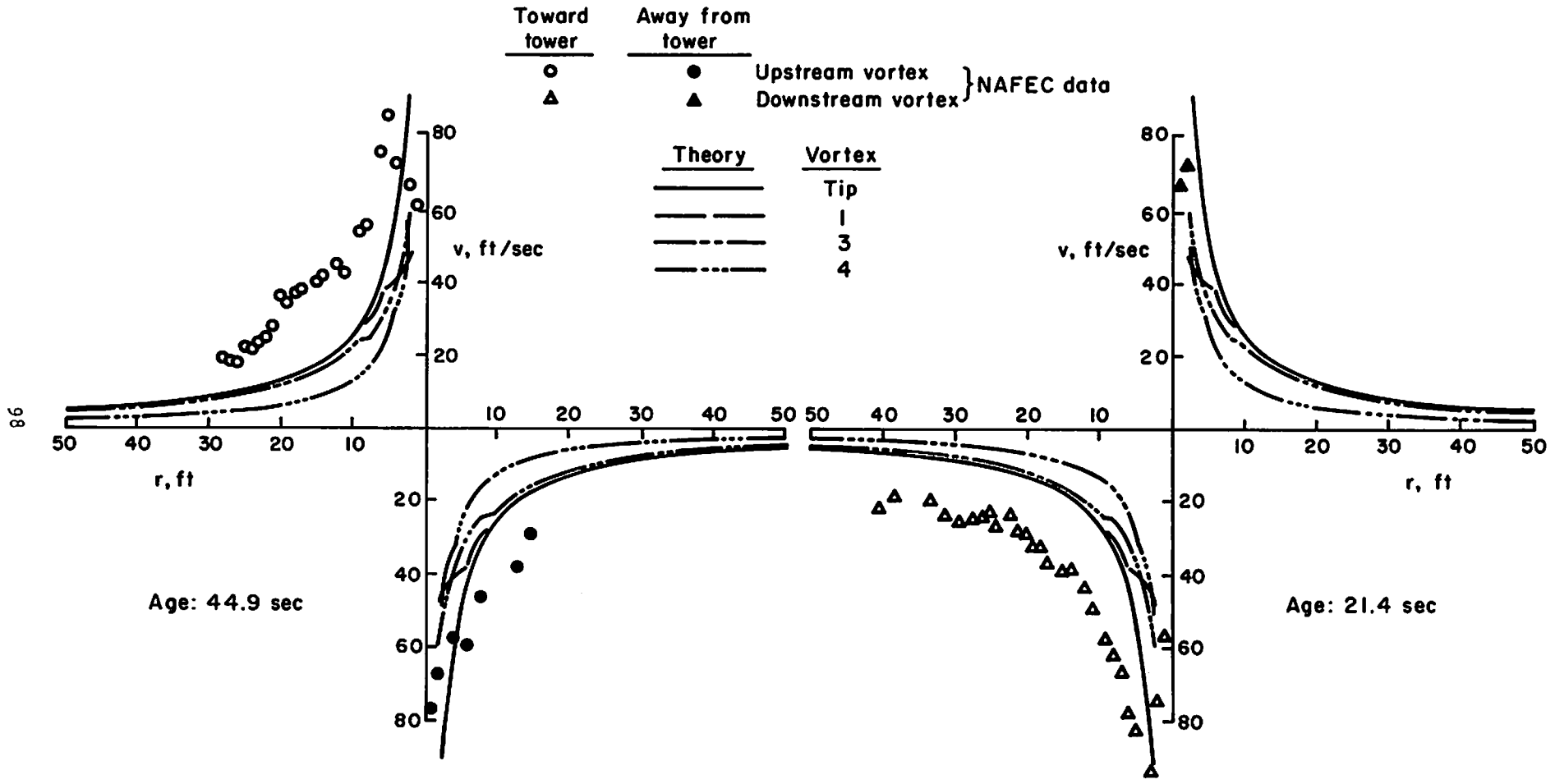

Fig. A-15. L-1011 Take-off/Approach. NAFEC Run 11

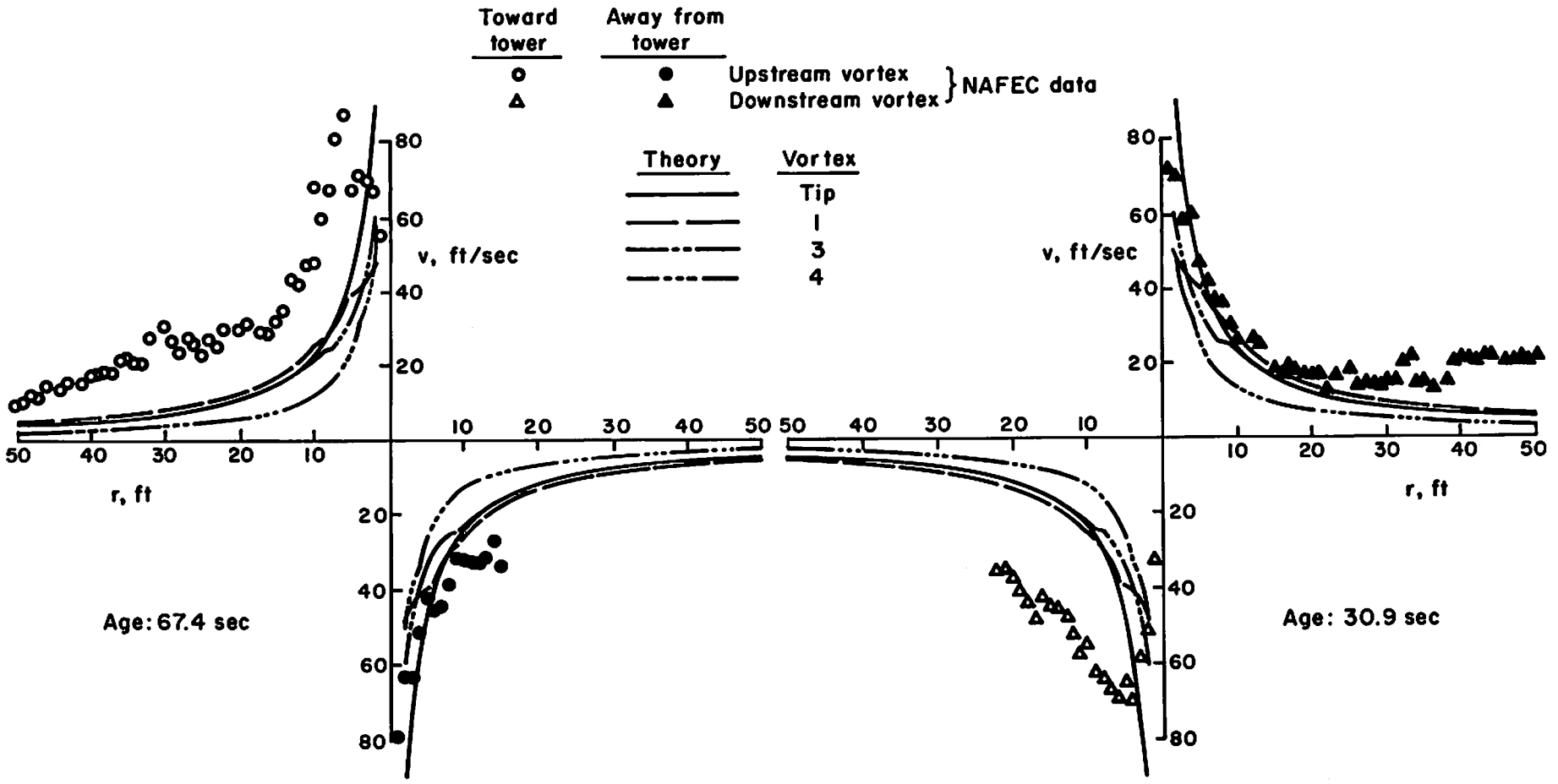

Fig. A-16. L-1011 Take-off/Approach. NAFEC Run 12

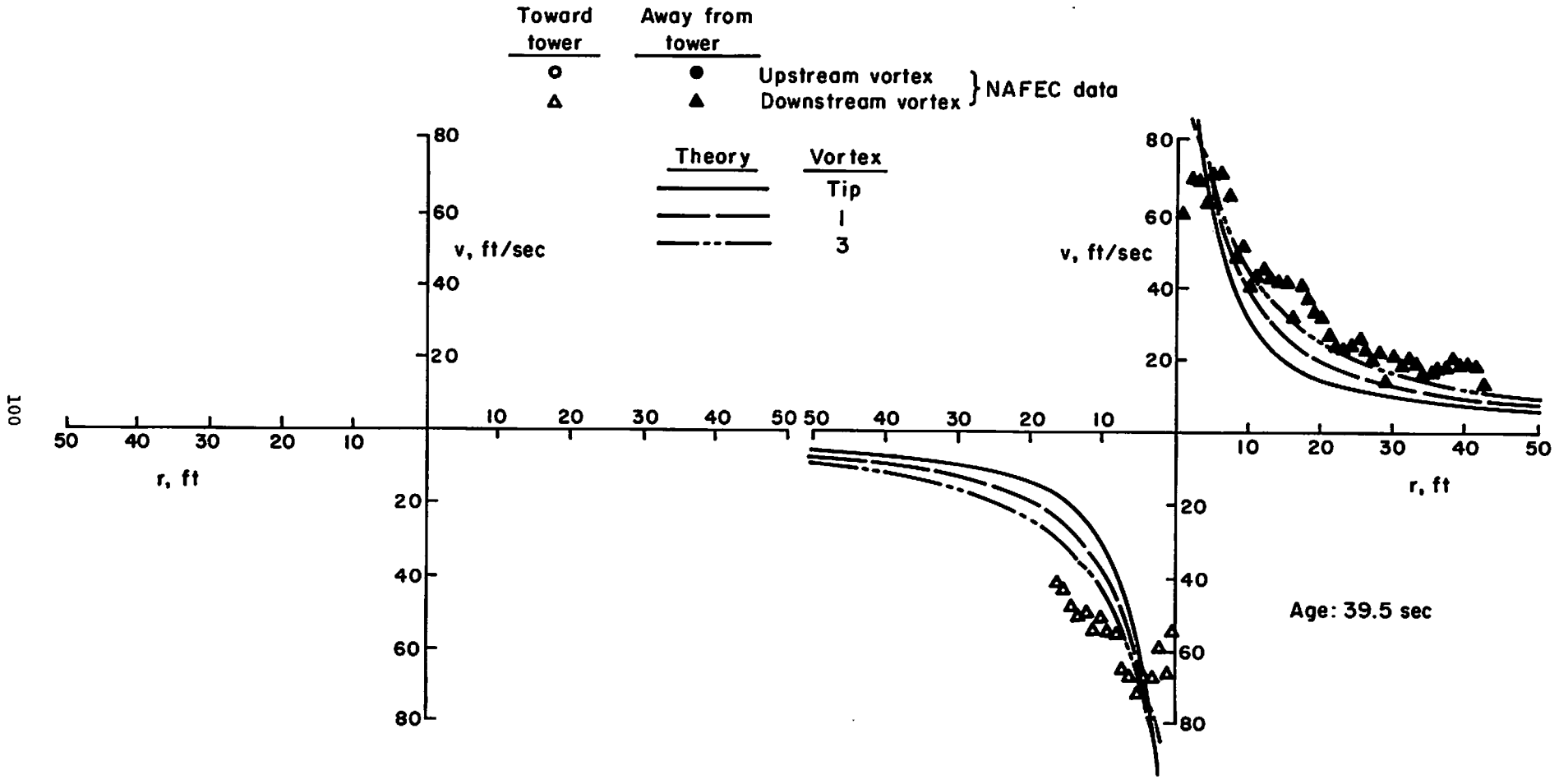

Fig. A-17. L-1011 Landing. NAFEC Run 2

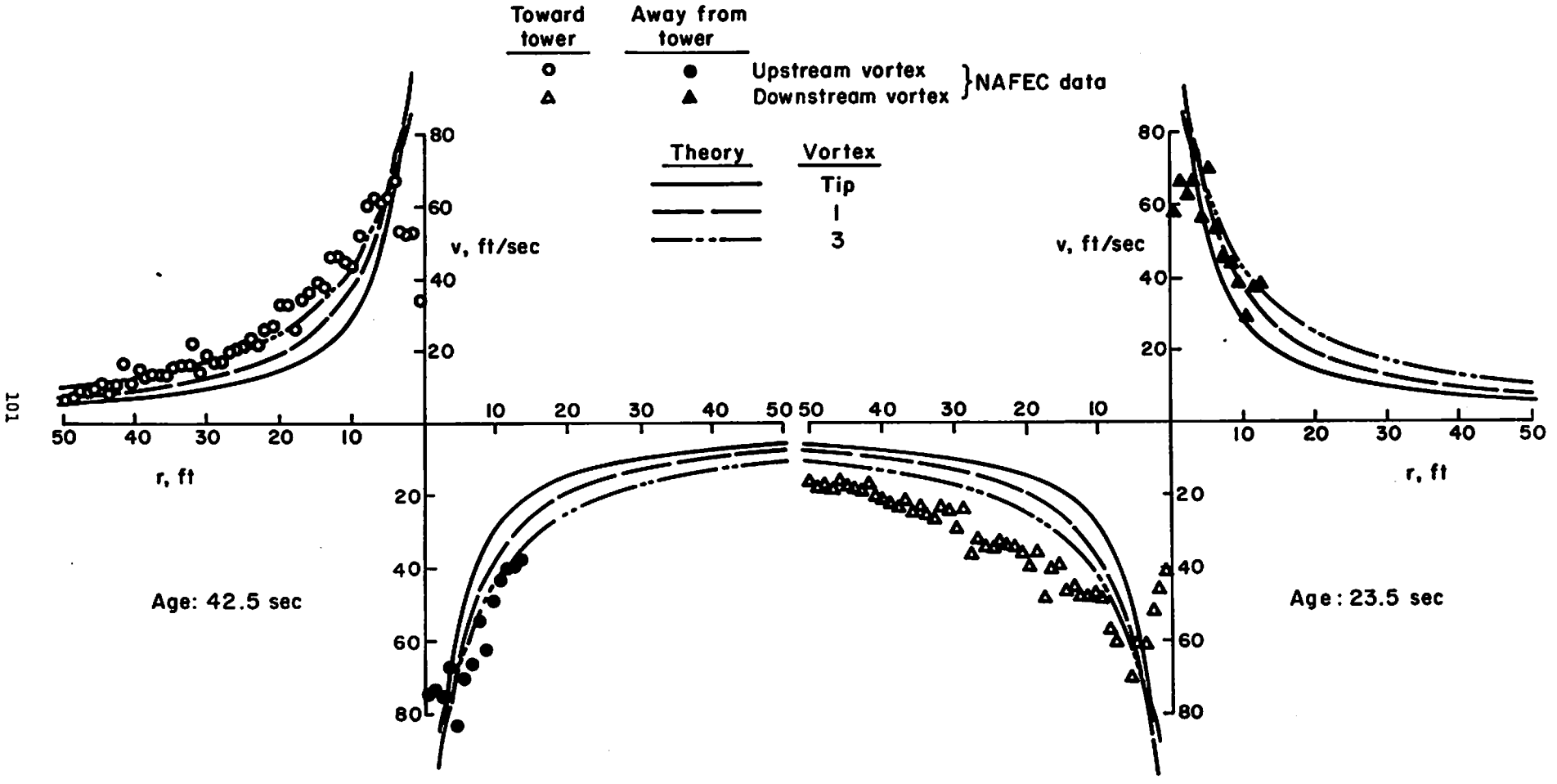

Fig. A-18. L-1011 Landing. NAFEC Run 6

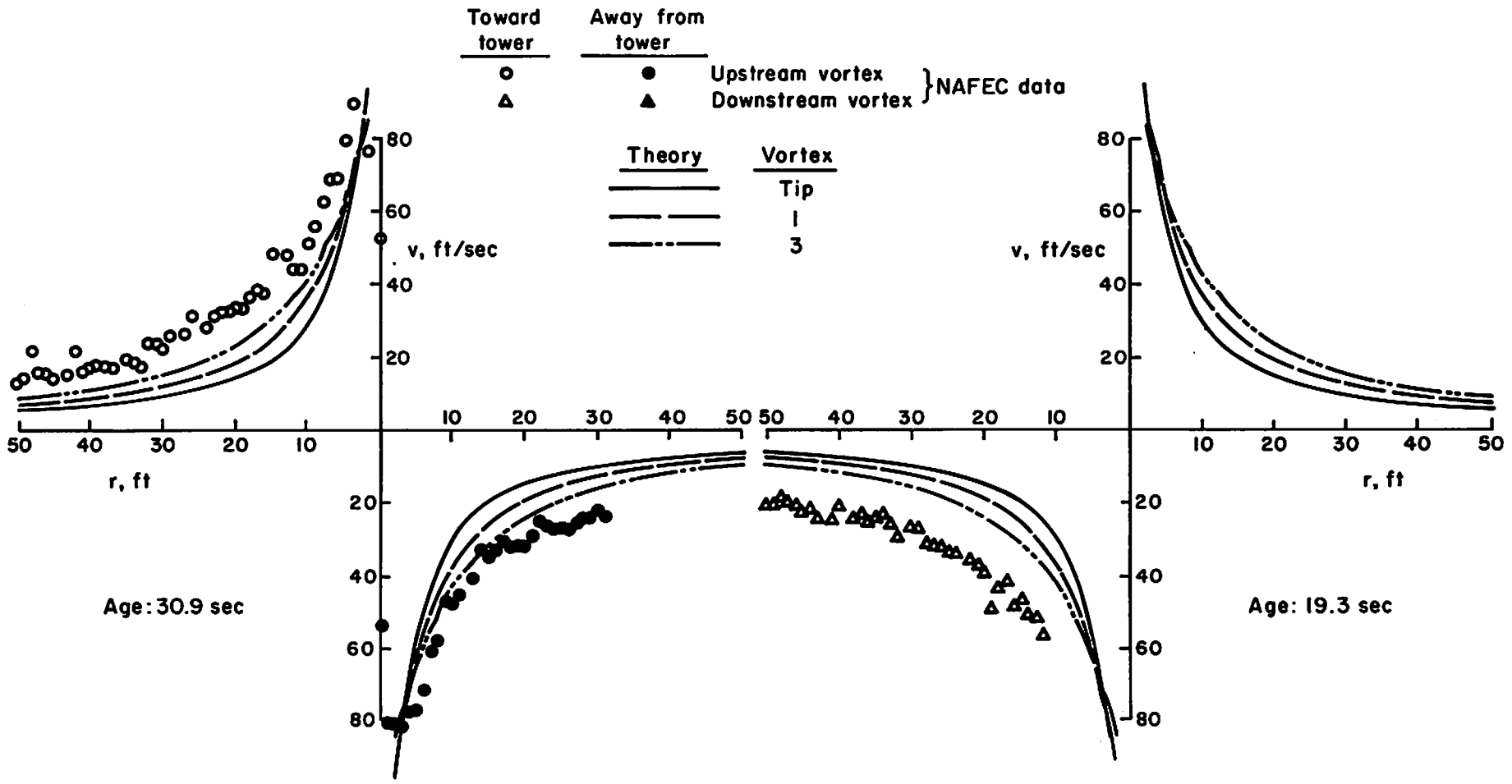

Fig. A-19. L-1011 Landing. NAFEC Run 7

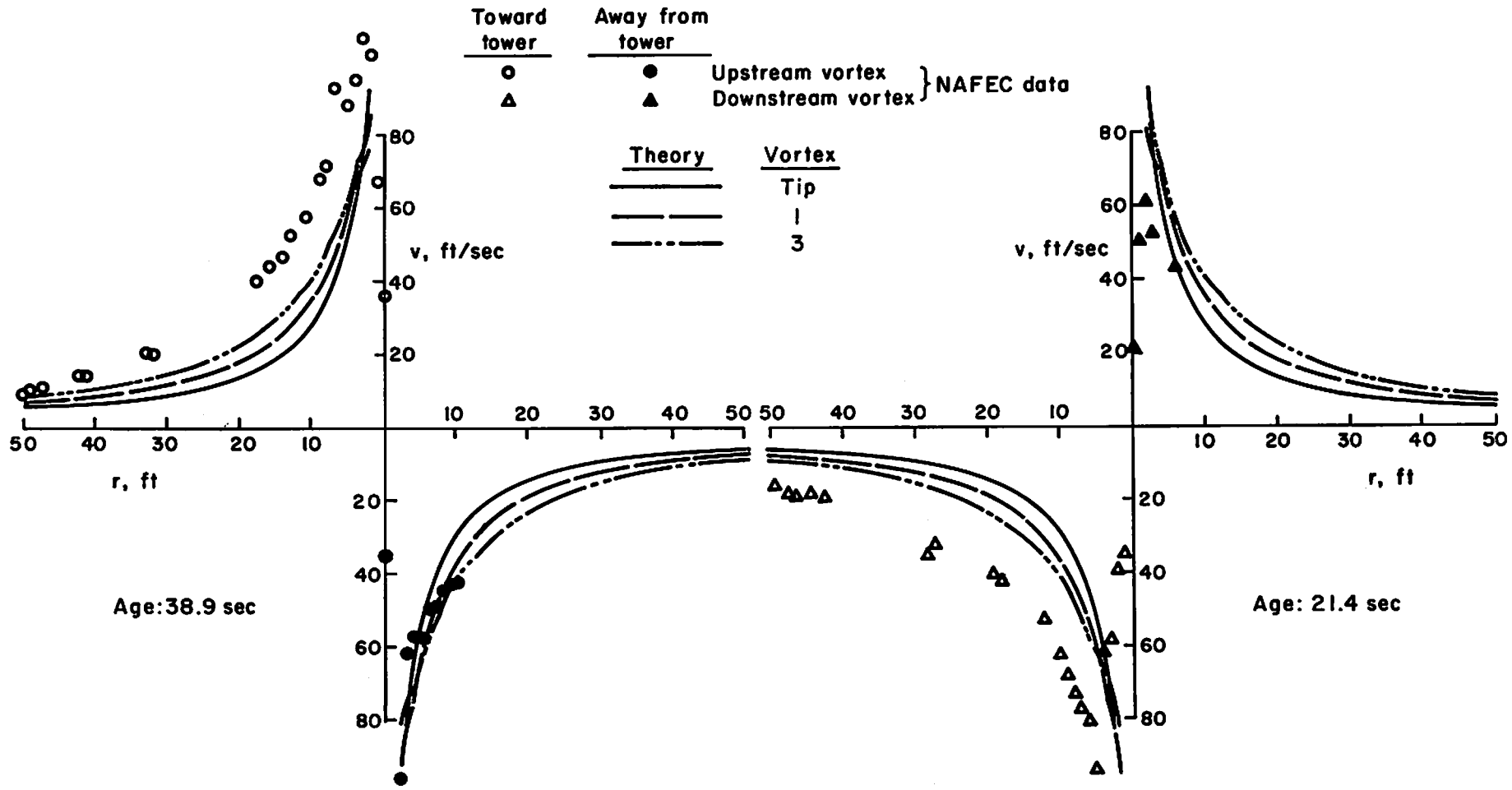

Fig. A-20. L-1011 Landing. NAFEC Run 18

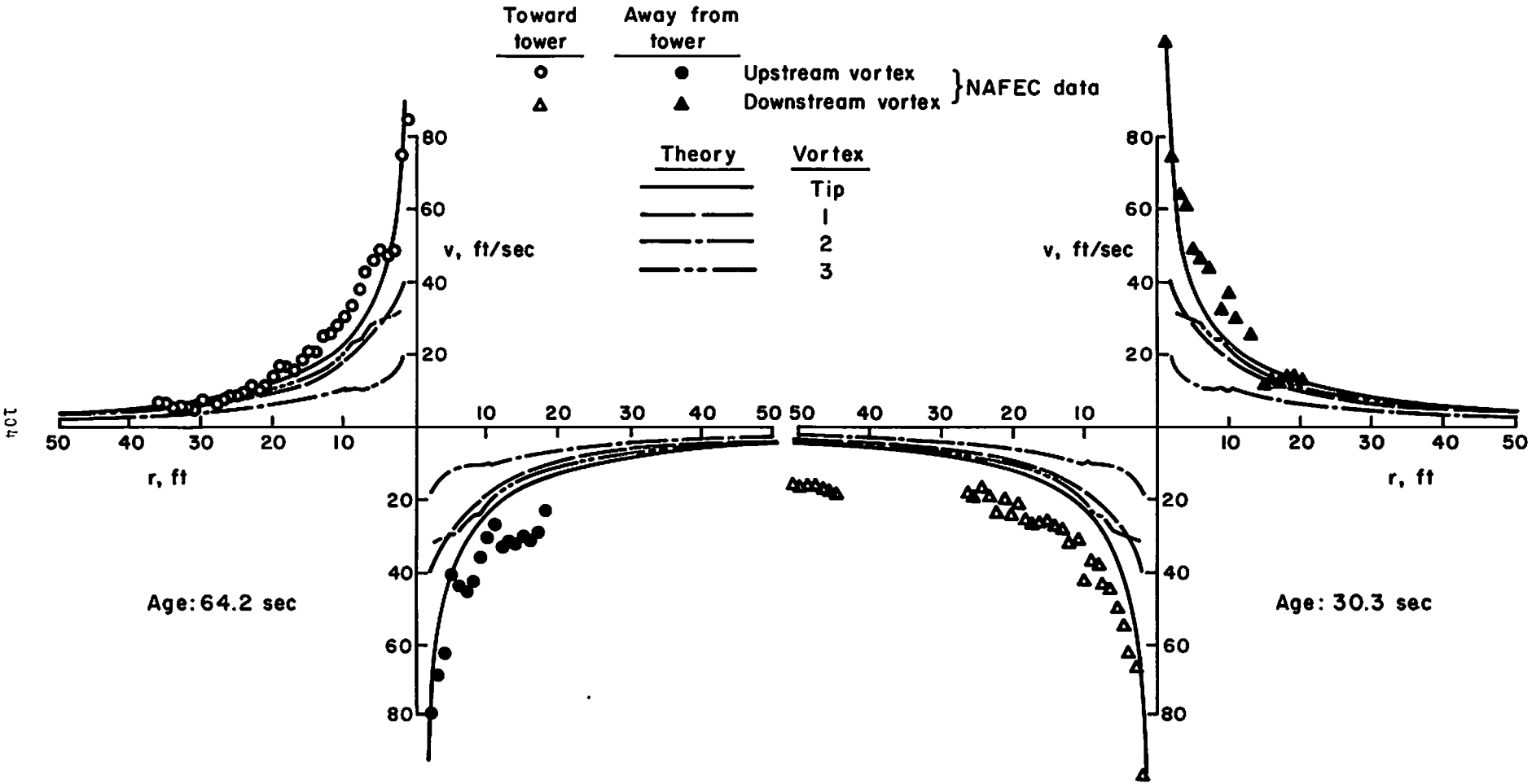

Fig. A-21. DC-10 Take-off. NAFEC Run 3

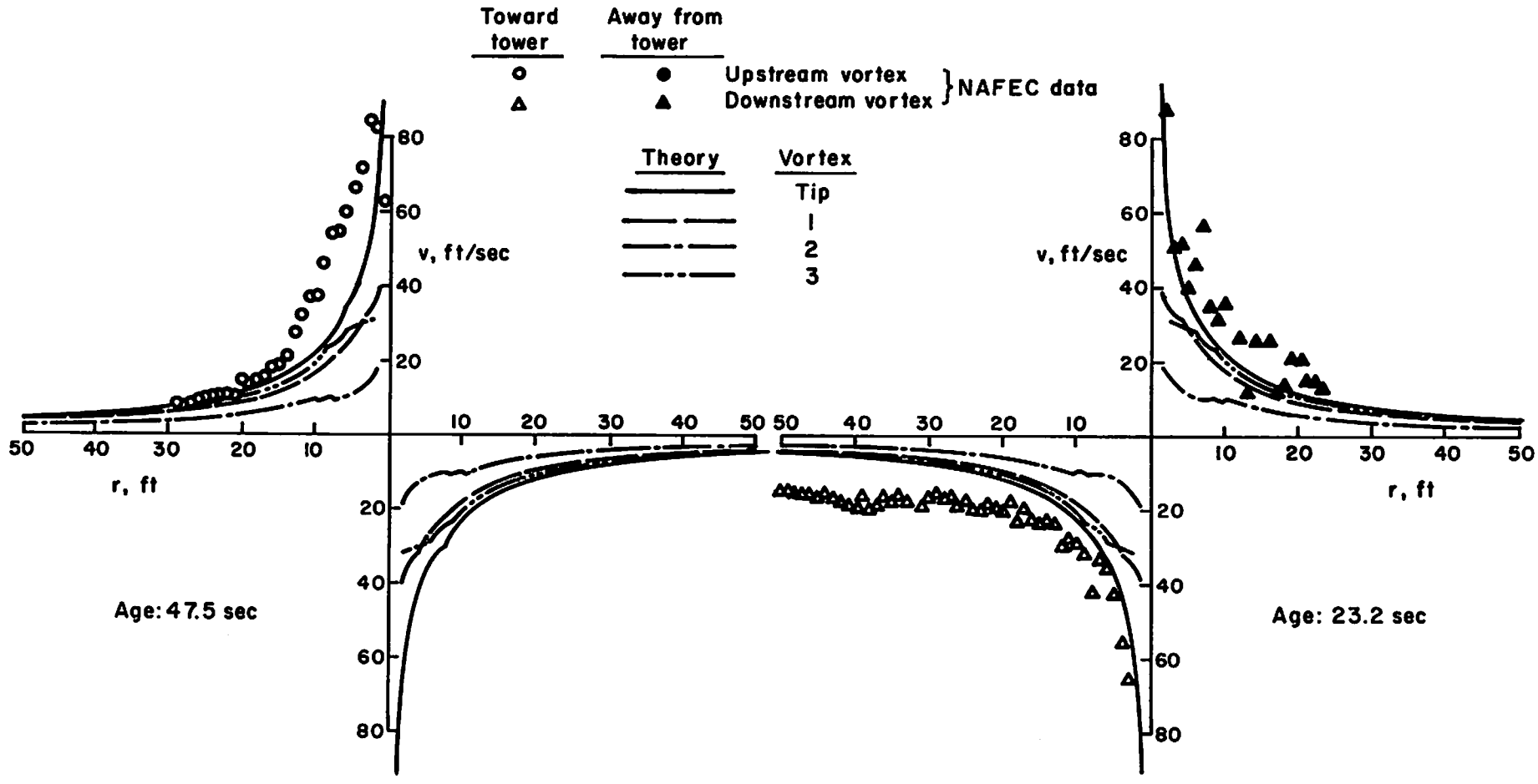

Fig. A-22. DC-10 Take-off. NAFEC Run 4

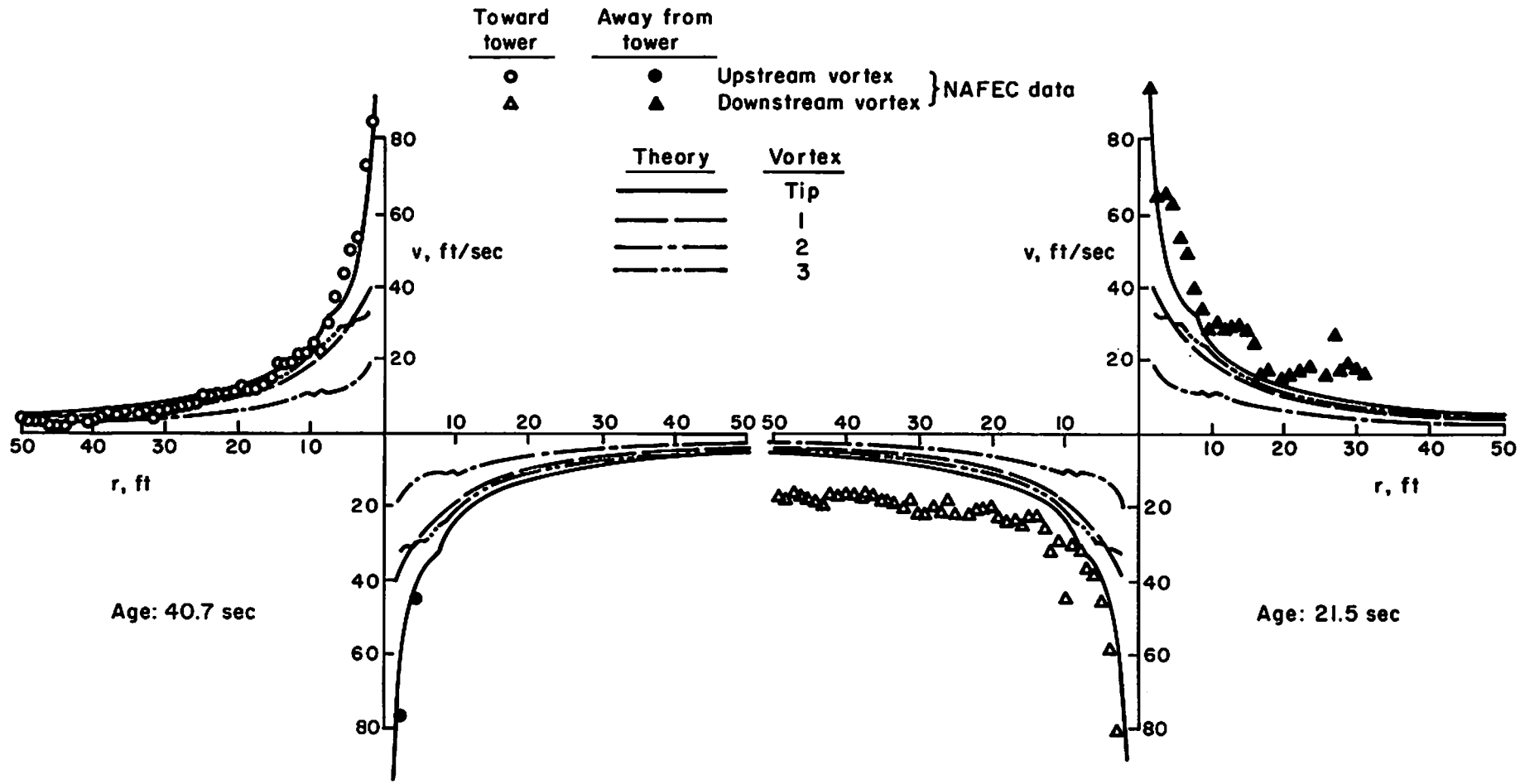

Fig. A-23. DC-10 Take-off. NAFEC Run 5

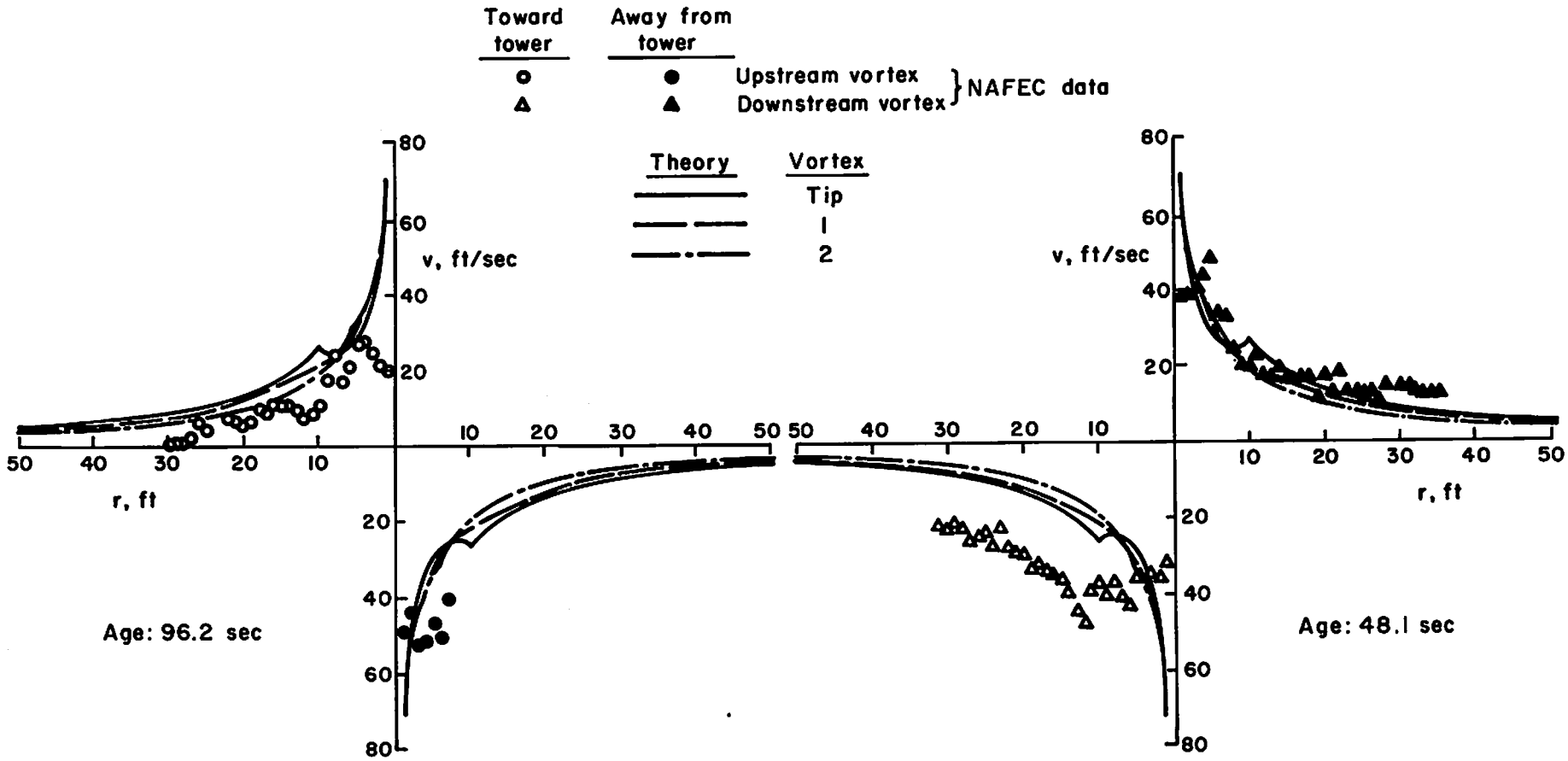

Fig. A-24. DC-10 Take-off/Approach. NAFEC Run 19

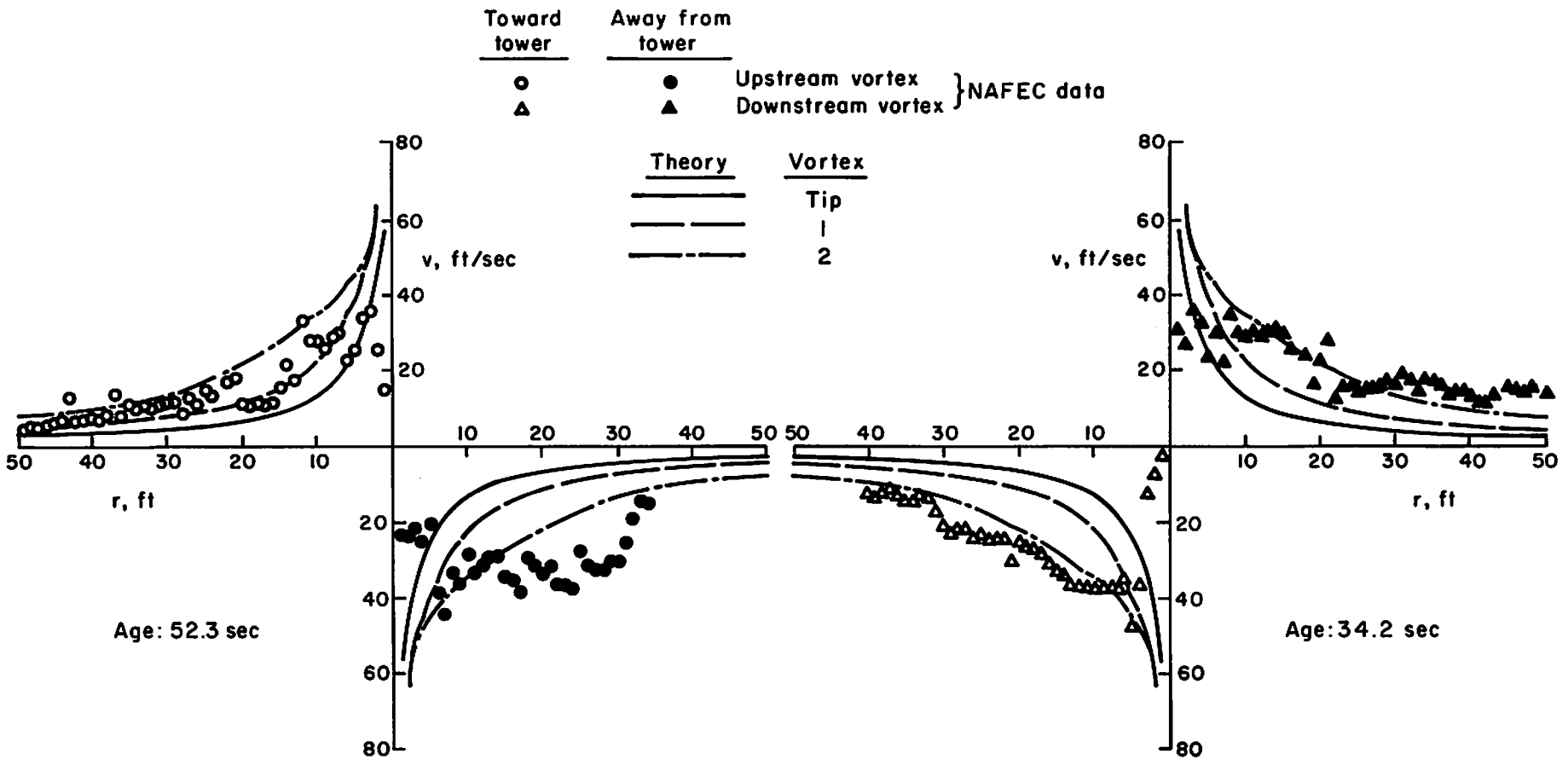

Fig. A-25. DC-10 Landing. NAFEC Run 14

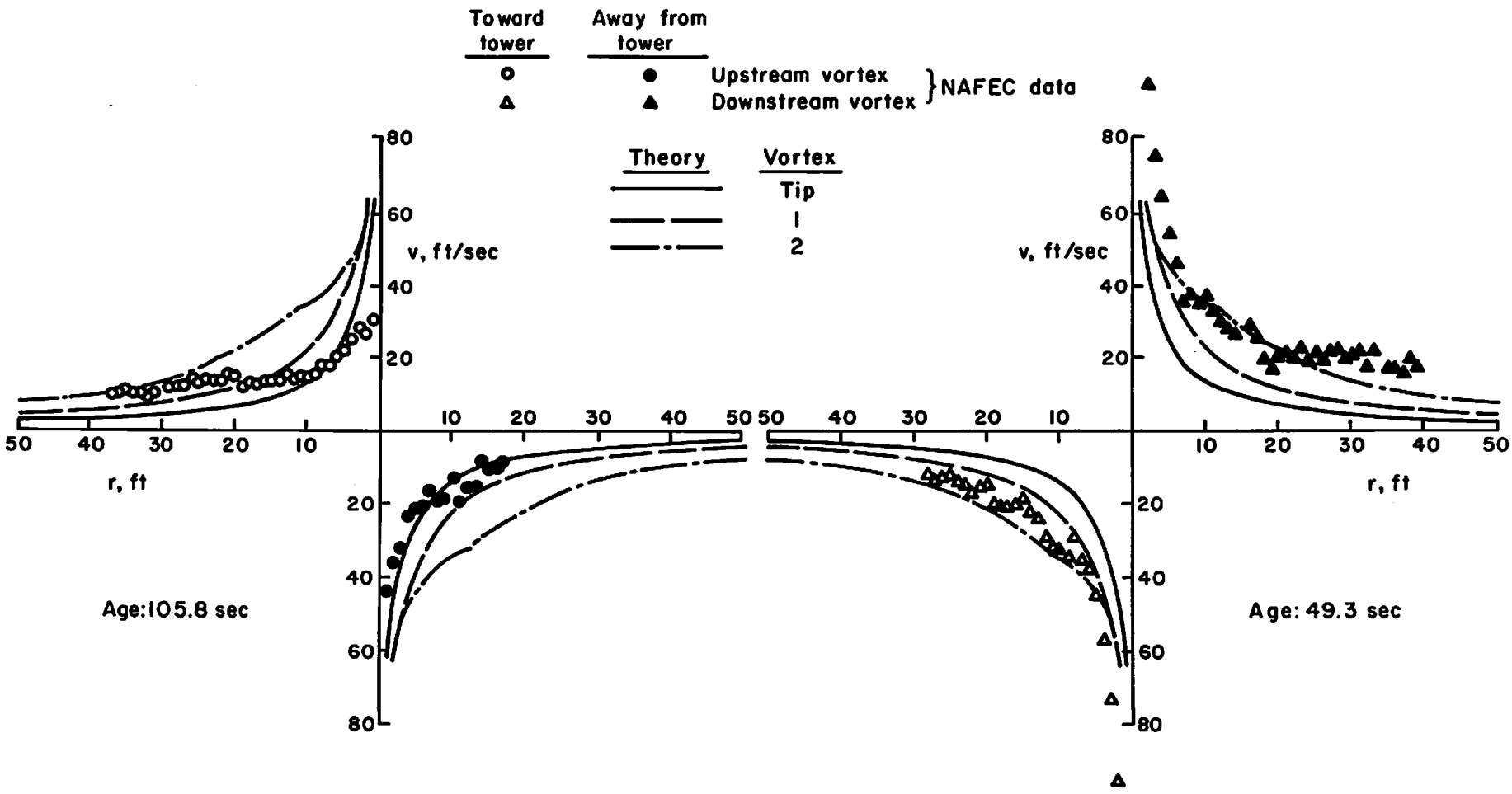

Fig. A-26. DC-10 Landing. NAFEC Run 16

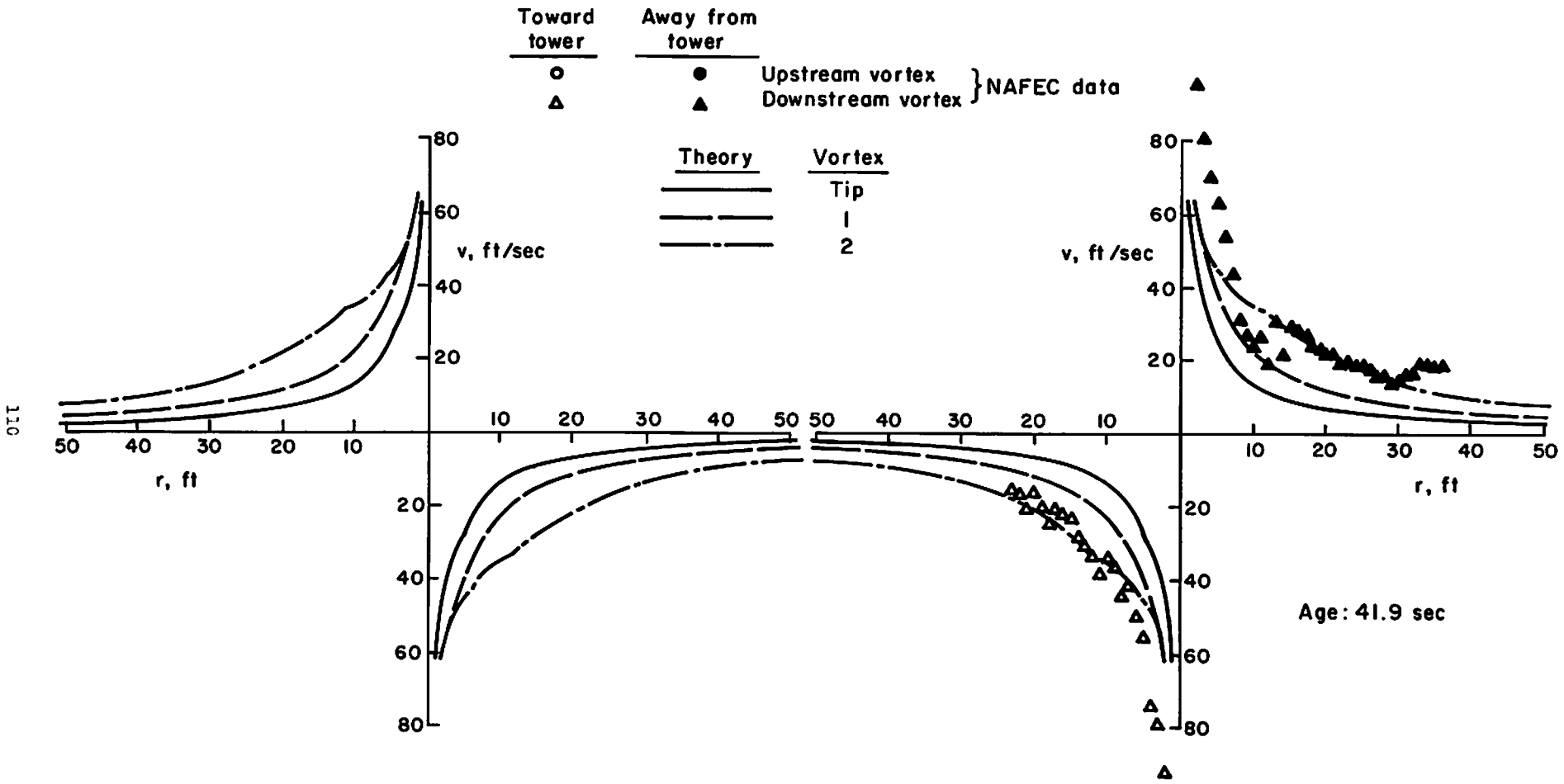

Fig. A-27. DC-10 Landing. NAFEC Run 17

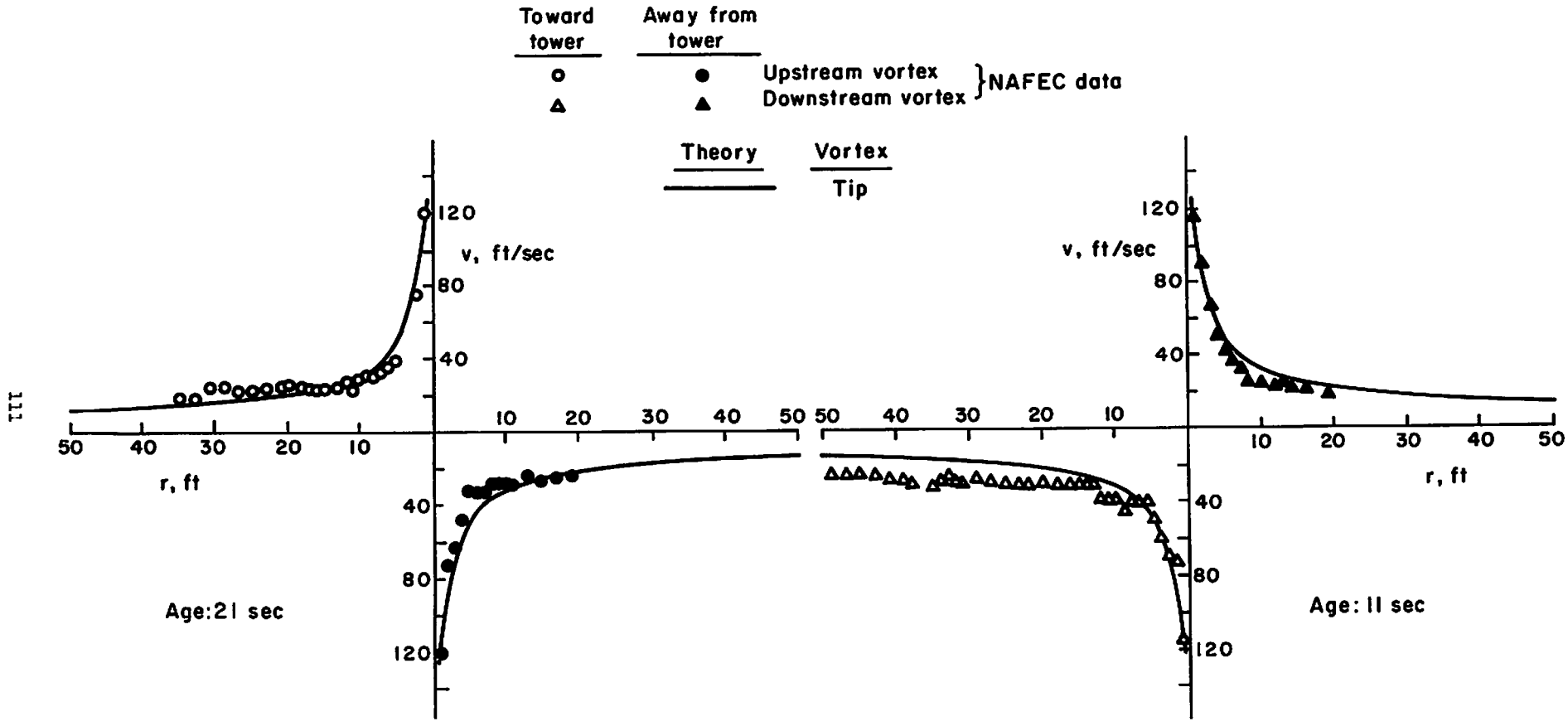

Fig. A-28. 747 Holding. NAFEC Run 44

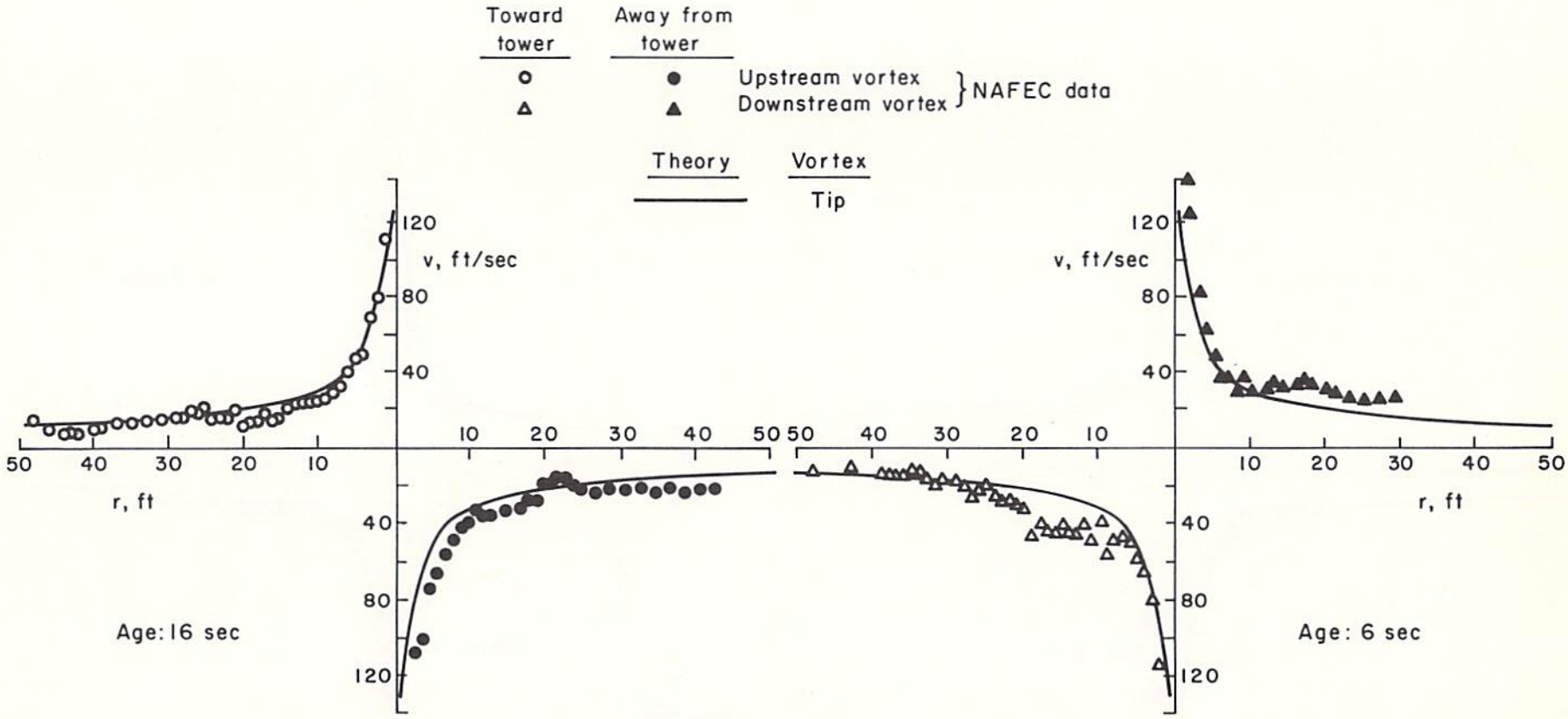

Fig. A-29. 747 Holding. NAFEC Run 53

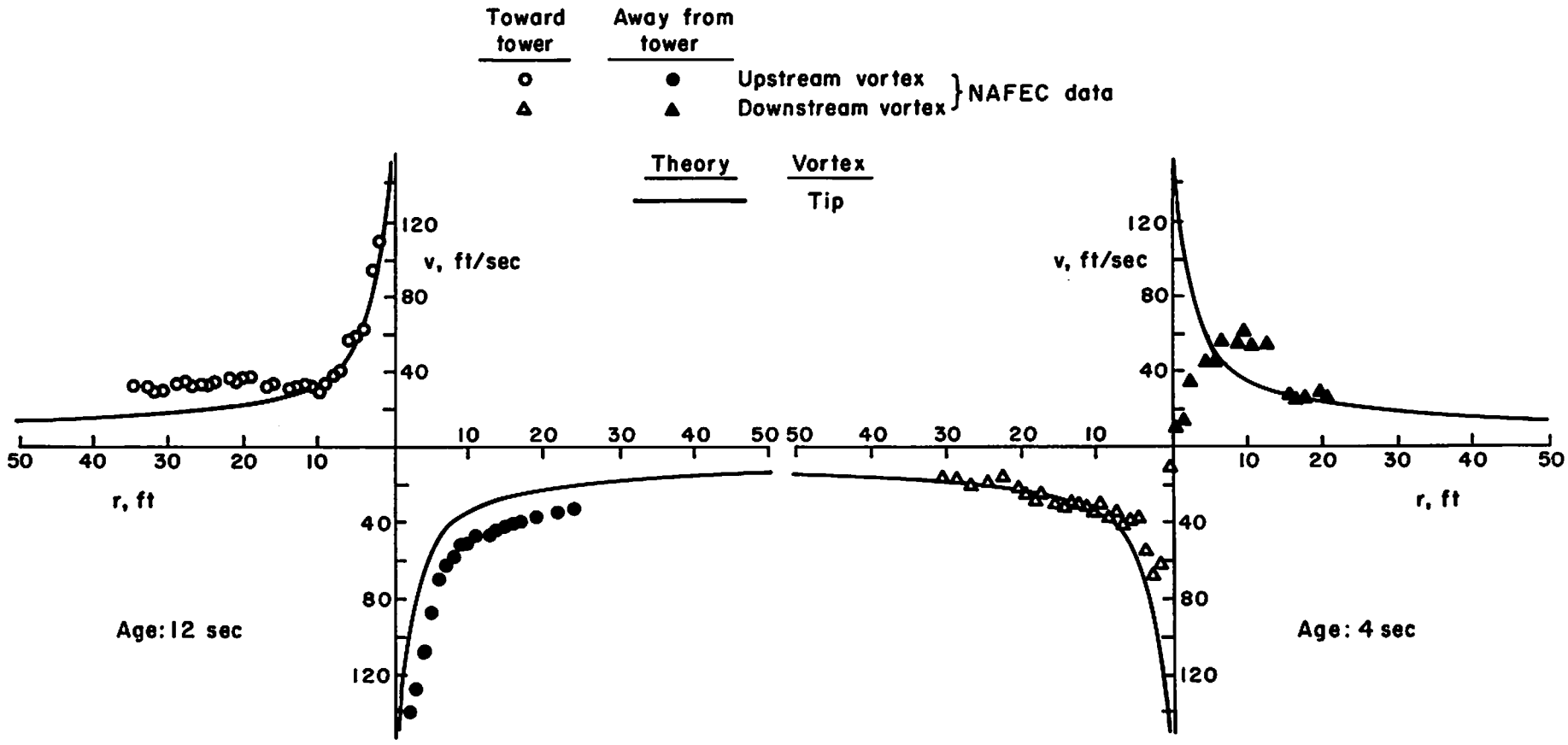

Fig. A-30. .747 Holding. NAFEC Run 55

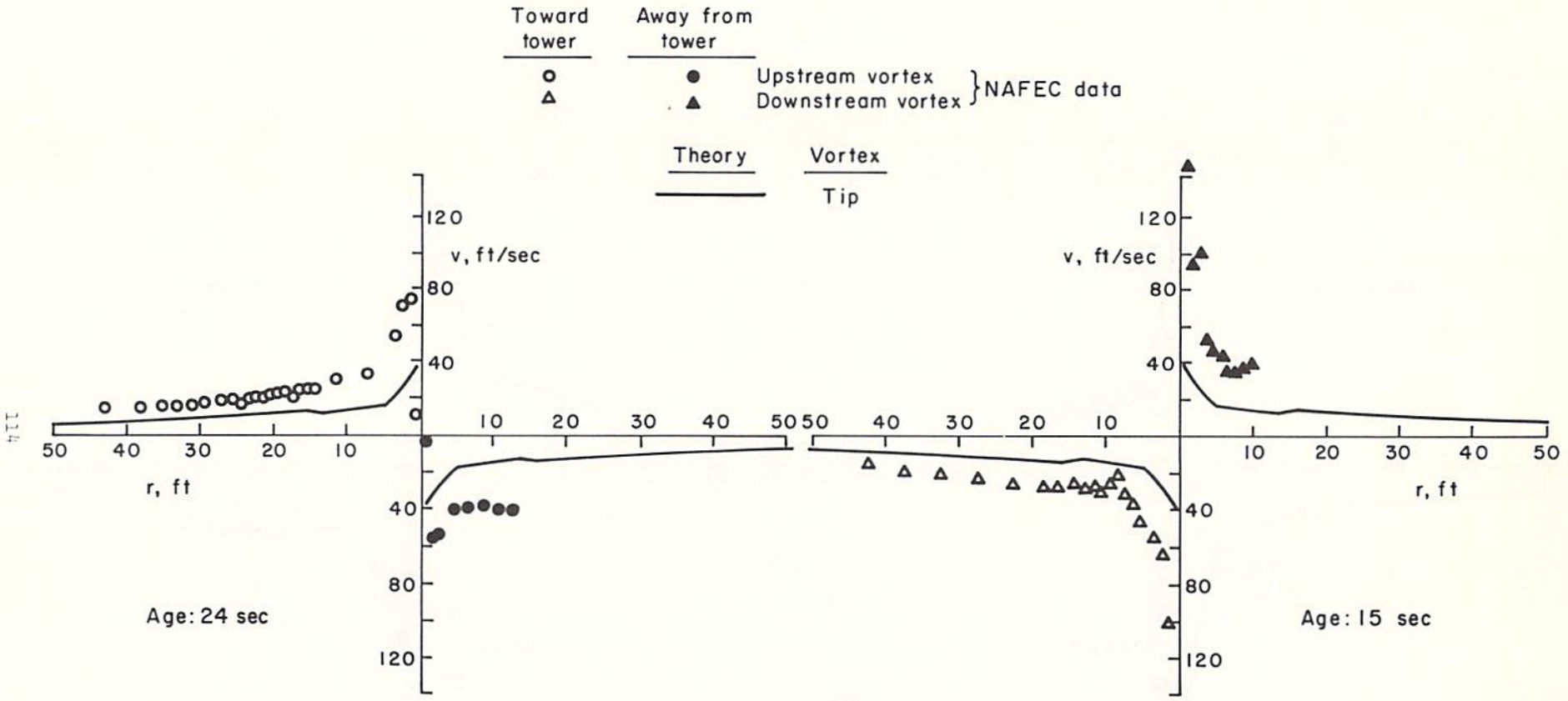

Fig. A-31. 747 Holding. NAFEC Run 68

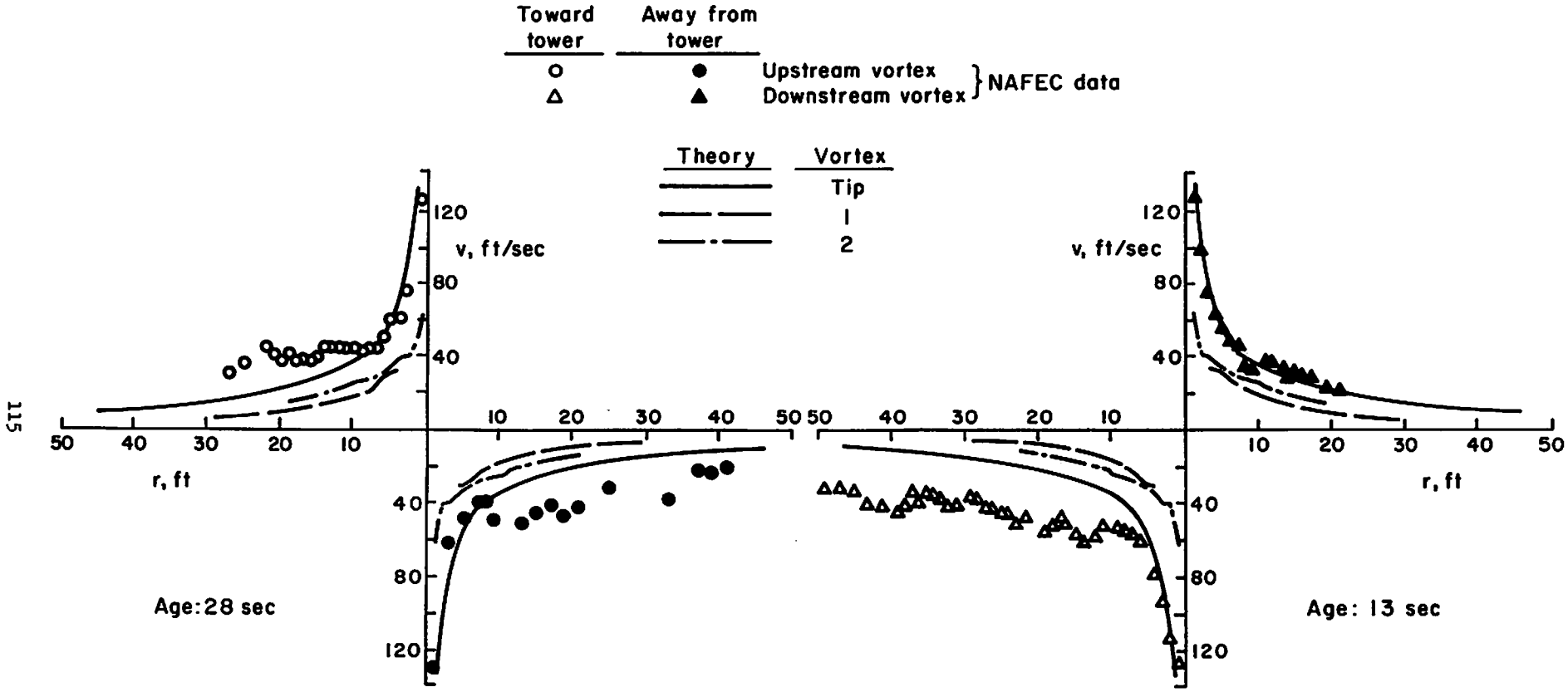

Fig. A-32. 747 Take-off. NAFEC Run 28

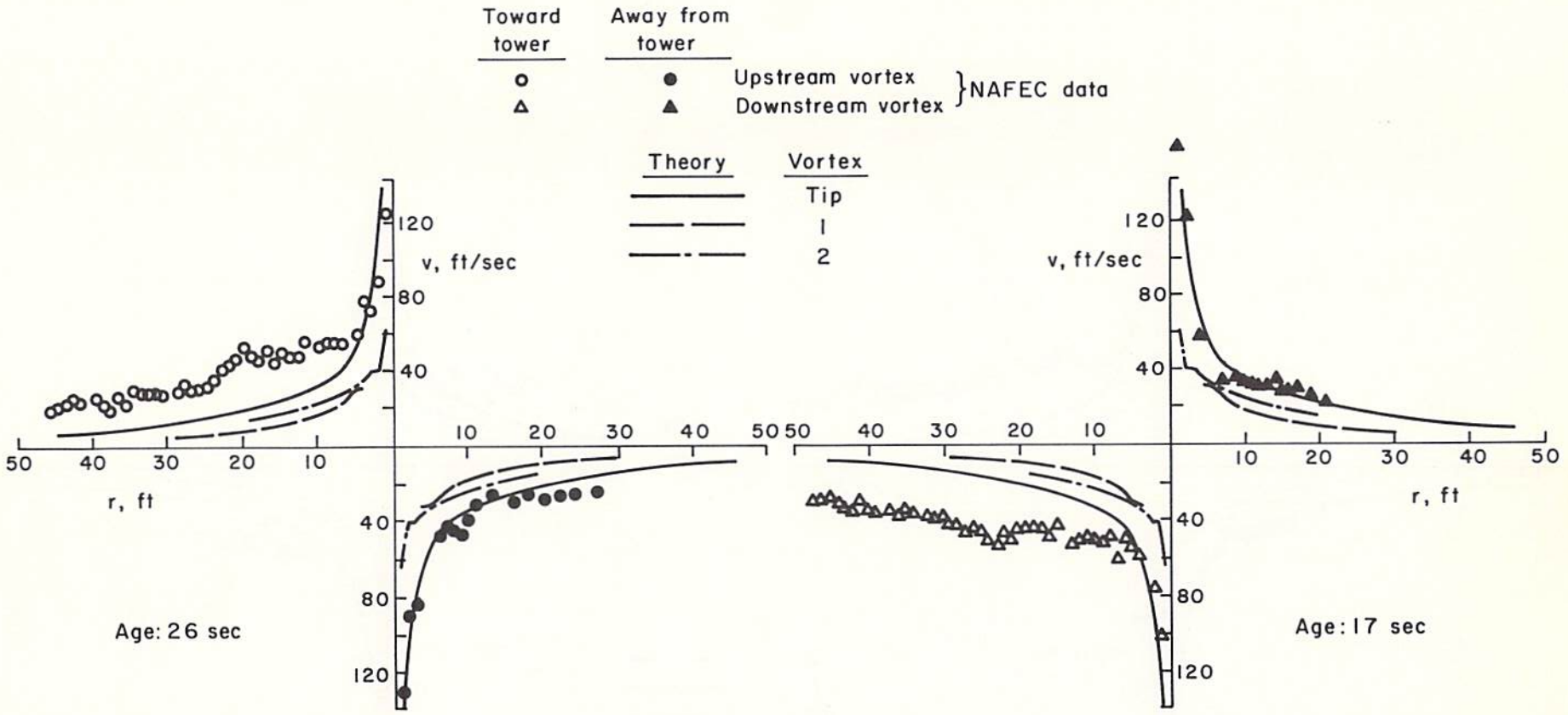

Fig. A-33. 747 Take-off. NAFEC Run 29

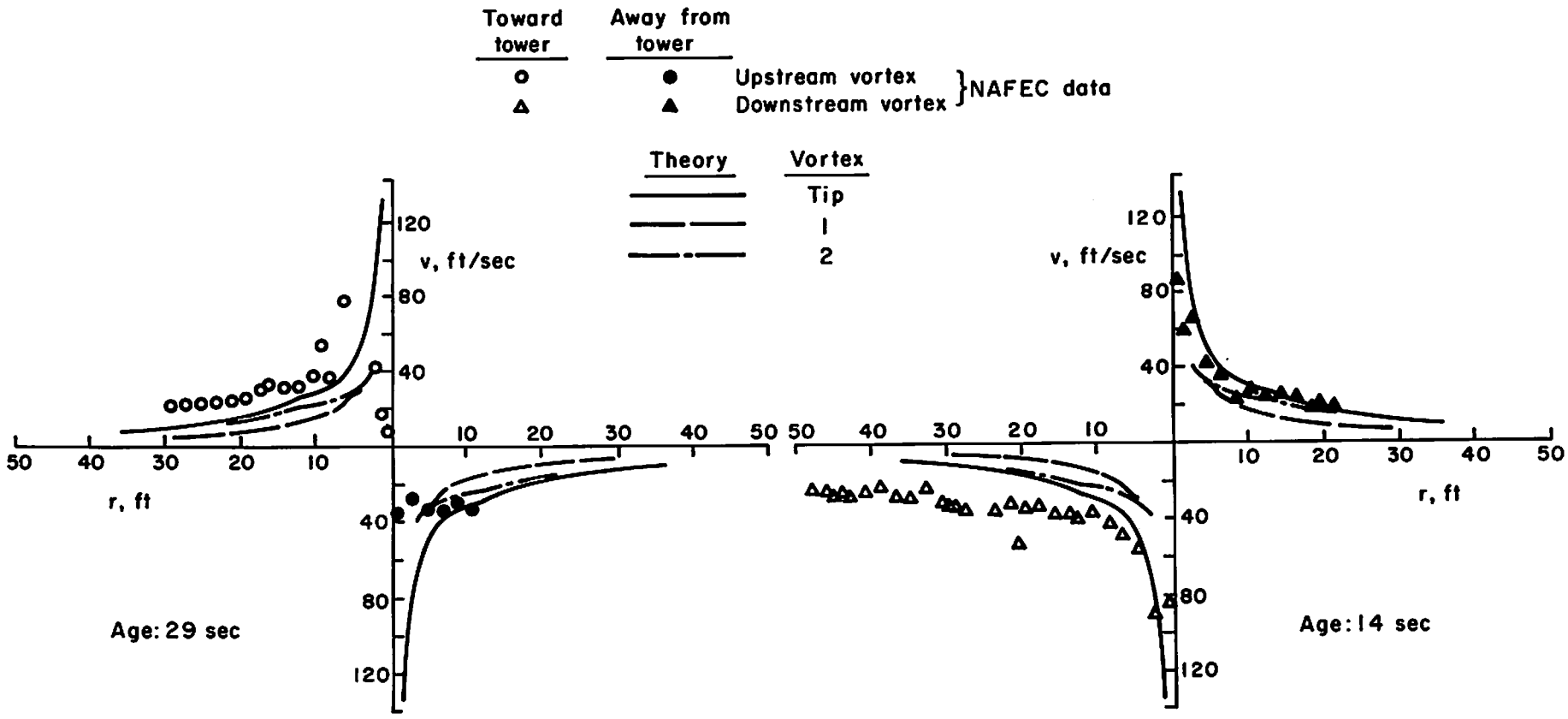

Fig. A-34. 747 Take-off. NAFEC Run 42

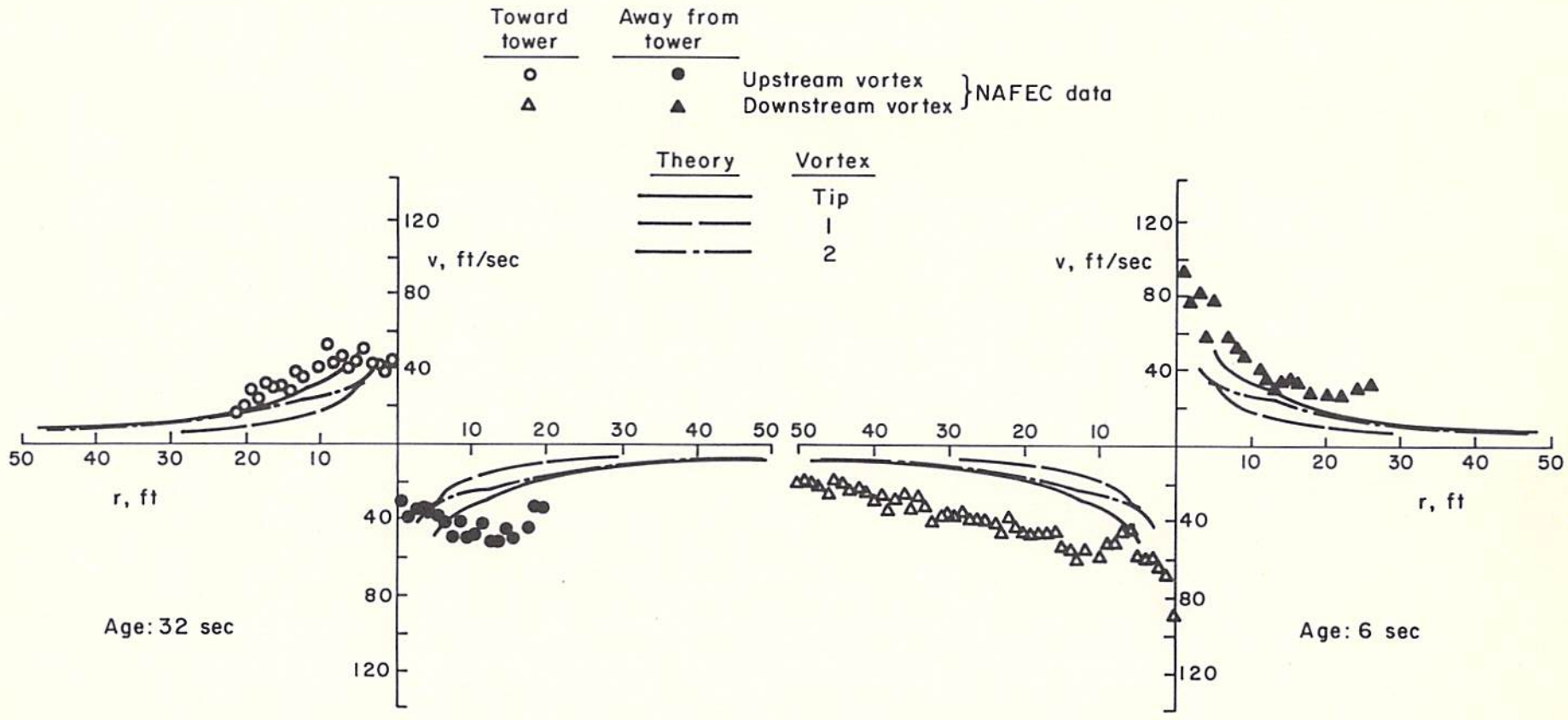

Fig. A-35. 747 Take-off. NAFEC Run 64

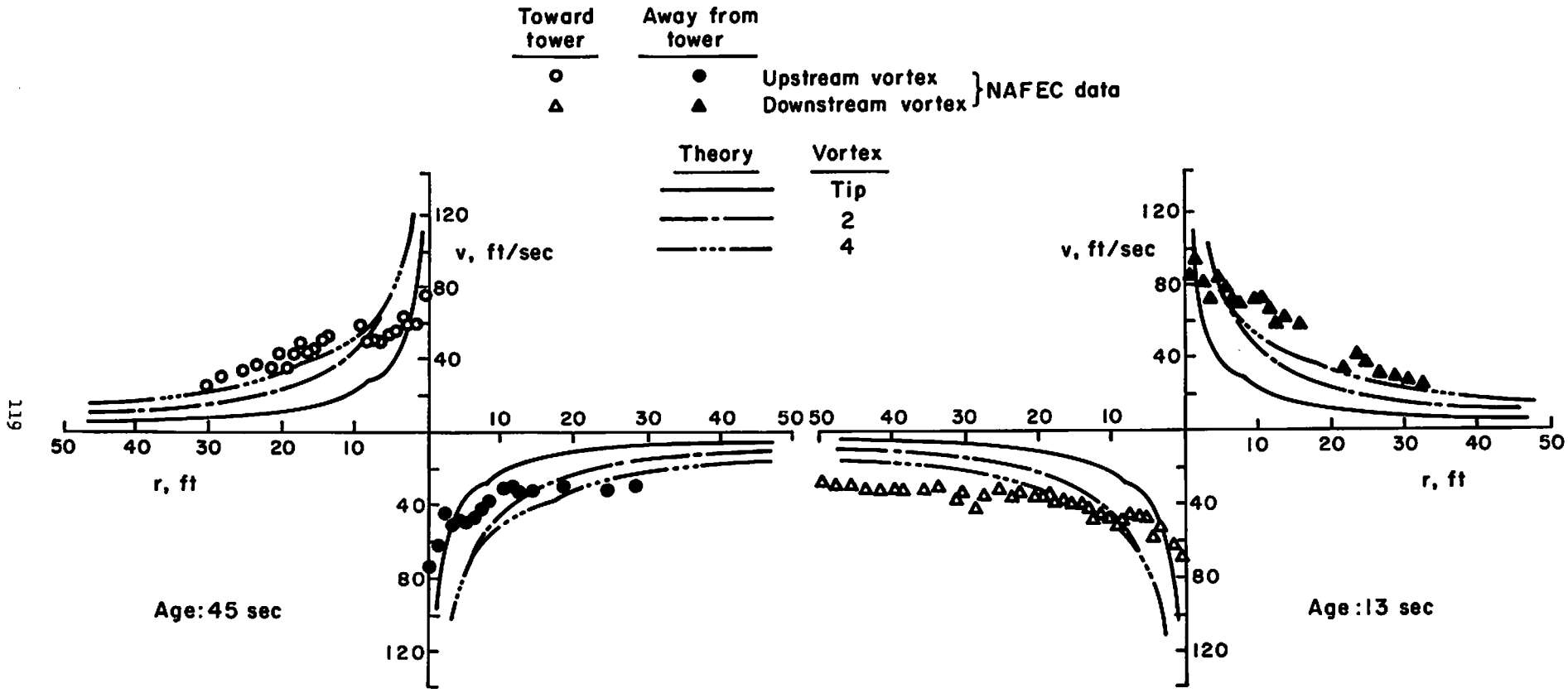

Fig. A-36. 747 Landing. NAFEC Run 11

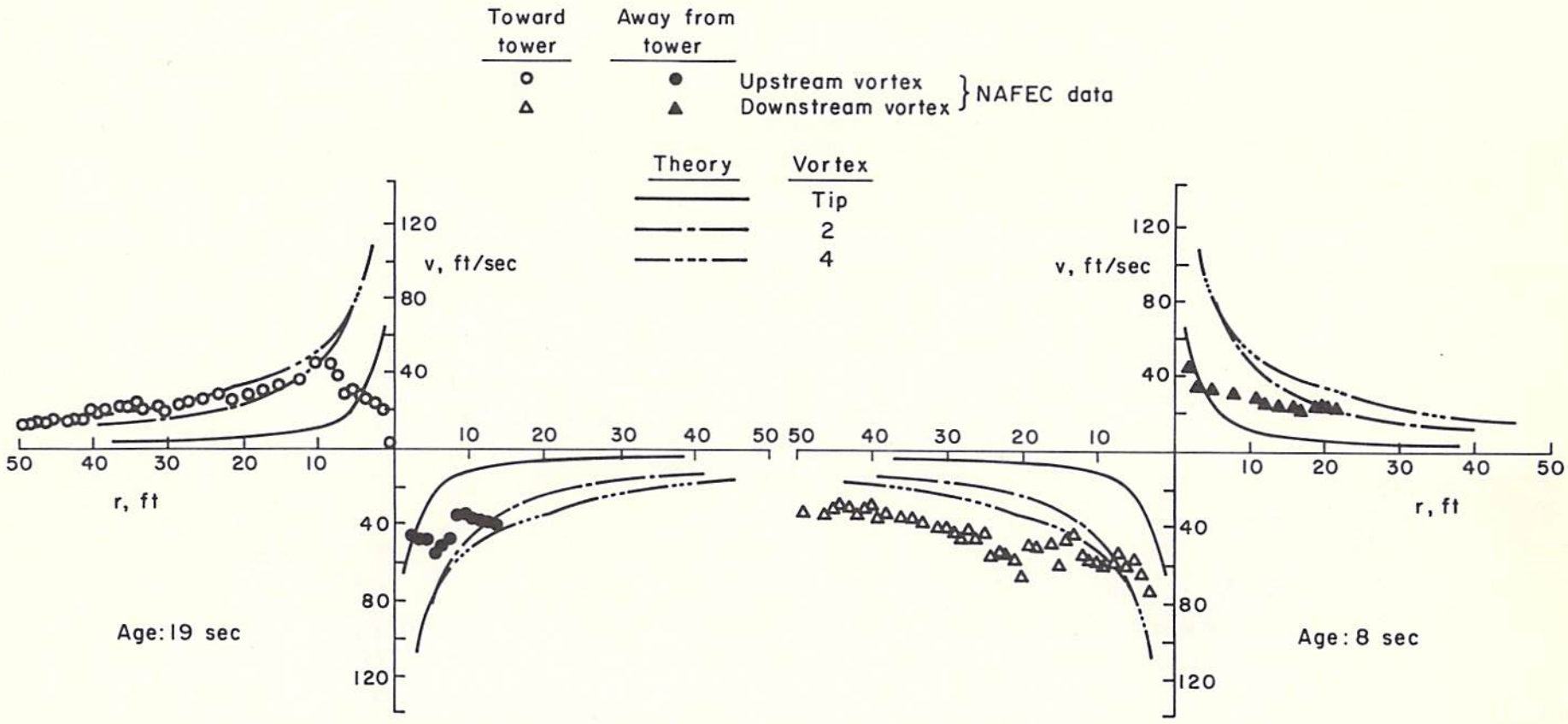

Fig. A-37. 747 Landing. NAFEC Run 38

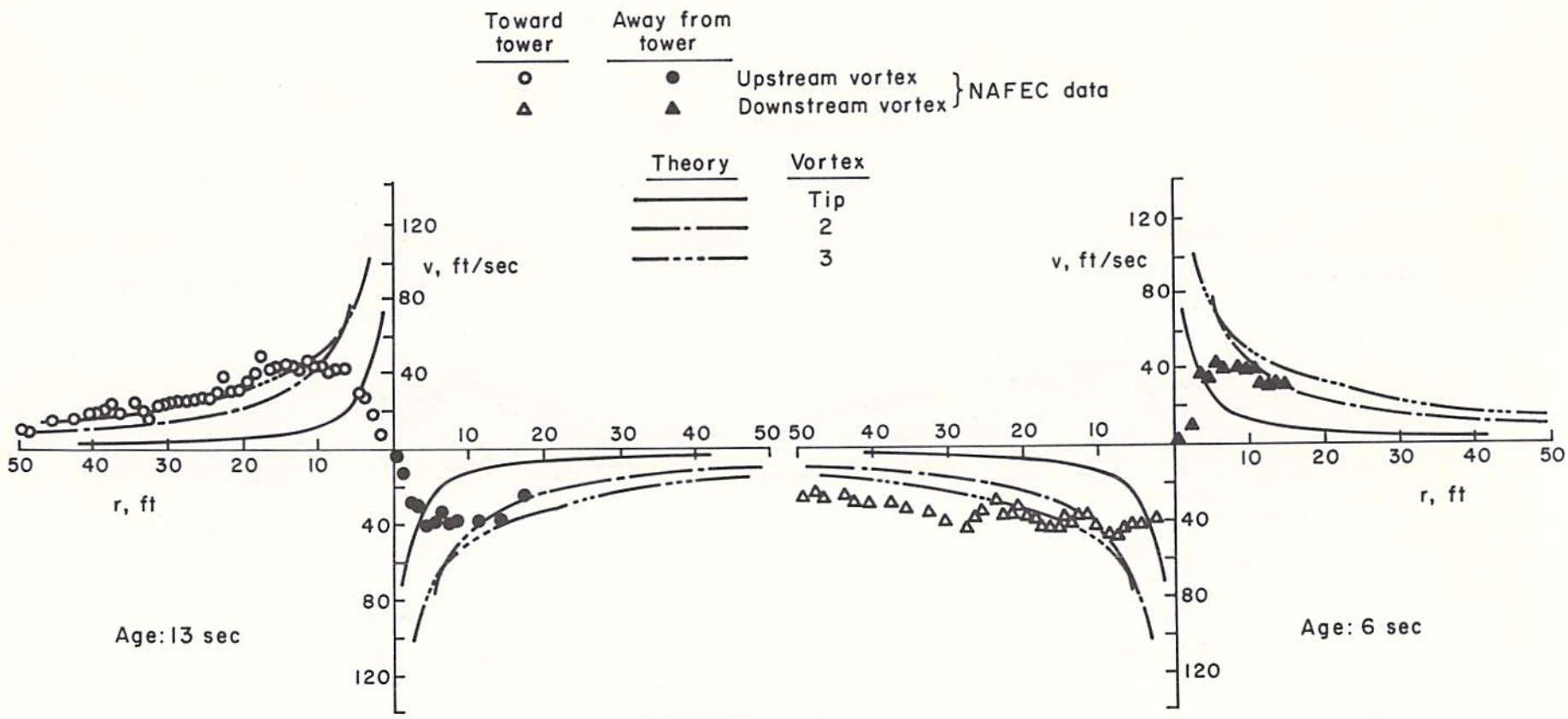

Fig. A-38. 747 Landing. NAFEC Run 49

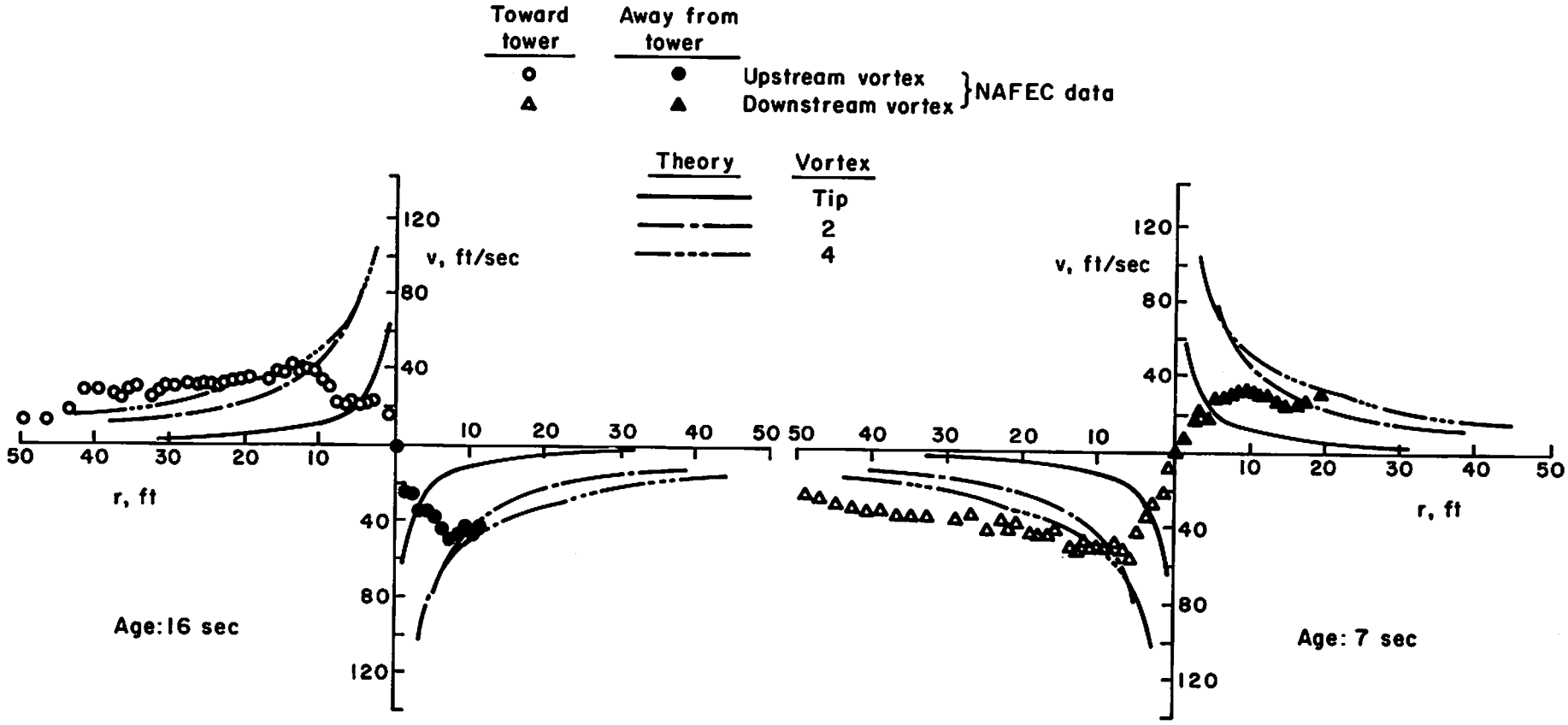

Fig. A-39. 747 Landing. NAFEC Run 51

REFERENCES

1. Betz, A., Behavior of Vortex Systems. NACA TM 713 (trans. from ZAMM, Vol. XII.3, 1932).

2. Donaldson, C. duP., A Brief Review of the Aircraft Trailing Vortex Problem. AFOSR-TR-71-1910, May 1971 (presented at Nat'l Aerospace Electronics Conf., Dayton, Ohio, May 1971).

3. Donaldson, C. duP., Snedeker, R.S., and Sullivan, R.D., A Method of Calculating Aircraft Wake Velocity Profiles and Comparison with Full-Scale Experimental Measurements. J. Aircraft 11, 9, September 1974, pp. 547-555.

4. Mason, W.H. and Marchman, J.F., III, Farfield Structure of an Aircraft Trailing Vortex. J. Aircraft 10, 2, February 1973, pp. 86-92.

5. Orloff, K.L. and Grant, G.R., The Application of a Scanning Laser Doppler Velocimeter to Trailing Vortex Definition and Alleviation. AIAA Paper No. 73-680, AIAA 6th Fluid and Plasma Dynamics Conference, 1973.

6. Bilanin, A.J., Donaldson, C. duP., and Snedeker, R.S., An Analytic and Experimental Investigation of the Wakes Behind Flapped and Unflapped Wings. AFFDL-TR-74-90, May 1974.

7. Donaldson, C. duP. and Bilanin, A.J., Vortex Wakes of Conventional Aircraft, AGARDograph 204, May 1975.

8. Rossow, V., On the Inviscid Rolled-Up Structure of Lift-Generated Vortices. J. Aircraft 10, 11, November 1973, pp. 647-650.

9. Jordan, P., Structure of Betz Vortex Cores. J. Aircraft 10, 11, November 1973, pp. 691-693.

10. Yates, J.E., Calculation of Initial Vortex Roll-Up in Aircraft Wakes. J. Aircraft 11, 7, July 1974, pp. 397-400.

11. Verstynen, H.A., Jr. and Dunham, R.E., Jr., A Flight Investigation of the Trailing Vortices Generated by a Jumbo Jet Transport. NASA TN D-7172, April 1973.

12. Durand, W.F. (Ed.), Aerodynamics Theory, Vol. II, Division E., California, Durand Reprinting Committee, 1943, pp. 328-330.

13. Brown, C.E., Aerodynamics of Wake Vortices. AIAA Journal 11, 4, April 1973, pp. 531-536.

14. Garodz, L.J., Lawrence, D., and Miller, N., The Measurement of the Boeing 727 Trailing Vortex System Using the Tower Fly-by Technique, Federal Aviation Administration Rept. No. FAA-RD-74-90, August 1974.

15. Garodz, L.J., Lawrence, D., and Miller, N., The Measurement of the Boeing 747 Trailing Vortex System Using the Tower Fly-by Technique, Federal Aviation Administration Rept. No. FAA-RD-73-156, June 1974.

16. Barber, M.R., Kurkowski, R.L., Garodz, L.J., Robinson, G.H., Smith, H.J., Jacobsen, R.A., Stinnett, G.W., Jr., McMurtry, T.C., Tymczyszyn, J.J., Devereaux, R.L., and Bolster, A.J., Flight Test Investigation of the Vortex Wake Characteristics behind a Boeing 727 during Two-Segment and Normal ILS Approaches, NASA TM X-62,398 - FAA-NA-75-151, January 1975.

17. Dunham, R.E., Jr., Model Tests of Various Vortex Dissipation Techniques in a Water Towing Tank. NASA LWP-1146, January 1974.